AN ANALYSIS OF HIGH-IMPACT, LOW-PREDICTIVE SKILL SEVERE WEATHER EVENTS IN THE NORTHEAST U.S.

by

Matthew T. Vaughan

A Thesis

Submitted to the University at Albany, State University of New York in Partial Fulfillment of

the Requirements for the Degree of

Master of Science

College of Arts & Sciences

Department of Atmospheric and Environmental Sciences

December 2015

ABSTRACT

An objective evaluation of Storm Prediction Center slight risk convective outlooks, as well as a method to identify high-impact severe weather events with poor-predictive skill are presented in this study. The objectives are to assess severe weather forecast skill over the northeast U.S. relative to the continental U.S., build a climatology of high-impact, low-predictive skill events between 1980–2013, and investigate the dynamic and thermodynamic differences between severe weather events with low-predictive skill and high-predictive skill over the northeast U.S. Severe storm reports of hail, wind, and tornadoes are used to calculate skill scores including probability of detection (POD), false alarm ratio (FAR) and threat scores (TS) for each convective outlook. Low predictive skill events are binned into low POD (type 1) and high FAR (type 2) categories to assess temporal variability of low-predictive skill events.

Type 1 events were found to occur in every year of the dataset with an average of 6 events per year. Type 2 events occur less frequently and are more common in the earlier half of the study period. An event-centered composite analysis is performed on the low-predictive skill database using the National Centers for Environmental Prediction Climate Forecast System Reanalysis 0.5° gridded dataset to analyze the dynamic and thermodynamic conditions prior to high-impact severe weather events with varying predictive skill. Deep-layer vertical shear between 1000–500 hPa is found to be a significant discriminator in slight risk forecast skill where high-impact events with less than 31-kt shear have lower threat scores than high-impact events with higher shear values. Case study analysis of type 1 events suggests the environment over which severe weather occurs is characterized by high downdraft convective available

potential energy, steep low-level lapse rates, and high lifting condensation level heights that contribute to an elevated risk of severe wind.

ACKNOWLEDGEMENTS

First, I would like to thank my family for their endless support of my academic and career aspirations. Their contribution to this work goes far beyond the encouragement I've received from them in the past 2.5 years that comprised my M.S. education and I am grateful for the love.

I thank my academic advisors, Profs. Brian Tang and Lance Bosart for their guidance, support, and willingness advise on a host of meaningful topics, both scientific and otherwise. It has been an absolute pleasure to work alongside these tremendous scientists who have prioritized my development as a scientist. They are professors and individuals of the highest order and I will always be grateful of my time under their tutelage.

In the same vein, I'd like to thank the faculty and staff of the UAlbany Department of Atmospheric and Environmental Sciences. The department maintains the highest standards in research and teaching and I have benefitted immensely from the hard work of the teachers and administrative staff here. I thank Kevin Tyle and David Knight for their technical assistance with the department computer system on which my M.S. work depended. I also thank Denise Church, Sandra George, Barbara Zampella, and Chaina Porter for their administrative support and willingness to help this bumbling graduate student.

My National Weather Service focal points, Mike Evans and Joe Villani, have provided very helpful advice and shared unique operational perspectives from their local offices. Additionally, I'm grateful to Mike for his help in organizing local workshops during my M.S. tenure to provide platforms to share my research results presented here to operational forecasters in the Northeast.

I wish to thank my fellow graduate students who, through their shared experience in pursuing graduate education, became invaluable friends. In particular, I'd like to thank Joshua Alland, Jeremy Berman, Michael Fischer, and Casey Peirano for their help, support, and camaraderie.

Lastly, I want to thank all my past teachers over the years. At my undergraduate institution, I am indebted to Drs. Randell Barry, Thomas Guinn, Frederick Mosher, and Bradley Muller who inspired and prepared me to pursue a graduate education. In addition, I thank my past teachers in Berkshire County, Massachusetts who instilled an appreciation for the pursuit of knowledge for which I will always be grateful.

This research was supported by the National Oceanic and Atmospheric Administration (NOAA) grant NA13NWS4680004, awarded to the University at Albany, SUNY, as part of the Collaborative Science, Technology, and Applied Research (CSTAR) program.

M. T. V.

Albany, New York

December 2015

TABLE OF CONTENTS

LIST OF TABLES

LIST OF FIGURES

1. Introduction

1.1 Motivation

Forecasting severe convective weather and its associated hazards is a pressing challenge for the meteorological community. In particular, storm severity, coverage, and track have magnified societal impacts in the densely populated northeastern United States (hereafter, Northeast). Major metropolitan areas are particularly vulnerable to severe weather, which can threaten millions of people over a small area. Figure 1.1 illustrates the large population densities around several cities across the Northeast. Specifically, the corridor following Interstate 95 from Boston through Philadelphia is densely populated with residential and commercial properties. The large volume of air traffic further exacerbates severe weather impacts over the Northeast states. Eight of the top twenty-five busiest airports in the United States are found north of Washington D.C. and east of Pittsburg, PA [Airports Council International (2013)]. Flight delays and reroutes are often necessary during severe weather events over the Northeast, causing disruptions in national air travel as major airports are affected (Evans et al. 2009). The U.S. Bureau of Transportation Statistics lists weather as causing 63.88% of all National Aviation System delays between 2003–2015 (www.transtats.bts.gov). Individuals and businesses with time-sensitive operations (e.g. UPS, FedEx, Amazon, etc.) as well as companies that directly service airline flights (e.g. Coca-Cola, Biscoff by Lotus Bakeries, etc.) are negatively impacted by unexpected, weather-related disruptions to air commerce. Therefore, accurately forecasting severe weather events over the Northeast is important to ensure proper societal preparation in such a vulnerable portion of the country.

Forecasting hazardous severe weather in the Northeast is often a difficult task. As an example, Figure 1.2 depicts verification of the National Oceanographic and Atmospheric Administration (NOAA) Storm Prediction Center (SPC) convective outlook forecast for 1200 UTC 19 August 2011 – 1200 UTC 20 August 2011 issued at 0600 UTC 19 August 2011. The coverage and density of severe reports over several northeastern states suggest a convective outlook depicting a higher probability of severe weather over the region was warranted for the observed magnitude of severe weather. Likewise, Figure 1.3 illustrates similarly poor verification over the Northeast for 1200 UTC 4 July 2012 – 1200 UTC 5 July 2012 for the 0600 UTC 4 July 2012 outlook. The recency of these events suggests severe weather forecasting in the Northeast remains a challenge and careful examination of these poorly forecast events is necessary to improve the state of convective forecasting in the region.

The Northeast harbors a varied landscape of mountains, valleys, lakes, rivers, and borders the Atlantic Ocean and the easternmost Great Lakes (Fig. 1.4). Interactions between the planetary boundary layer flow and the Northeast terrain create complex convective environments that can influence storm development and severity (e.g., Riley and Bosart 1987; Wasula et al. 2002; LaPenta et al. 2005; Bosart et al. 2006; Lericos et al. 2007). Lake and ocean boundaries, along with aforementioned terrain variations, create additional sources of vertical motion through surface convergence and upslope flow and may modify low-level winds and enhance low-level vertical wind shear (Bosart et al. 2006). Consequently, results from numerous studies of severe weather environments over the Great Plains may not be fully representative of severe weather environments over the Northeast. Therefore, restricting study to events over the Northeast will tailor results to the regional environment, enhancing the relevance of research results to local operational forecasters.

As a result of ongoing research on convective storms and, in large part, the work done during the NOAA Hazardous Weather Testbed, severe weather forecasters now have access to convection-allowing numerical weather prediction models (CAMs), ensembles of CAMs, high-resolution satellite data, and a wide range of regional and global models to aide in the forecasting process. Despite these new forecast tools, severe weather forecasting requires significant human involvement. Human insight remains a vital part of the severe weather forecasting process providing valuable guidance to various users of weather data. Analyzing the performance of SPC convective outlooks captures the predictive skill of the entire severe weather forecasting system including forecaster adjustments to model output. It is useful to identify cases of poor forecast performance, such as those illustrated in Figures 1.2 and 1.3, to focus further research and case studies concerning environments with low-predictive skill. Thus, our understanding of Northeast severe weather would benefit from an identification algorithm and subsequent analysis of severe weather environments with poor-predictive skill.

1.2 Literature Review

1.2.1 Northeastern United States convection

Previous studies have investigated the seasonal variability, mode, and synoptic environment of convection, including severe convection, across the Northeast. Hurlbut and Cohen (2012) examined severe convection over Pennsylvania, New Jersey, New York, Connecticut, Rhode Island, Massachusetts, New Hampshire, Vermont and Maine between 1999–2009. They found severe reports of hail, wind and tornados occur most frequently during the meteorological summer (defined as June–August) season (Fig. 1.5) with 498 of 742 (67%)

severe weather days occurring in these three months. Meteorological spring (defined as March–May) is the second-most active season with 144 events (19%). Within the 11-year study period, some interannual and interseasonal variability exists, with severe reports peaking in 2007 and 2008 (Fig. 1.6). Nevertheless, given the variability, the vast majority of severe weather reports occur during the summer in the Northeast.

Severe convection in the Northeast tends to mimic the diurnal heating cycle, suggesting diabatic heating of the surface through solar insolation is important to thunderstorm initiation and maintenance (Hurlbut and Cohen 2012). The peak time for the first severe report of a severe event is 1900 UTC. First severe reports occur infrequently in the overnight hours, especially between 0600 and 1200 UTC when only 4% of first reports occur. Meanwhile, the last severe reports rarely occur during the late morning and early afternoon with 2% of last reports occurring between 1500 and 1700 UTC whereas the peak time for last reports is 0000 UTC.

Severe convective wind is the dominant severe weather threat in the Northeast (Fig. 1.5). 10161 severe wind reports occurred over the 11-year study period of Hurlbut and Cohen (2012) compared to 1732 reports of hail greater than 1 in. (4413 reports of hail greater than 0.75 in.). Meanwhile, a total of 190 tornado reports occurred during the study period, suggesting tornadoes are a rare phenomenon, as they are in the rest of the nation, and solidifying severe wind as the primary severe convective threat in the Northeast.

Lombardo and Colle (2011, hereafter LC11) documented convective storm structures and ambient conditions associated with severe storms over the Northeast. Their study used the 2007 warm season (May–August) and a warm season comprising randomly selected days from the 2002–2006 warm seasons. The convective storms are categorized, through manual examination of 2-km National Operational Weather Radar reflectivity imagery (NOWrad), and binned into

three types of cellular convection, five types of quasi-linear systems, and nonlinear systems identical to the method used in Gallus et al. (2008) (Fig. 1.7). LC11 define a severe event when a convective element produces at least one severe report. Linear structures (NS, TS, PS, LS, and BE in Fig. 1.7), while the least common convective mode in the Northeast (Lombardo and Colle 2010), are responsible for one-third of all severe events. Conversely, cellular convection comprises approximately half of all warm season convection (Lombardo and Colle 2010), but contributes 39% of all severe events in the Northeast. Lastly, nonlinear convective systems compose about one-third of all warm season convection as well as severe reports.

Figure 1.8 from LC11 illustrates the number of severe events, separated into severe wind, hail, and tornado categories, associated with each convective organizational structure over the Northeast. The numbers of severe wind events for each of the three main convective types (cellular, linear, nonlinear) are comparable. However, cellular clusters produce significantly more severe wind events than isolated cells. Additionally, linear convection with trailing stratiform or no stratiform precipitation produces significantly more severe wind events than other linear types. The numbers of severe hail events for each of the main convective types is comparable however cellular convection is responsible for ~1.3 times as many hail events as both linear and nonlinear systems (85% significance). LC11 found linear convective structures are less common than cellular and nonlinear convection but produce significantly more severe wind reports per event. Furthermore, cellular clusters, followed by trailing stratiform linear convective structures, produce the highest number of hail reports per event.

For context, a comparison of severe convective organizational structures over the central and northeastern United States is warranted. Gallus et al. (2008) identifies convective structures responsible for various types of severe weather (wind, hail, tornadoes) over the central United

States using the methodology described in Lombardo and Colle (2010, 2011). Cellular convection is responsible for 48% of all severe events in the central United States (Gallus et al. 2008, their Fig. 6) whereas 39% of all severe events are produced by cellular convection in the Northeast. The fraction of severe events produced by linear structures is higher over the Northeast (32%) compared to the central Unites States (23%). Nonlinear events produce 29% of all severe reports over both the Northeast and the central United States (No uncertainty values given).

The differences in severe convection between the Northeast and the central United States extend to the environmental parameters prior to convective passage. LC11 evaluates ambient environmental conditions using the closest 3-h North American Regional Reanalysis (NARR) time prior to the first severe weather report of a particular convective element. Variables are taken at four locations in the coastal region of the Northeast. Mean most-unstable convective available potential energy (MUCAPE) values for cellular and linear events are ~1200 J kg^{-1}, while for nonlinear events the mean is ~460 J kg^{-1} (Fig. 1.9a). Thompson et al. (2003) found mean mixed-layer CAPE (MLCAPE) values of 1645 and 1280 J kg^{-1} for non-tornadic supercells and nonsupercells, respectively, over the central Great Plains. Therefore, we infer the mean MLCAPE of severe cells near the coastal Northeast is lower than the mean MLCAPE for nonsupercells over the central Great Plains. Additionally, for Northeast severe linear events, the mean MUCAPE (1200 J kg^{-1}) is half as large as the mean surface-based CAPE observed during derecho-producing mesoscale convective systems (MCSs) over the central United States [2394 J kg^{-1}; Coniglio et al. (2004)]. MUCAPE values during coastal Northeast linear events (Fig. 1.9a) are more consistent with MLCAPE observed during nonsevere MCSs over the central Great Plains (Cohen et al. 2007, their Fig. 8a). Notably, Northeast MUCAPE varies substantially for

severe events. The 25th to 75th quartiles for the more populated cellular and linear bins range from ~700 J kg^{-1} to ~1600 J kg^{-1} with the entire severe convection envelope ranging from less than 100 J kg^{-1} to greater than 3000 J kg^{-1} (Fig. 1.9a).

The average 0–1-km shear value during coastal Northeast severe cellular events is ~2.6 m s^{-1} (Fig. 1.9b), a smaller mean value than for central U.S. non-supercells [3.8 m s^{-1}; Thompson et al. (2003)], and is significantly (95% level) less than coastal Northeast severe linear events (4.5 m s^{-1}). However, 4.5 m s^{-1} is substantially smaller than during derecho-producing MCSs in the central and eastern United States [10.6 m s^{-1}; Coniglio et al. (2004)]. Furthermore, 0–1-km shear values during coastal Northeast severe linear events are 1.5 times less than 0–1-km shear values observed during weakly forced (500-hPa **Q**-vector convergence) central U.S. derecho events (Coniglio et al. 2004). Notably, the interquartile range (IQR) of severe cellular events (N=49) is relatively small, ranging from 1.4 to 2.6 m s^{-1}, while the IQRs for severe linear (N=45) and nonlinear (N=15) events are substantially larger (Fig. 1.9b). The NARR may not fully represent the near-storm environment, but the confined distribution of severe cellular events and the significantly smaller mean value of 0–1-km shear suggest environments with strong 0–1-km shear tend to favor linear and nonlinear structures while environments with very weak 0–1-km shear favor cellular convective modes.

The mean 0–6-km shear values for coastal Northeast severe events increase from cellular to linear to nonlinear convective modes (Fig. 1.9c). Deep-layer shear magnitudes for coastal Northeast linear severe events are smaller than central and eastern U.S. severe and derecho-producing quasi-linear systems (Cohen et al. 2007). An earlier study of derechos developing east of the Rockies found the IQR of 0–6-km shear is 11.8–20.0 m s^{-1} (Evans and Doswell 2001), which is consistent with coastal Northeast severe linear events (Fig. 1.9c). Cellular and linear

severe convective modes over the coastal Northeast display large variability in deep-layer shear, with values ranging from less than 5 m s^{-1} to more than 40 m s^{-1}, suggesting severe weather can initiate and develop under fairly weak deep-layer shear values. This is similar to the findings of Evans and Doswell (2001), stating derechos can form in 0–6-km shear environments as low as 1 m s^{-1}. These events usually lack strong synoptic forcing, such as a cold front or vigorous midlevel trough, developing in regions of warm air advection under more unstable conditions compared to events with larger shear values (Evans and Doswell 2001).

Given the previous results above, it is apparent that many severe events over the coastal Northeast occur in environments with weaker CAPE and vertical wind shear than over the central U.S. Recognizing the challenge inherent to forecasting these more subtle conditions, Hurlbut and Cohen (2014) examined severe weather over an 11-year period across a large portion of the northeastern U.S. (Fig. 1.1). Manual selection of representative soundings for each severe event day precludes a larger climatology. Figure 1.10 illustrates observed MLCAPE for severe events grouped by severe report count. Neglecting events producing more than 101 reports, median MLCAPE values are less than 1000 J kg^{-1}. Cohen et al. (2007) found a median MLCAPE value of ~1400 J kg^{-1} for nonsevere MCSs and a median MLCAPE value above 2000 J kg^{-1} for severe MCSs in the central Great Plains. Additionally, the median MLCAPE values across the Northeast are below the mean MLCAPE values given by Thompson et al. (2003) for non-tornadic supercells and nonsupercells. This suggests severe weather develops in weaker instability, not only across the coastal portion of the northeastern U.S. but also across a large portion of the Northeast, than supercells and MCS structures over the central and eastern U.S.

Median 0–6-km shear observations during severe events hover between 13 and 16 m s^{-1} over the Northeast (Fig. 1.11). Interestingly, the bottom 25th percentile for events featuring at

least 101 reports is below 10 m s^{-1} while events with significant wind (>33.4 m s^{-1}) reports have a broad range of shear values. Hurlbut and Cohen (2014) did not find 0–6-km shear to be a significant discriminator of severe event severity, but the wide range of shear values indicates that large deep-layer shear values are not necessary for widespread severe weather events in the Northeast. Coincidentally, downdraft CAPE (DCAPE) was found to be a significant (99% level) parameter in distinguishing between events with at least 101 reports and events with fewer reports (Fig. 1.12). DCAPE is representative of the energy available to a descending saturated air parcel and can be used as a theoretical predictor of downdraft wind speed. Thus, in environments with reduced wind shear and weak tropospheric flow preventing substantial downward transport of horizontal momentum, high DCAPE can indicate another avenue for the formation of strong, convectively-driven wind speeds at the surface.

Hurlbut and Cohen (2014) utilize observed 0000 UTC and 1200 UTC proximity sounding data for their study. The authors note, especially in the data sparse regions of central New York and central and western Pennsylvania, there can be up to a 250-km gap between the sounding sites and the report distribution. Such broad distances, in addition to a temporal discrepancy of up to 6 hours between report time and sounding launch time, can introduce error in the representation of the near-storm environment. LC11 uses 3-hourly NARR data collocated with the passage of convective elements producing severe weather. While the temporal and spatial errors between severe reports and model-derived soundings are lessened with this approach, reliance on reanalysis data introduces inherent model errors and biases to the results. Additionally, the relatively small number of severe weather events (310) spanning the early-to-mid 2000s limits the usefulness of the results and subjects the findings to interannual variability

described in Hurlbut and Cohen (2014). Our approach, described in chapter 2, seeks to mitigate some of these issues by using a more robust 34-year climatology.

1.2.2 Predictive skill of U.S. severe convection

The SPC started issuing convective outlooks in 1955 (Corfidi 1999) and has added convective outlook categories with increasing lead time and more frequent updates over the years. Evaluations of the SPC's forecasts are challenging since severe thunderstorm reports are needed in order to get verification. Unfortunately, reporting practices have varied substantially through time and space in the United States (Doswell et al. 2005, 2009). Past evaluation studies have focused on watches (Doswell et al. 1993, Vescio and Thompson 2001) but less verification has been done on convective outlooks. Hitchens and Brooks (2012) evaluated early morning SPC convective outlooks from 1973–2010 over the continental United States (CONUS). Day 1 slight risk outlooks, issued at 0600 UTC and valid for the 24-h period beginning at 1200 UTC and ending at 1200 UTC the following day, are verified using valid storm reports.

The performance of the SPC's day 1 slight risk convective outlook areas are evaluated over time using measures from a Roebber performance diagram (Fig. 1.13) including probability of detection (POD), frequency of hits [FOH or 1−false alarm ratio (FAR)], critical success index (CSI), and bias. A complete description of these measures is found in chapter 2. Hitchens and Brooks (2012) found POD increases more than any other measure between 1973 and 1993 but changes very little over the remainder of the period. FOH scores remain relatively flat until 1993 when scores improve marginally over the rest of the period. The increasing POD suggests slight risk outlooks were better located to enclose more severe events over the first two decades of the

period, but the accompanying stable FOH values indicate the POD improvement is also a result of an increase in areal extent of slight risk outlooks (Hitchens and Brooks 2012). Figure 1.14 supports this assertion, showing an increasing cumulative area covered by slight risk outlooks through the mid-1990s with a consistent upward trend in observed storm report area. The increase in FOH values through the remainder of the period is likely due to well-placed risk areas that are smaller in size, reducing false alarms. Lastly, CSI increases modestly from 1973–2010, indicating improvement in slight risk outlook placement and coverage through the period (Fig. 1.13). A logical next step is to compare the regional differences in verification metrics within the CONUS domain and, in chapter 3, we compare the verification skill over the Northeast to the rest of the CONUS.

Hitchens and Brooks (2014) verified a range of SPC day 1 through day 3 products, providing skill scores for the 1300, 1600, and 2100 UTC updates to the day 1 slight risk convective outlooks. Between 1999–2011, continual improvement in the skill of each day 1 convective outlook was observed, although there is often little difference in skill between consecutive outlook updates (Fig. 1.15). Nevertheless, using a persistence-style approach (e.g. calculate the skill of the 0600 UTC day one outlook using the reported events valid for the 1300 UTC day one outlook) to evaluate skill of the updates, it was found that these outlooks improved upon the preceding outlook more than 70% of the time each year (Fig. 1.16).

1.3 Research goals and thesis structure

The work presented herein attempts to build on the results of previous work [e.g. Hurlbut and Cohen (2014), LC11, Hitchens and Brooks (2012)] and identify environments conducive to

low-predictive skill of severe convective weather over the Northeast. To this end, we will evaluate the predictive skill of SPC slight risk outlooks over the Northeast and target poorly predicted events with particularly high impact. Events with low-predictive skill will be categorized and climatological, composite, and case study analyses will be conducted to investigate the ambient synoptic, dynamic, and thermodynamic environments associated with these events.

Chapter 2 describes the methodology for verifying the SPC convective outlooks, as well as the criteria for constructing the climatology. We use a 34-year dataset of Northeast severe weather events to provide more robust climatology results than previous studies using fewer events. We also present a method for identifying high-impact events as well as the techniques and data used for the composites and case studies. Chapter 3 describes the results of the 34-year (1980–2013) evaluation of SPC slight risk outlooks over the Northeast and the climatology of events with low-predictive skill. Synoptic flow patterns and thermodynamic parameters characteristic of low-predictive skill environments are presented and compared with high-predictive skill environments. Chapter 3 also examines the dynamic and thermodynamic differences between high-impact and low-impact severe events over the Northeast. And finally, chapter 3 presents four case studies illustrating the differences in ambient conditions between high-impact severe weather with low-predictive skill within varying CAPE and shear environments. Chapter 4 synthesizes the results in chapter 3 and discusses the implications for convective forecasting over the Northeast, as well as providing suggestions for future work.

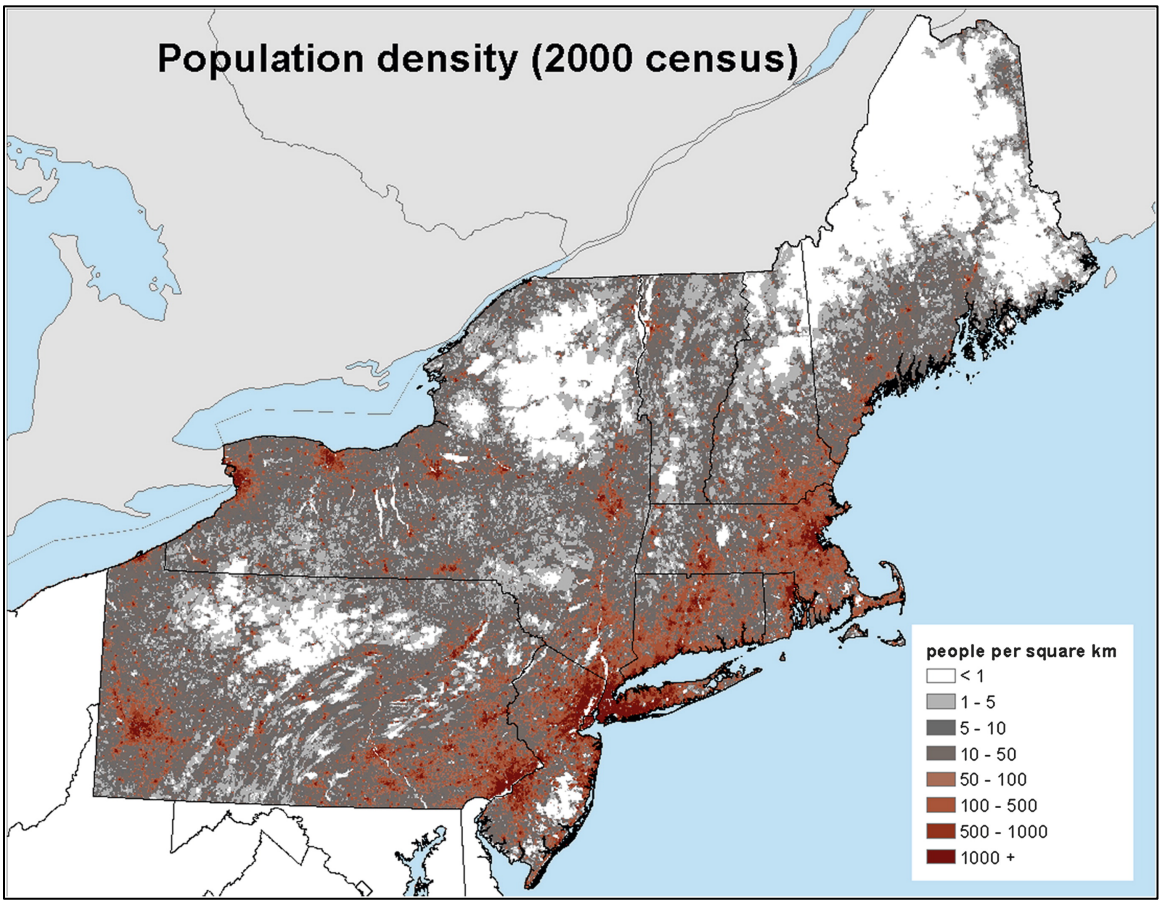

Figure 1.1. Population density map of the northeastern United States from the 2000 census [From Hurlbut and Cohen (2014)].

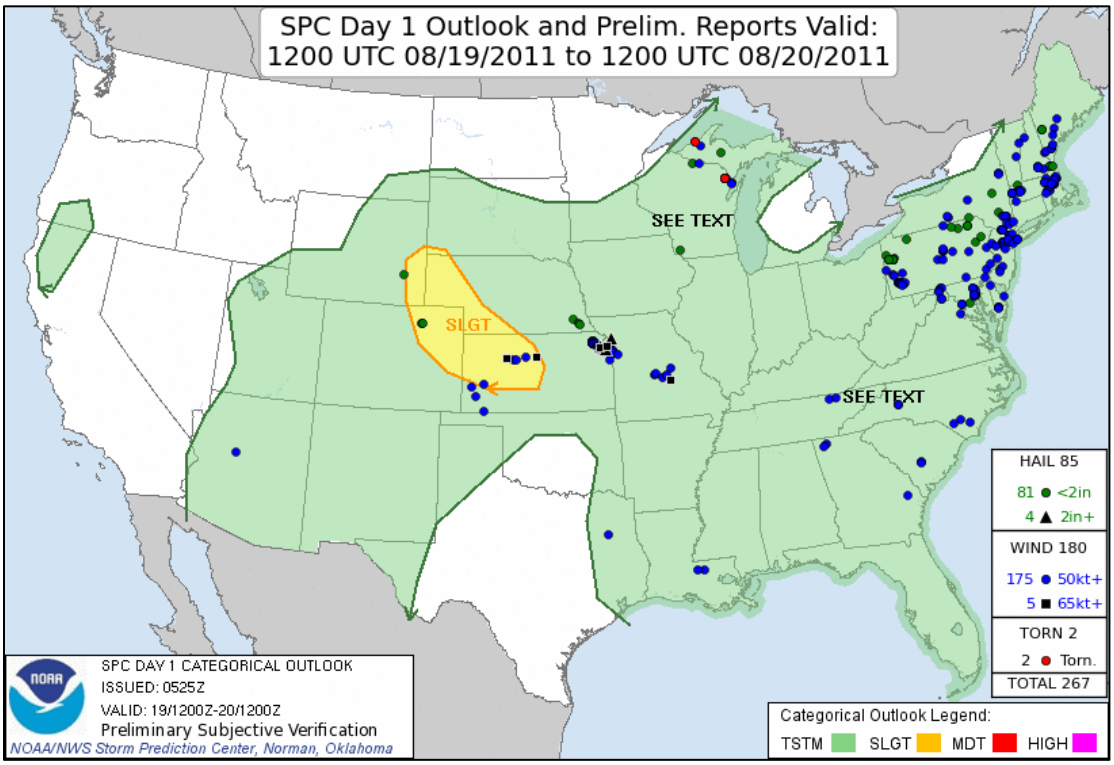

Figure 1.2. Storm Prediction Center day 1 convective outlook issued at 0600 UTC 19 August 2011 with verifying storm reports.

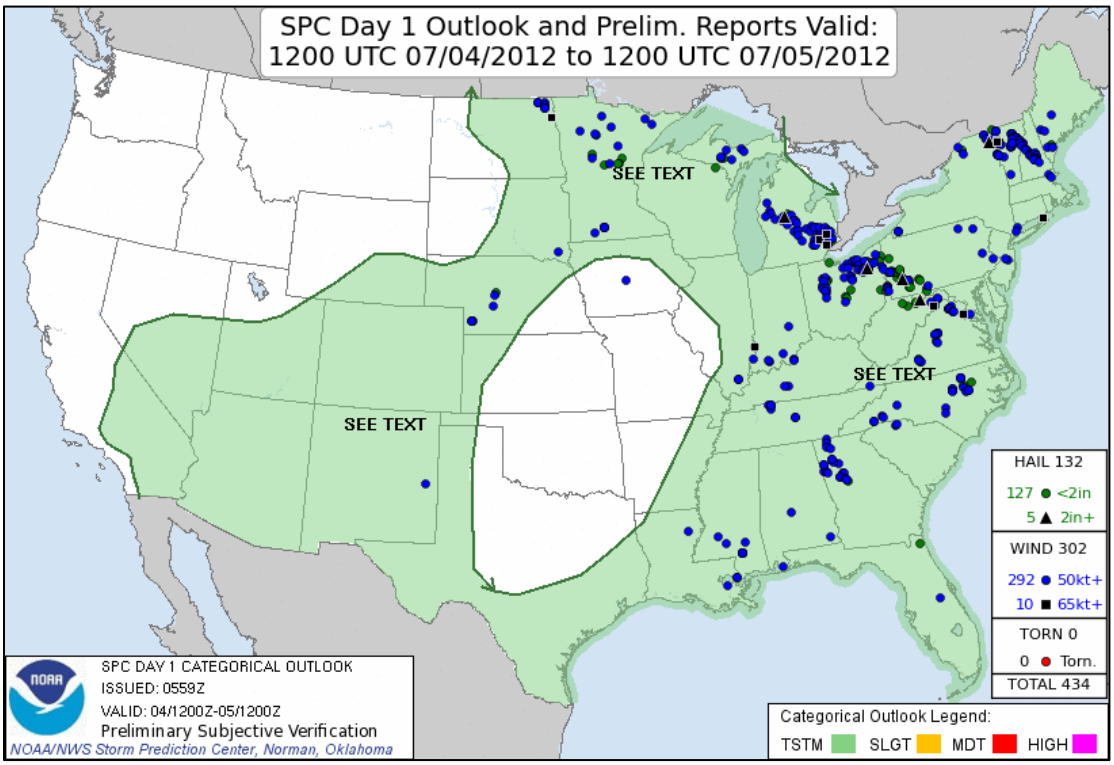

Figure 1.3. Storm Prediction Center day 1 convective outlook issued at 0600 UTC 5 July 2012 with verifying storm reports.

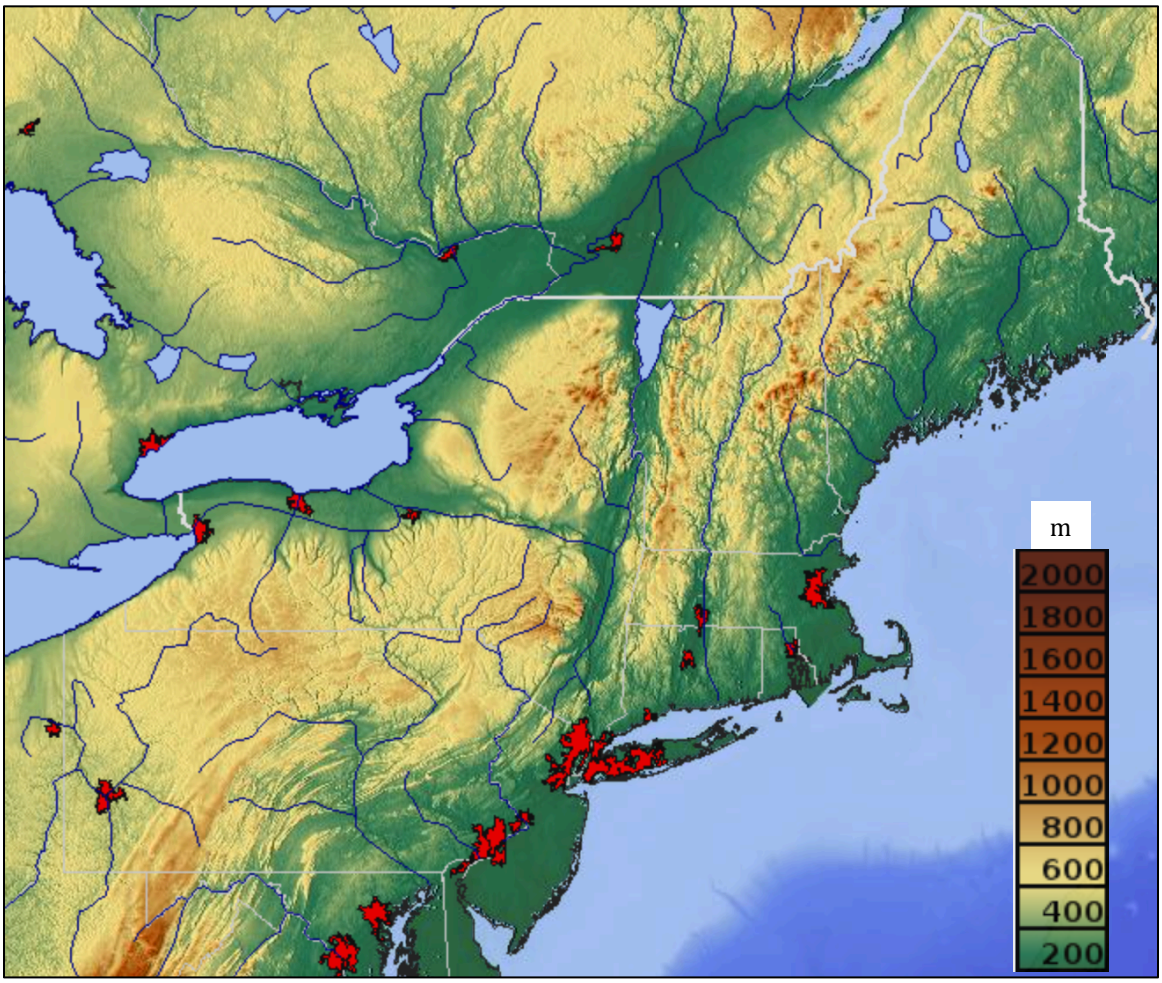

Figure 1.4. Relief map of the northeastern United States (meters). Urban areas are in the red shading (From http://www.maps-for-free.com).

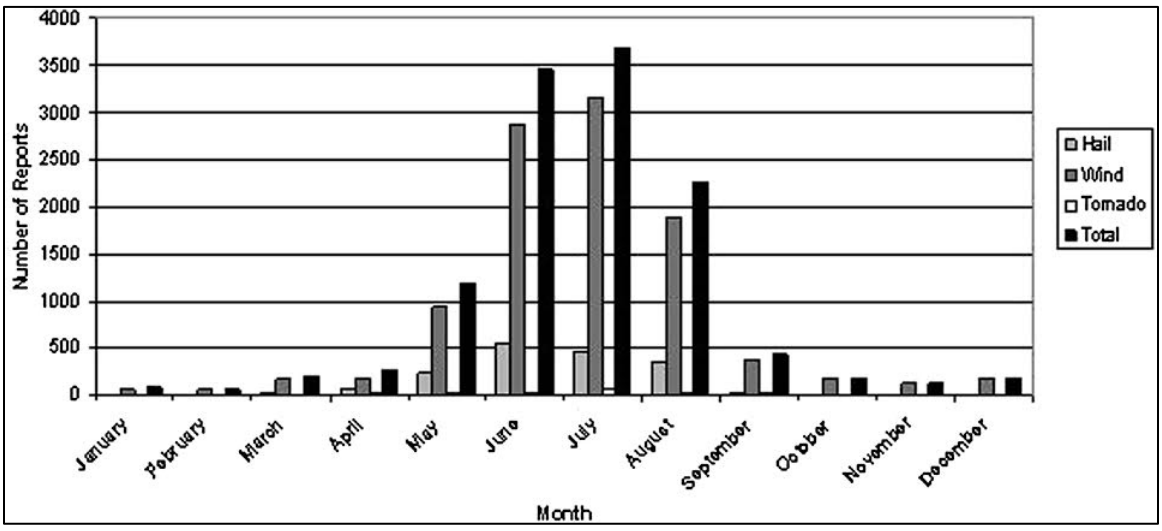

Figure 1.5. Number of severe thunderstorm reports by month and type of report from 1999 to 2009 in the Northeast [From Hurlbut and Cohen (2014)].

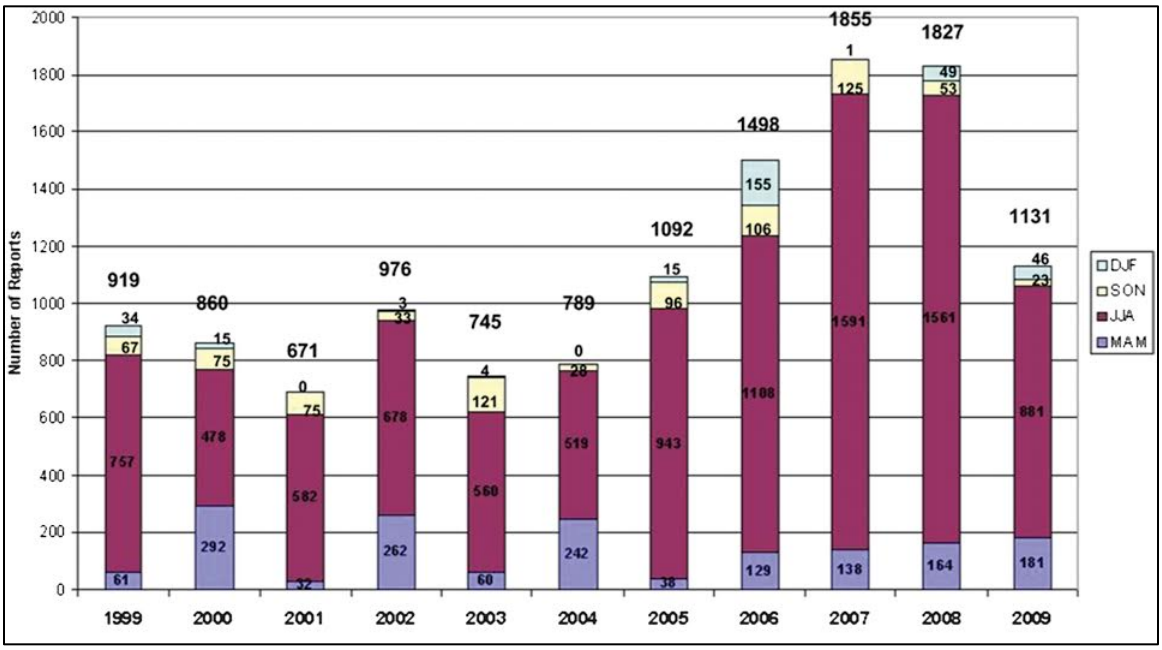

Figure 1.6. Number of severe thunderstorm reports by season from 1999 to 2009 in the Northeast [From Hurlbut and Cohen (2014)].

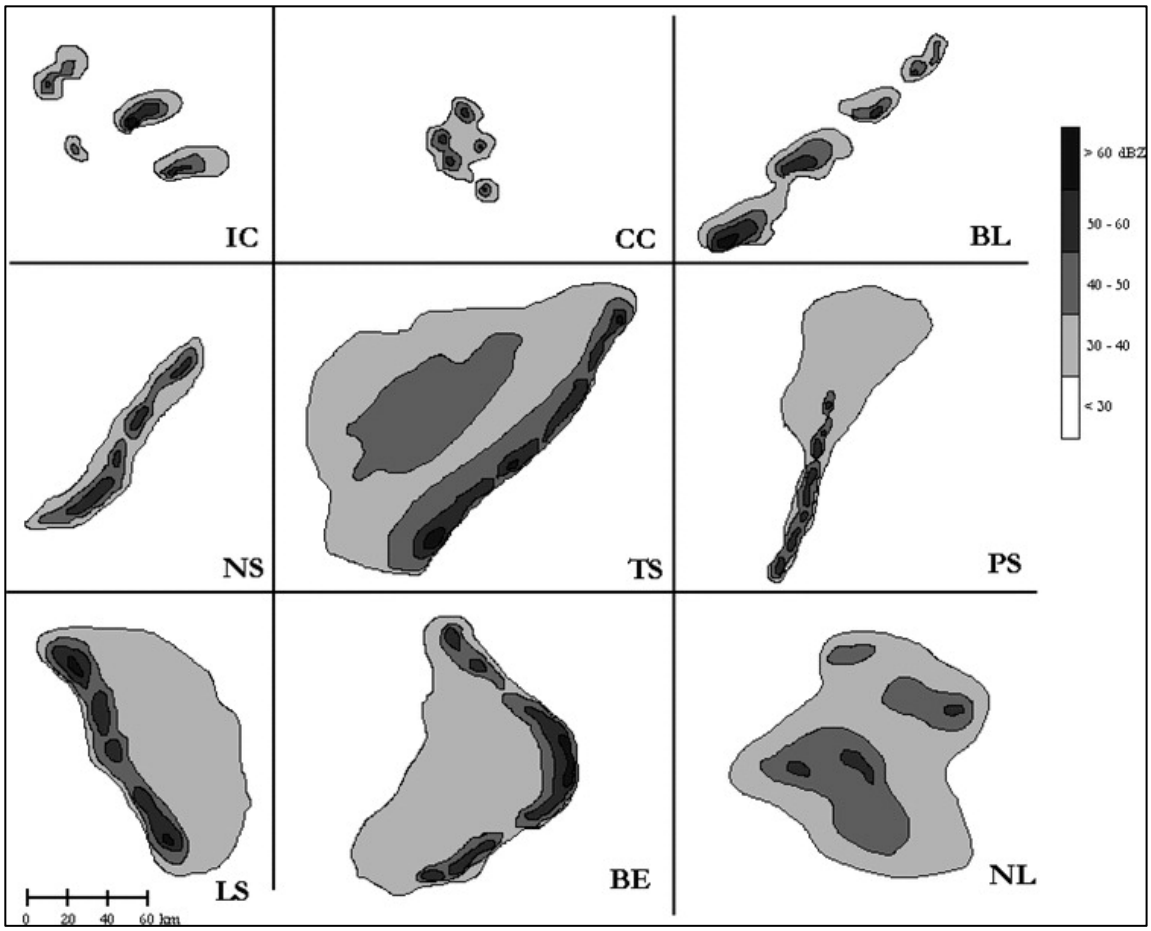

Figure 1.7. Schematic demonstrating each of the nine storm morphologies used in the LC11 classification system. Morphologies are abbreviated as follows: IC, isolated cells; CC, clusters of cells; BL, broken line; NS, squall line with no stratiform rain; TS, squall line with trailing stratiform rain; PS, squall lone with parallel stratiform rain; LS, squall line with leading stratiform rain; BE, bow echo; and NL, nonlinear system. [From Gallus et al. (2008)].

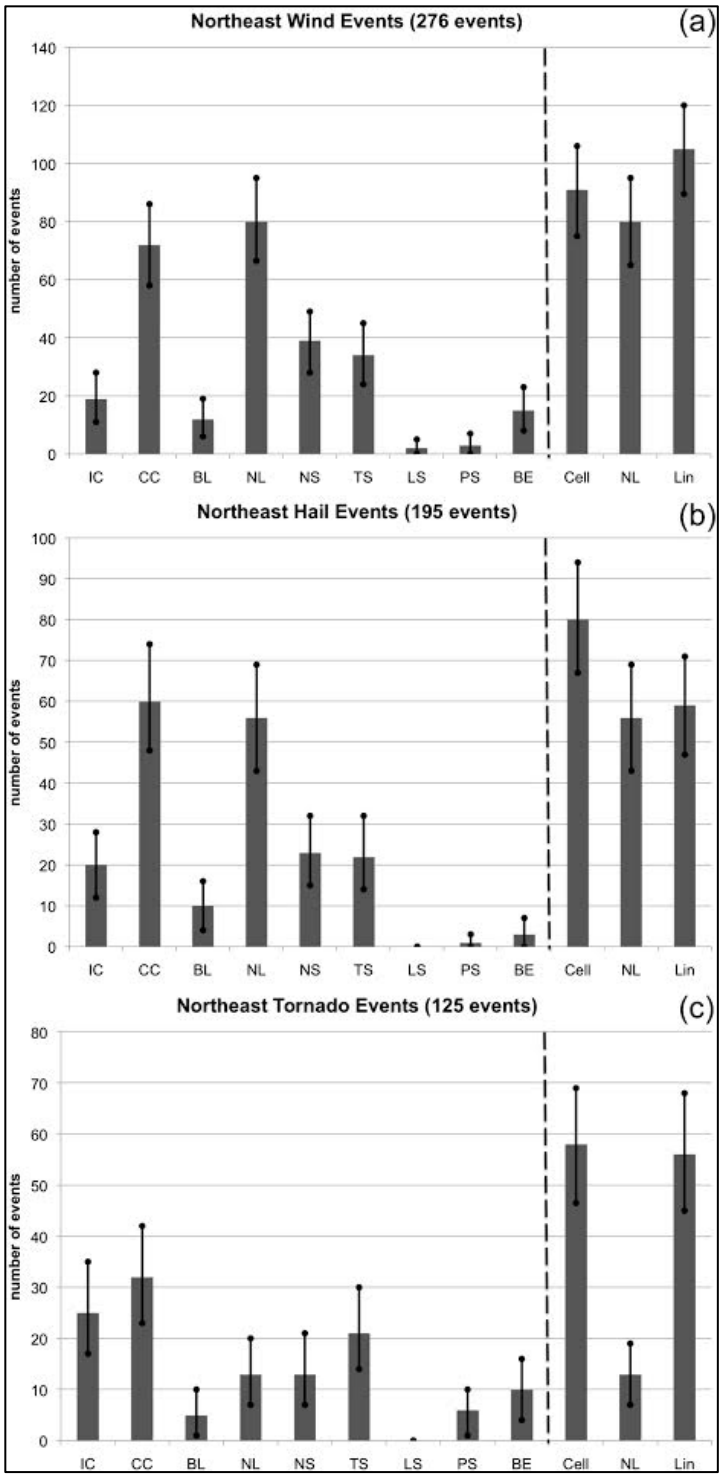

Figure 1.8. Number of northeastern U.S. severe (a) wind and (b) hail events from 2007 and a random aggregate of the 2002–2006 warm seasons (May–August), and (c) tornado events from the 1996–2007 warm seasons for each of the nine convective types individually and grouped into three main organizational types (cellular, nonlinear, linear). Error bars (solid black) mark the range of the 95% significance level [From Lombardo and Colle (2011)].

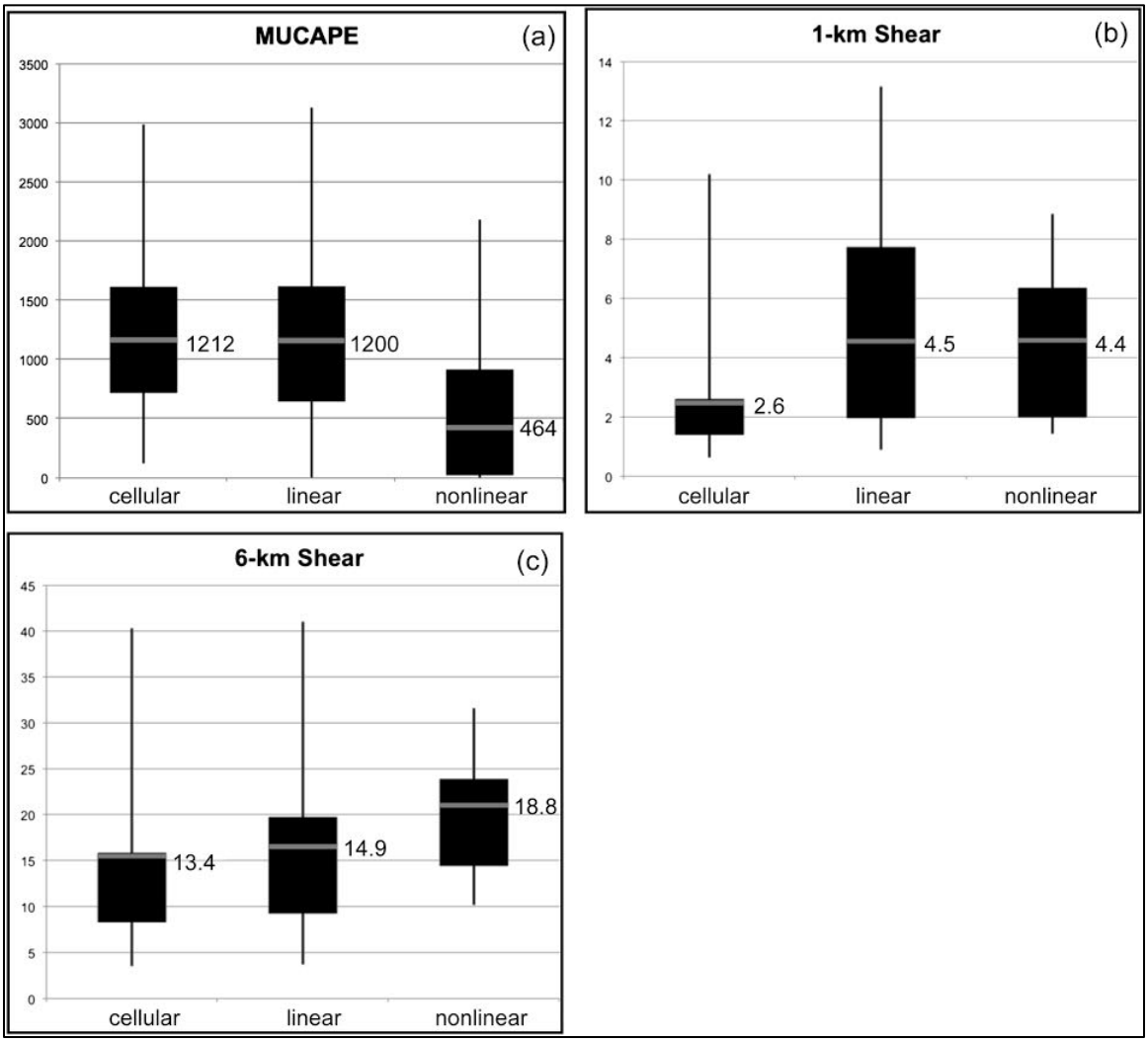

Figure 1.9. Box-and-whisker plots averaged over four points within the coastal region showing (a) MUCAPE (J kg^{-1}), (b) 0–1-km shear (m s^{-1}), and (c) 0–6-km shear (m s^{-1}) for the 49 cellular, 45 linear, and 15 nonlinear severe coastal events. The bottom and top of the solid black box mark the 25th and 75th quartiles, respectively. The gray bar denotes the mean and the value has been included. The maximum and minimum outliers are the top and bottom of the solid vertical black lines [From Lombardo and Colle (2011)]. Note the large MLCAPE distribution differences between cellular/linear convection and nonlinear convection. Additionally, 1-km shear for cellular convection is significantly (95% level) less than other convective structures. Lastly, 6-km mean shear values are comparable between cellular, linear, and nonlinear convective structures.

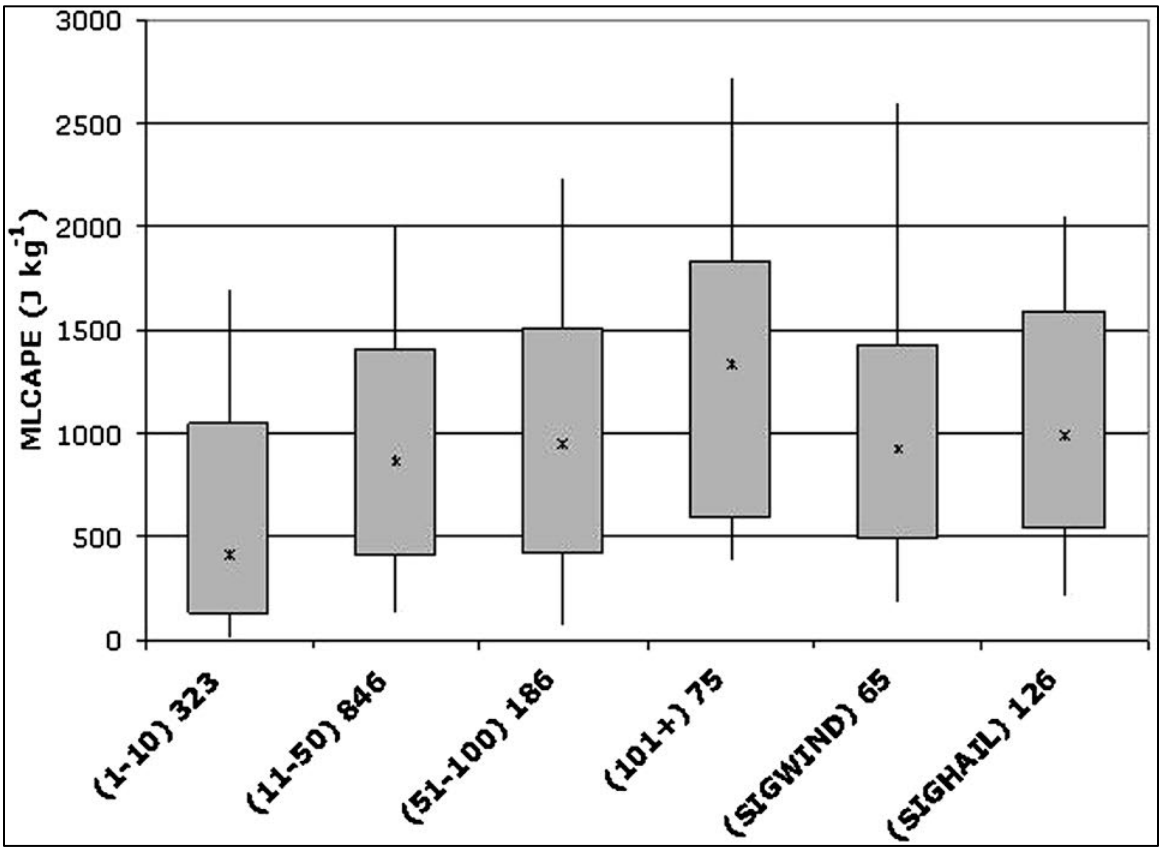

Figure 1.10. Box-and-whisker plots for summer MLCAPE. The ends of the solid boxes represent the 25th and 75th percentiles of the distribution with the ends of the whiskers representing the 10th and 90th percentiles of the distribution and the asterisks depicting distribution medians. Sample sizes (corresponding to the number of sounding observations considered) are listed beside event categories along the abscissa. Northeast states used in the study are highlighted in Fig. 1 [From Hurlbut and Cohen (2014)].

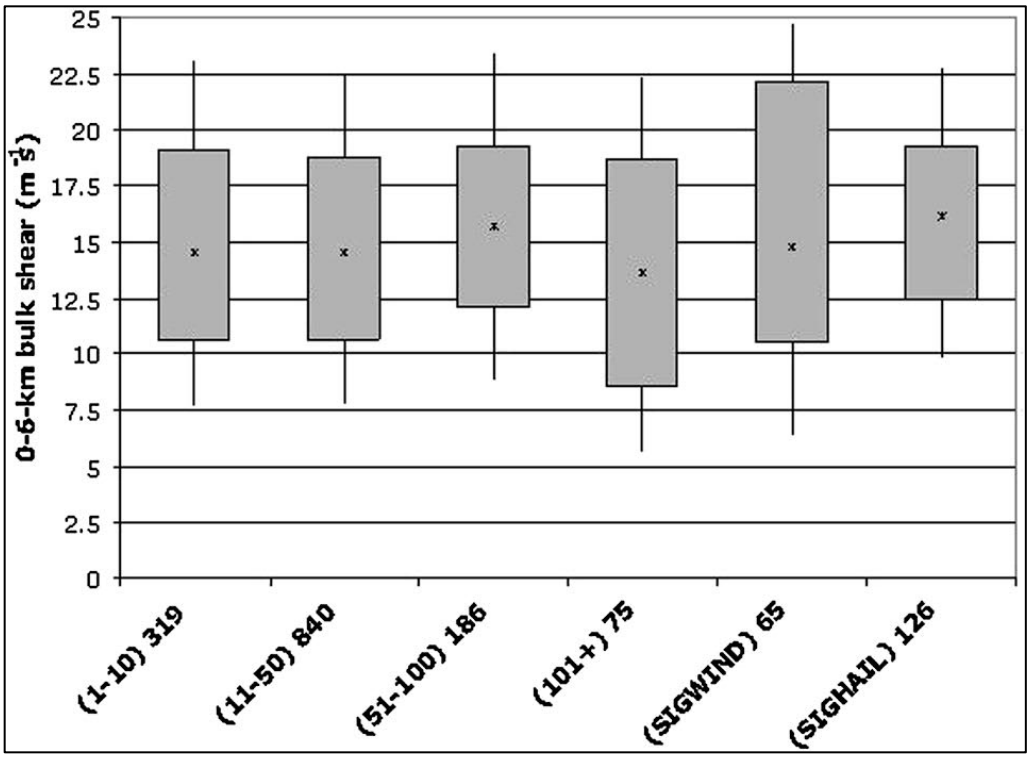

Figure 1.11. Same as Fig. 1.9, but for 0–6-km vertical wind shear [From Hurlbut and Cohen (2014)].

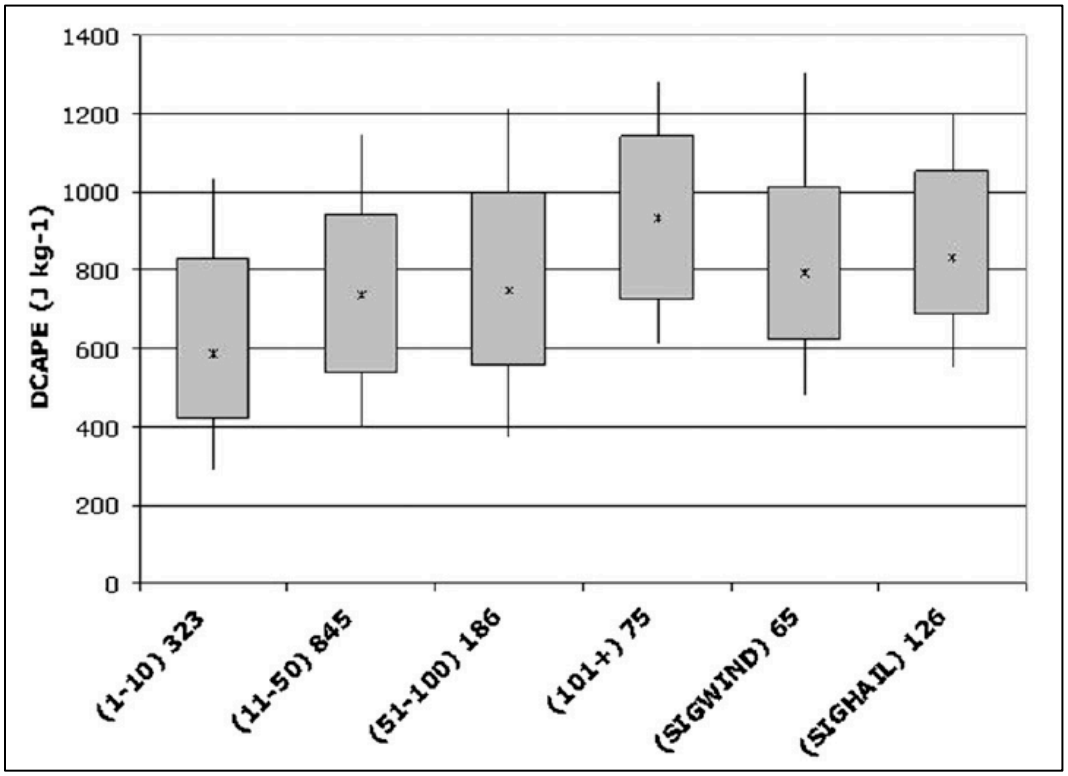

Figure 1.12. Same as Fig. 1.9, but for DCAPE [From Hurlbut and Cohen (2014)].

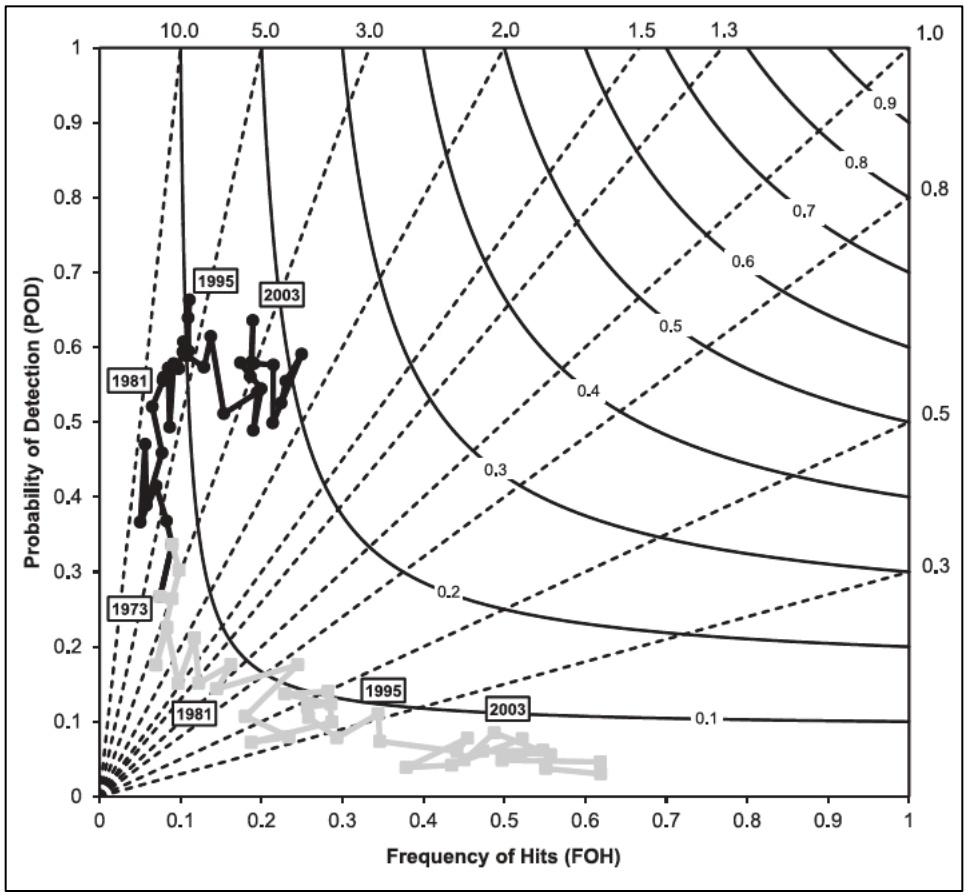

Figure 1.13. Performance diagram [see Roebber (2009) for details] of annual convective outlook performance for slight risk areas (black circles and line) and moderate risk areas (gray squares and line) from 1973 to 2010 Labeled years are provided for context [From Hitchens and Brooks (2012)].

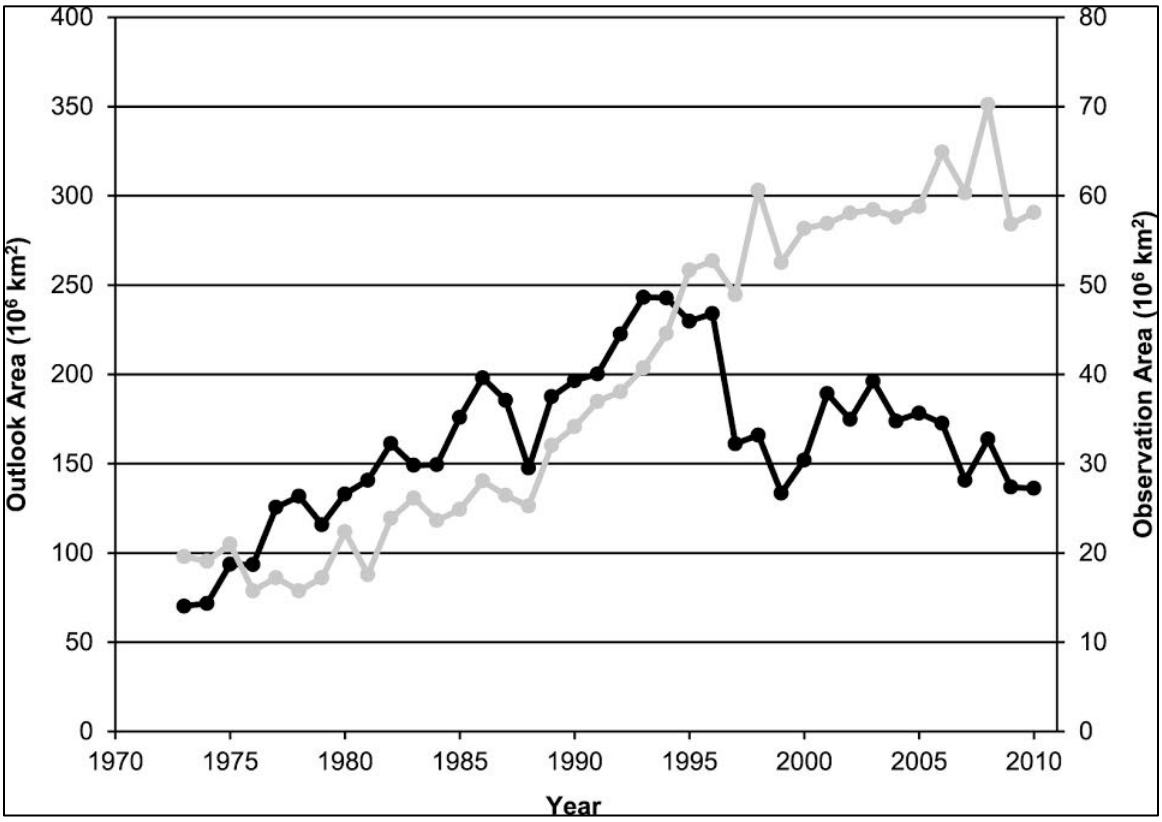

Figure 1.14. Annual sums of convective outlook area (black line, left axis) and observed storm report area (gray line, right axis) [From Hitchens and Brooks (2012)].

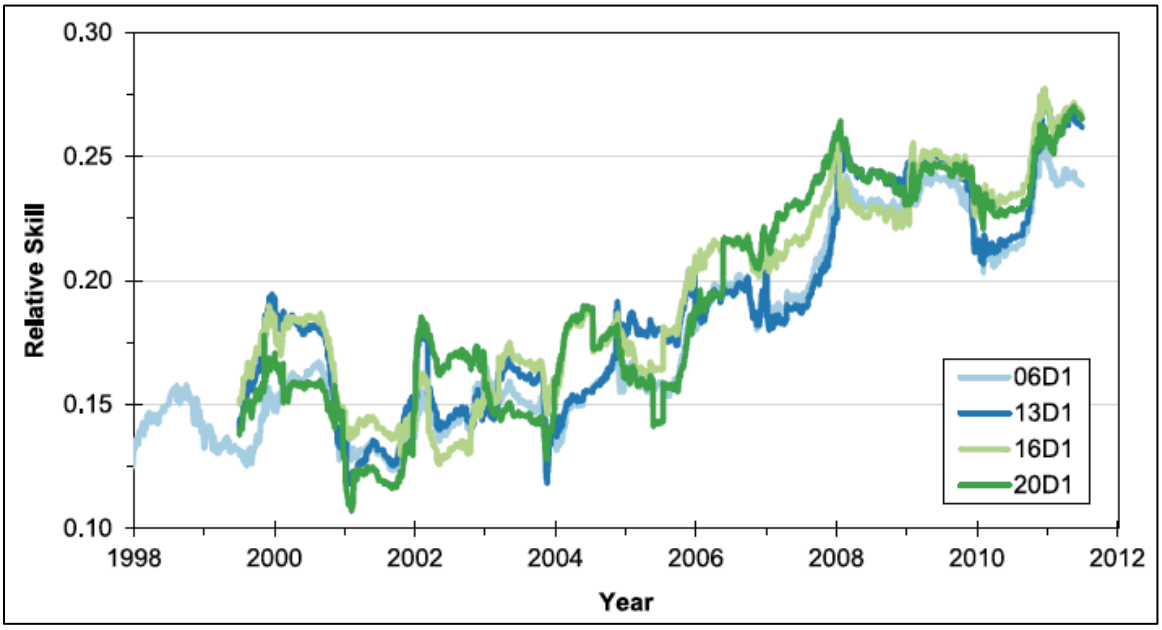

Figure 1.15. Relative skill of the Storm Prediction Center's initial day 1 outlook (0600 UTC) and updates to this forecast calculated as the relative position of each outlook's critical success index value [From Hitchens and Brooks (2014)].

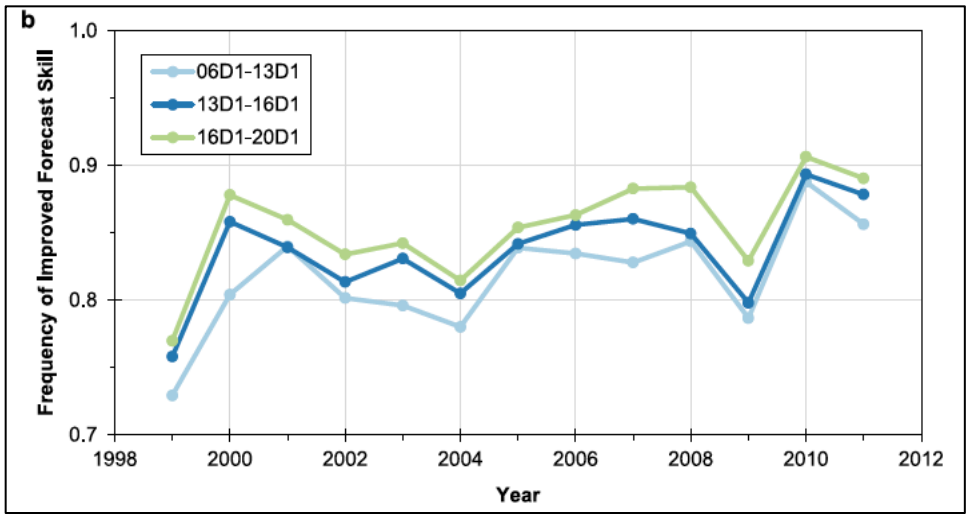

Figure 1.16. Frequency of improvement in daily forecast skill between consecutive forecasts based on the relative skill of the earlier outlook calculated with the reported events from the time period associated with the later outlook [From Hitchens and Brooks (2014)].

2. Data and methodology

2.1 Verification technique

This study attempts to distinguish between Northeast severe convective events with high-predictive skill and those with low-predictive skill. Motivated by the results of Hitchens and Brooks (2012), we use the SPC convective outlooks to gauge severe weather forecast skill. There are four risk categories that can be issued in a convective outlook: see text, slight, moderate, and high. As of 22 October 2014, SPC added an "enhanced slight" risk category between slight and moderate and renamed the see text category to "marginal". The 1980–2013 study period precludes the newer convective outlook classification scheme and limits the present study to the previous four categories. Additionally, we use only the slight-risk outlook areas for verification due to their higher rate of occurrence than moderate-risk areas, especially in the Northeast, and the higher probability of severe, impactful weather implied by the slight-risk category than the lower, see text category.

Notably, when assigning heightened risk areas, the current convention is to enclose them within the lower risk areas; for instance, a high-risk area is contained within both a moderate-risk and a slight-risk area. This was not always the case, as through at least the mid-1980s, a moderate risk might be issued without a surrounding slight risk. Similarly, a high-risk area might be contained within a slight-risk area without a moderate-risk area. For this study, we examine only slight-risk outlooks and days with only moderate-risk areas without an attendant slight risk are not included. In addition, the area within a slight-risk outlook, even if it contains a higher risk area, is treated the same as the rest of the slight-risk area.

Hitchens and Brooks (2012) took a holistic approach and verified both slight-risk and moderate-risk convective outlooks over the entire CONUS domain. Their nationwide approach presents the opportunity to compare the CONUS domain predictive skill to the smaller, Northeast regional domain illustrated in Figure 2.1. Regional verification of convective outlooks enhances the usability of the results to local forecasters by ensuring predictability scores and, importantly, the events on the extreme ends of the convective storm predictability spectrum, are representative of the region. Additionally, full CONUS verification averages regional variations in population and terrain, which may impact the size and magnitude of severe report distributions. The comparison of the CONUS and Northeast predictive skill scores will suggest whether predictive skill has any regional dependence or is fairly uniform across the CONUS.

To accomplish the comparison of predictive skill, a verification scheme similar to Hitchens and Brooks (2012, 2014) is used. A 40-km grid is placed over the CONUS region to calculate skill metrics as SPC probabilities for convective outlooks are calibrated for severe weather within 40 km of a point. For a given day, the day 1 slight-risk convective outlooks, issued at 0600 UTC, are plotted on the 40-km grid outlining areas of the CONUS under a higher threat for severe weather (Fig. 2.2). These outlooks are valid for a 24-hour period beginning at 1200 UTC and ending at 1200 UTC the following day. The 0600 UTC day 1 convective outlook has been consistently issued since 1973, making the product suitable for developing a climatology of low-predictive skill events.

Individual storm reports that meet the National Weather Service's criteria for severe weather are used to verify the day 1 convective outlooks (storm report data available from the SPC at http://www.spc.noaa.gov/wcm/#data). Severe weather is defined as a wind gust equal to or in excess of 25.7 m s^{-1}, hail equal to or in excess of 19.1 mm, or a tornado. As of 5 January

2010, the severe hail criterion changed to 25.4 mm and from that date on, the present study uses the 25.4 mm threshold. Reports are grouped into 24-hour blocks beginning at 1200 UTC each day and plotted on a 40-km grid with the same specifications as those used with the convective outlooks. Lastly, a radius of influence of 40 km, centered on each storm report, is applied to match the intended scale of the convective outlooks issued by the SPC.

The 40-km grid is evaluated with the convective outlooks and valid storm reports for each day from 1980–2013. The storm reports and grid points are considered dichotomous such that a grid point surrounded by multiple storm repots in a 24-hour period do not have more influence than a grid point with a single report in the vicinity. Therefore, the grid can be evaluated using a 2 × 2 contingency table (Table 2.1). Grid points enclosed by slight-risk convective outlooks are assigned a "forecast yes" value while grid points within the area of influence of a storm report are assigned an "observed yes" value. Correct hit, false alarm, miss, or null is assigned to each grid point depending on the verification performance for a particular day (Fig. 2.3).

This process is repeated for the Northeast domain illustrated in Fig. 2.1. A variety of verification metrics are calculated using the contingency table, but those used herein are probability of detection (POD), false alarm ratio (FAR), and critical success index (CSI) or threat score (TS):

$$POD = \frac{A}{A + C} \qquad (1)$$

$$FAR = \frac{B}{A + B} \qquad (2)$$

$$CSI = TS = \frac{A}{A + B + C} \qquad (3)$$

where A is the number of correctly forecasted grid points with severe weather, B is the number of incorrectly forecasted grid points without severe weather, and C is the number of grid points with unpredicted severe weather. We compare the predictive skill of severe convection over the CONUS and the Northeast using these metrics.

The 34-year predictive skill study using convective outlooks consists of all days with a slight risk convective outlook covering a portion of the respective CONUS and Northeast domains. The study is performed with the expectation that slight-risk outlooks are not designed to encapsulate all severe reports during a given period; thus, near-perfect skill scores are unrealistic. Rather, the slight-risk outlooks seek to highlight areas with a greater probability of severe weather occurrence. No attempt is made to include events that did not contain a slight-risk convective outlook when comparing the predictive skill of the Northeast and the CONUS.

The practice of neglecting events without slight-risk areas ignores potentially high-impact severe weather with no slight-risk outlook and many severe weather events that have a POD of zero. It is important to include these poorly predicted events when assessing skill but caution must be taken to determine which events should be considered. As an example, an event with no slight-risk outlook that produces 2 reports over the entire Northeast has too low of an impact to be considered a "bad" forecast and counted against the forecaster. Importantly, the severities of reports are not considered in this study (e.g. 2 reports of an EF-3 tornado would be treated the same as 2 reports of 1-in hail). Contrast the previous event with a scenario of prolific wind damage from a long-lived bowing line segment producing over 150 reports that was not captured in a slight-risk outlook. The latter case should be considered in a study assessing predictive skill, but how should more ambiguous, borderline events be handled? We present a method of

determining whether an event is of sufficiently high impact to warrant inclusion in the study later in this chapter.

2.2 High impact, slight-risk database

In addition to the predictive skill comparison between the CONUS and the Northeast, we compile a database consisting of slight-risk events and high-impact severe weather events in the Northeast. However, as previously mentioned, slight-risk areas are not intended to capture all severe reports within a given domain. Sampling days with few severe reports and, justifiably, no slight-risk area, will skew POD and CSI scores down, as these days would be assigned a zero for POD and CSI. Therefore, additional criteria must be applied to prevent oversampling of low-impact events and ensure only severe events of sufficiently high impact are included.

On first glance, a lower-limit threshold for number of severe reports over the Northeast for a given day is necessary for building a database of high-impact events. However, several issues arise when using an absolute number of reports to define a high-impact event. The number of severe reports each year has increased since the 1980s as population swelled and the advent of the digital communication age made reporting much easier. Additionally, a severe storm in a rural area may elicit a handful of reports whereas severe weather over a densely populated area garners many more reports due to the large number of observers (Doswell et al. 2005).

To accommodate the aforementioned issues, the number of grid points that observed severe weather is calculated for each severe weather event. Using a spatial metric to measure severe storm impact lessens the effect of report clustering around populated areas. Slight-risk outlooks suggest a higher risk of severe weather than lower risk outlook categories. Therefore,

we infer higher societal impacts are associated with slight risk days than days with lower risk outlooks. The distribution of the number of grid points observing severe weather on days with a slight-risk outlook within the Northeast domain provides the range of spatial area affected by severe weather during these higher-impact slight-risk events. Moreover, the middle portion of this distribution describes how much area is "typically" affected by severe weather when a slight-risk outlook is present. Thus, the distribution can provide helpful guidance to create a criterion for a high-impact event.

Figure 2.4 illustrates the median number of grid points within 40 km of at least one severe weather report in the Northeast on days with a slight-risk outlook in the same domain for every year in the dataset. An upward trend in area observing severe weather is notable. We hypothesize the upward trend is a result of an increase in population and the advent of ubiquitous electronic communication fostering improved reporting frequency rather than an increase in severe storm coverage over the study period. It is clear the upward trend in reporting frequency would render a static areal threshold for high-impact weather ineffective. An event with 40 grid points observing severe weather would span more than double the area of a median event in 1980 whereas an event with the same 40 grid points of coverage represents an event affecting about a third less area of a median event in 2006. Therefore, a dynamic lower limit of severe weather areal coverage through the period is needed.

Linear regression through the distribution of severe impact area provides a smooth threshold for defining a high-impact event. The 55th percentile of the number of grid points observing severe weather during slight-risk events is chosen for the linear regression. Choosing a percentile above the median for the lower spatial threshold lends further confidence that events with greater areal coverage than the linear regression line were, indeed, high impact. Secondly,

due to the relative scarcity of slight risk events in the Northeast compared to other areas of the CONUS, no lower limit of areal coverage is placed on slight-risk outlooks for inclusion in the database. The size of slight risk areas is moderately correlated to severe spatial coverage with a correlation coefficient of 0.65 over the 1980–2013 dataset; thus, choosing the 55th percentile—denoted by the red line in Figure 2.4—to center the regression will mitigate the lower severe report coverage attendant with small slight-risk areas and ensure high-impact events have a relatively large area of severe report coverage.

2.3 Composite analysis and case studies

For each case in the high-impact, slight-risk Northeast dataset, various atmospheric fields and parameters are calculated using the 0.5° Climate Forecast System Reanalysis (CFSR; Saha and Coauthors 2010). Analysis times are set at 1800 UTC for each event. Recall the peak time for the first severe report for Northeast severe events is 1900 UTC (Hurlbut and Cohen 2012). The 1800 UTC analysis attempts to capture the pre-convective environment in the majority of cases. The analyses are centered on either the point of maximum report density for high-impact events or the centroid of the slight risk area for events not classified as high-impact according to the linear regression technique discussed previously. The results are composited and grouped based on predictive performance.

There are three common types of low-predictive skill events. The first class of event, defined here as type 1, is an event with a low POD score commonly called a "missed" event (e.g. Figs. 1.2 and 1.3). To qualify as a type 1 event, a case must both be classified as high-impact and have a POD score in the lowest 25th percentile of all high-impact events. The second type,

defined as type 2, is an event with high FAR referred to as a "forecast bust" (e.g. Fig. 2.5). To qualify, a type 2 event must have both a false alarm area in the highest 25th percentile and a severe report coverage area in the lowest 25th percentile. Simply put, type 2 events have relatively large slight-risk outlooks and a small area covered by severe reports in the domain. Low POD and high FAR scores characterize type 3 events. However, due to the subjective nature of classifying the skill of these forecasts (e.g. severe conditions persist longer than expected and occur further downstream of the slight-risk outlook), no attempt was made to classify these events separately. A fourth category, designated good events, is created to facilitate comparisons between well-forecasted events and poorly forecasted events. Good events are any high-impact events that score a TS in the highest 25th percentile of all high-impact events. Events falling within these categories are binned and composited using the methods stated earlier. The top 10 events in each category are listed in Table 2.2.

The CFSR and other reanalysis data such as the North American Regional Reanalysis (Mesinger and Coauthors 2006) are subject to several model limitations including temporal and spatial resolution, microphysical and convective parameterization, and data assimilation. Gensini et al. (2014) quantified some of the error associated with the NARR data and observed soundings in convective environments. They found a substantial lack of correlation between the model atmosphere and the observed soundings using coefficients of determination for some atmospheric fields and indices (Tables 2.3 and 2.4). Dynamic variables away from the boundary layer, such as 200-hPa wind speed, are represented fairly well in the model whereas thermodynamic variables within the boundary layer, such as 850-hPa dew point, are poorly resolved. Gensini et al. (2014) solely considered the NARR in their study, however the CFSR

has similar model limitations—though, it has 64 vertical levels compared to 45 levels in the NARR—thus we consider the results to be applicable to the CFSR data as well.

Four case studies, 3 representing poorly predicted, high-impact events under various CAPE and shear conditions and 1 representing a type 2 “forecast bust”, are subjectively chosen to illustrate environments conducive to poor predictability. Surface, upper-air, satellite, and radar data are used to investigate mesoscale details of the events. Rapid Update Cycle (RUC) and Rapid Refresh (RAP) model data, when available, are used to inspect the synoptic conditions prior to the events and assess convective parameters such as CAPE and shear during the events. Storm report data for all case studies were obtained from the SPC (http://www.spc.noaa.gov/climo/).

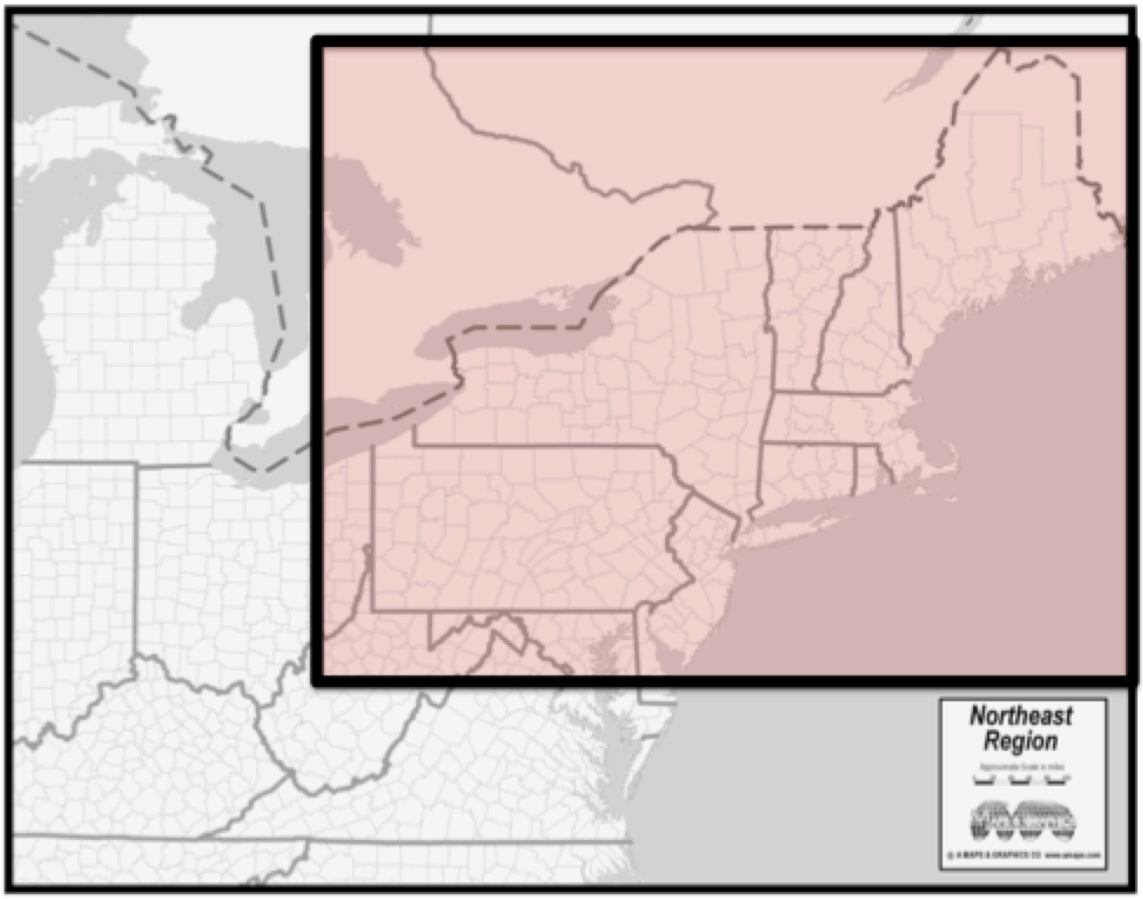

Figure 2.1. Political map of the northeastern United States. The red shaded area denotes the domain used in the present study (From http://www.amaps.com).

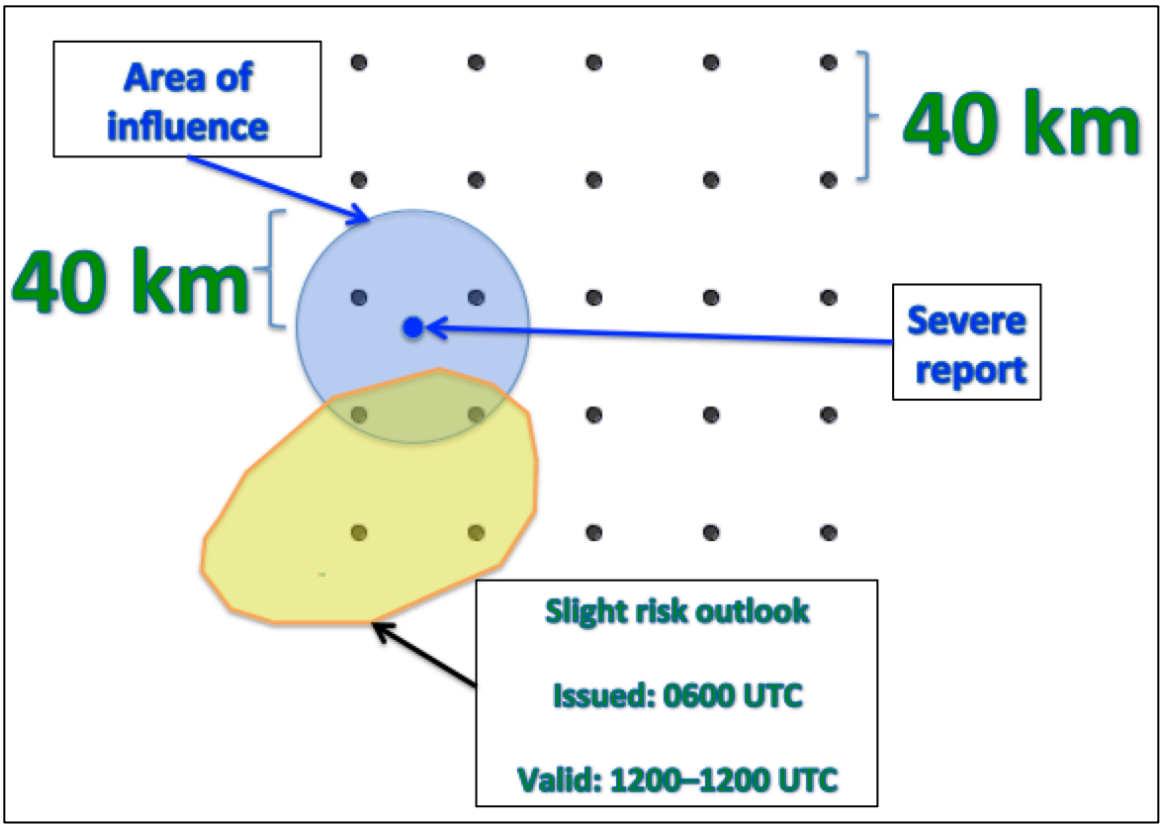

Figure 2.2. Schematic of the verification technique used here. Grid points are 40 km apart and all severe reports have a 40-km radius of influence. Slight-risk outlooks issued at 0600 UTC and valid from 1200–1200 UTC are used.

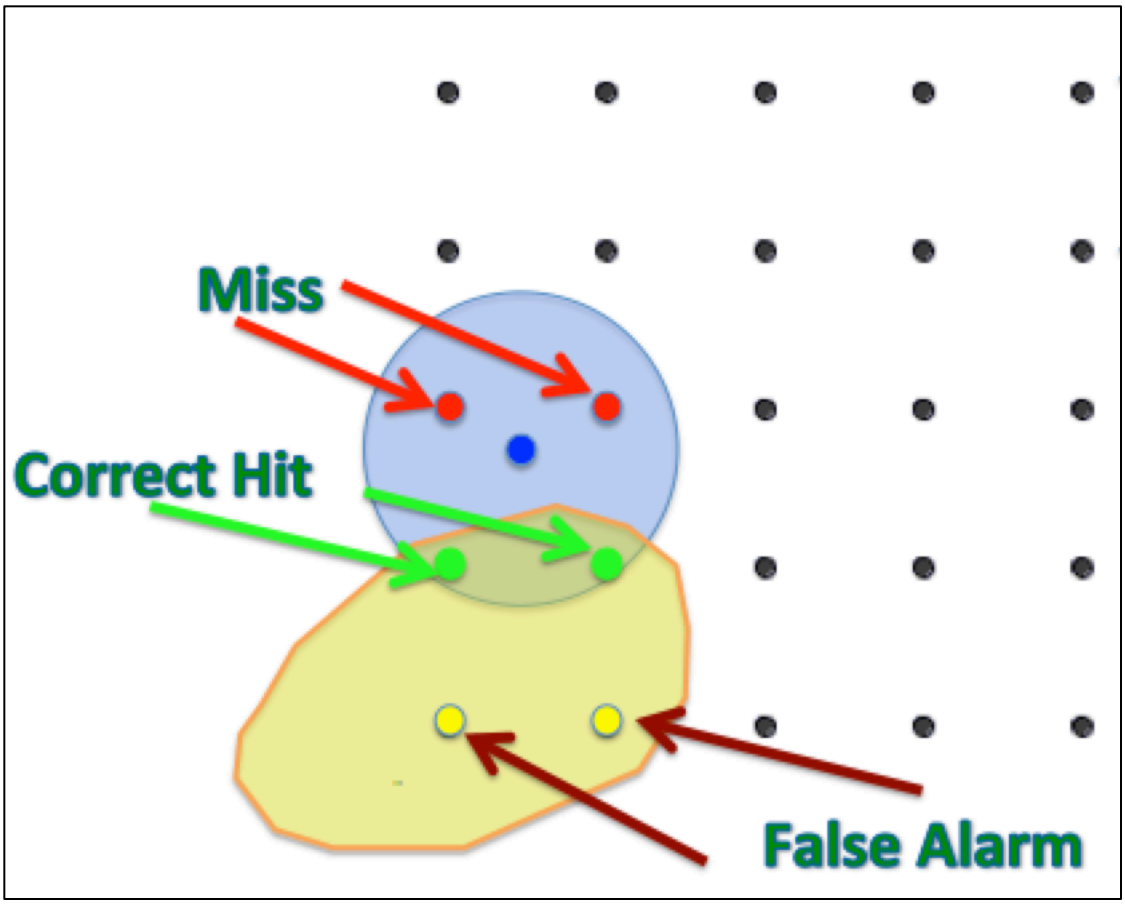

Figure 2.3. Schematic of the verification technique used here. Grid points impacted by the severe report and are outside (inside) the slight risk are designated as “misses” (“correct hits”). Grid points within the slight risk and not impacted by the severe report are designated “false alarm”.

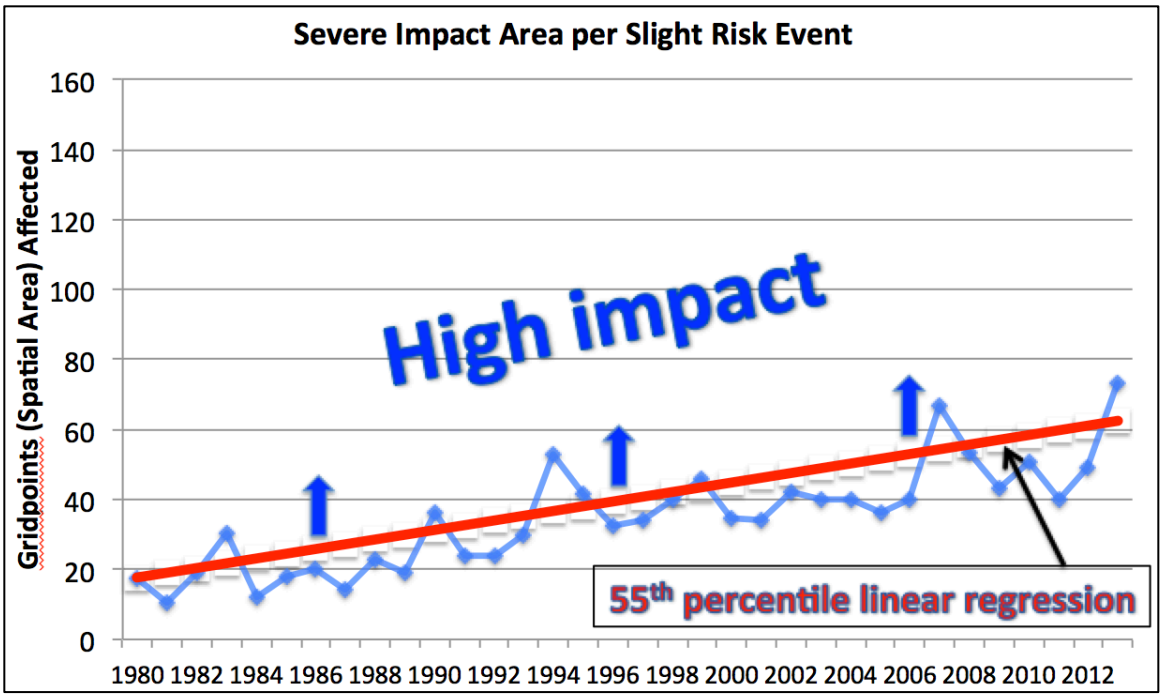

Figure 2.4. Graph depicting the median severe impact area per slight-risk event for each year of the study period in the Northeast. The red line denotes the 55th percentile linear regression through the study period. All events with more grid points observing severe weather than the red linear regression line for a given year are classified as high impact.

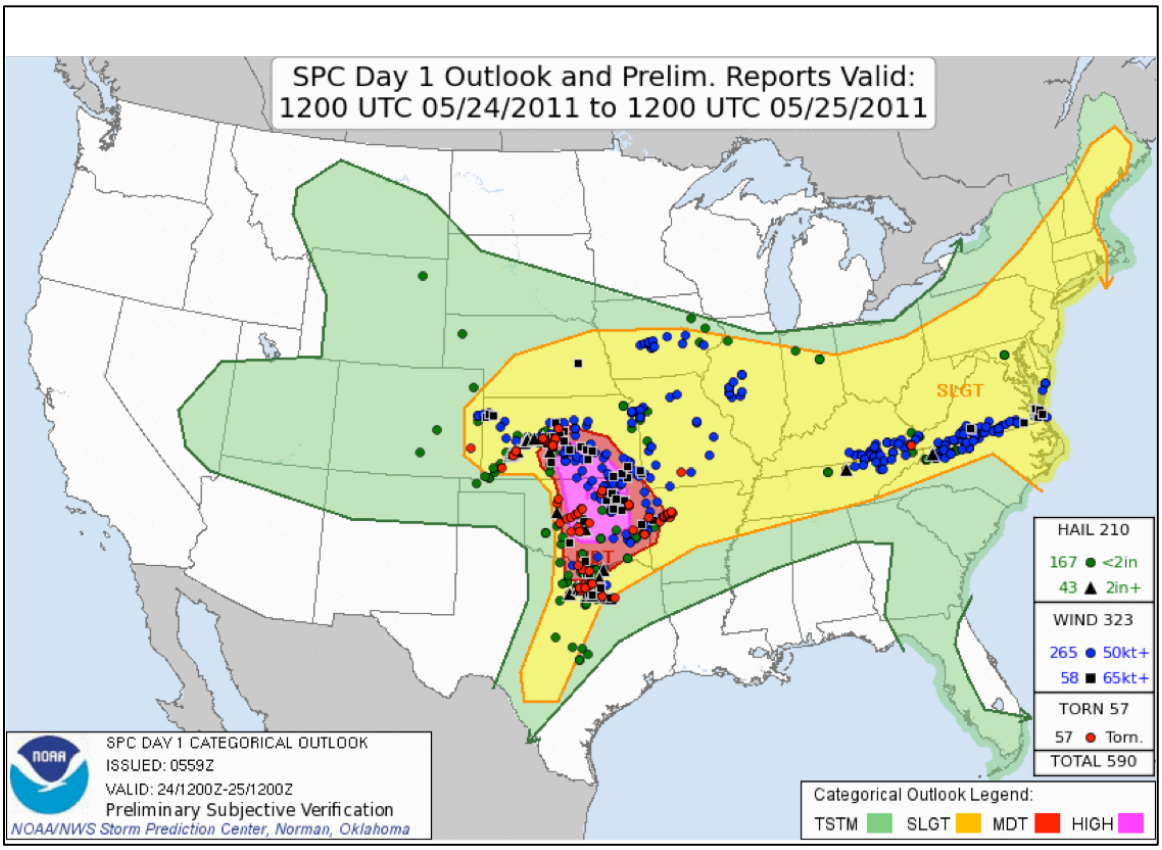

Figure 2.5. Storm Prediction Center day 1 convective outlook issued at 0600 UTC 24 May 2011 with verifying storm reports.

Contingency Table	Observed Y	Observed N
Forecast (Y)	Hit (A)	False Alarm (B)
Forecast (N)	Miss (C)	Correct null (D)

Table 2.1. 2 × 2 contingency table for observed events and forecasted events.

Type 1	Type 2	Good
19 August 2011	22 June 2004	29 May 1998
21 July 1983	29 July 1995	19 June 2007
10 May 2000	24 May 2011	8 June 2007
18 July 1997	4 September 1985	6 June 2005
15 July 1995	30 June 1996	28 April 2002
27 June 2002	4 October 1990	13 June 2007
24 June 2013	16 August 1993	29 May 2012
6 July 2007	13 May 1988	8 September 2012
4 July 2012	24 May 1988	26 May 2011
29 June 2012	5 October 1991	26 July 2005

Table 2.2. Top 10 type 1, type 2 and good events descending from top to bottom. Type 1 events are ranked using severe report area. Type 2 events are ranked using false alarm area. Good events are ranked using threat score.

Abbreviation	Parameter
SBCAPE	Surface-based convective available potential energy
MLCAPE	100-hPa mixed-layer convective available potential energy
SBCIN	Surface-based convective inhibition
MLCIN	100-hPa mixed-layer convective inhibition
SBLI	Surface-based lifted index (calculated at 500 hPa)
MLLI	100-hPa mixed-layer lifted index (calculated at 500 hPa)
SBLCL	Surface-based lifting condensation level
MLLCL	100-hPa mixed-layer lifting condensation level
03SRH	0–3-km storm relative helicity
01SRH	0–1-km storm relative helicity
7/5LR	700–500-hPa lapse rate
SCP	Supercell composite parameter (using a surface-based parcel)
STP	Significant tornado parameter (using a surface-based parcel)
01EHI	0–1-km energy helicity index (using a surface-based parcel)
FRZGLVL	Freezing level
SFCT_d	Surface dewpoint
850T_d	850-hPa dewpoint
200WND	200-hPa wind velocity
500WND	500-hPa wind velocity
850WND	850-hPa wind velocity
T_c	Convective temperature
6BWD	0–6-km bulk wind difference
CB	Craven–Brooks significant severe parameter (using a surface-based parcel)

Table 2.3. Convective variables and composite indices examined in Gensini et al. (2014).

	KTOP	KTBW	KRAP	KPIT	KOUN	KOAX	KMAF	KLZK	KLBF	KJAN	KGRB	KFFC	KDVN	KDRT	KDNR	KDDC	KBRO	KBNA	KBIS	KAMA	KALB	Avg
SBCAPE	0.43	0.17	0.35	0.24	0.41	0.38	0.13	0.31	0.39	0.21	0.40	0.19	0.37	0.32	0.19	0.37	0.33	0.32	0.50	0.33	0.25	0.31
MLCAPE	0.19	0.00	0.01	0.15	0.01	0.22	0.00	0.05	0.05	0.00	0.37	0.01	0.33	0.20	0.00	0.05	0.20	0.14	0.22	0.00	0.26	0.12
SBCIN	0.12	0.12	0.07	0.12	0.20	0.18	0.04	0.05	0.12	0.20	0.16	0.14	0.08	0.22	0.00	0.21	0.40	0.05	0.10	0.06	0.06	0.13
MLCIN	0.21	0.01	0.11	0.07	0.02	0.09	0.03	0.11	0.13	0.04	0.22	0.00	0.07	0.20	0.00	0.13	0.38	0.07	0.16	0.10	0.19	0.11
SBLI	0.46	0.27	0.23	0.22	0.46	0.48	0.16	0.35	0.37	0.25	0.39	0.24	0.37	0.30	0.14	0.37	0.36	0.31	0.44	0.30	0.23	0.32
MLLI	0.20	0.11	0.07	0.18	0.08	0.28	0.05	0.12	0.09	0.08	0.37	0.07	0.37	0.27	0.02	0.08	0.25	0.20	0.24	0.05	0.23	0.16
SBLCL	0.43	0.19	0.62	0.32	0.59	0.23	0.59	0.39	0.56	0.33	0.17	0.31	0.25	0.11	0.65	0.62	0.18	0.41	0.49	0.67	0.27	0.40
MLLCL	0.21	0.00	0.28	0.24	0.52	0.26	0.17	0.12	0.36	0.01	0.18	0.00	0.25	0.10	0.61	0.55	0.08	0.11	0.28	0.62	0.02	0.24
03SRH	0.62	0.55	0.24	0.72	0.56	0.48	0.38	0.73	0.42	0.74	0.58	0.75	0.64	0.39	0.32	0.35	0.35	0.78	0.40	0.33	0.68	0.52
01SRH	0.52	0.57	0.09	0.62	0.50	0.23	0.16	0.58	0.27	0.73	0.39	0.70	0.55	0.36	0.13	0.31	0.33	0.72	0.22	0.31	0.55	0.42
7/5LR	0.83	0.64	0.78	0.72	0.85	0.82	0.76	0.76	0.78	0.72	0.74	0.74	0.80	0.88	0.81	0.78	0.84	0.76	0.80	0.78	0.62	0.77
SCP	0.48	0.43	0.26	0.31	0.53	0.37	0.23	0.47	0.31	0.46	0.58	0.46	0.48	0.33	0.13	0.38	0.34	0.46	0.52	0.38	0.32	0.39
STP	0.16	0.00	0.00	0.16	0.00	0.06	0.00	0.03	0.00	0.00	0.20	0.01	0.24	0.30	0.00	0.01	0.25	0.11	0.05	0.00	0.08	0.08
01EHI	0.44	0.12	0.20	0.28	0.43	0.23	0.06	0.36	0.24	0.33	0.36	0.23	0.42	0.29	0.03	0.29	0.22	0.36	0.23	0.28	0.41	0.28
FRZGLVL	0.96	0.87	0.97	0.94	0.95	0.96	0.92	0.93	0.96	0.91	0.96	0.90	0.95	0.93	0.95	0.93	0.90	0.93	0.97	0.94	0.92	0.94
SFCT_d	0.49	0.42	0.46	0.49	0.49	0.47	0.41	0.46	0.58	0.42	0.63	0.42	0.60	0.48	0.38	0.49	0.46	0.51	0.49	0.56	0.49	0.49
850T_d	0.12	0.00	0.05	0.40	0.12	0.12	0.00	0.04	0.05	0.10	0.29	0.12	0.10	0.07	N/A	0.02	0.00	0.33	0.11	0.00	0.44	0.12
850WND	0.88	0.76	0.62	0.83	0.87	0.77	0.66	0.83	0.80	0.87	0.84	0.85	0.86	0.82	N/A	0.88	0.77	0.88	0.84	0.75	0.82	0.81
500WND	0.93	0.88	0.84	0.90	0.92	0.88	0.85	0.90	0.85	0.88	0.87	0.94	0.92	0.95	0.74	0.85	0.92	0.93	0.86	0.89	0.90	0.89
200WND	0.93	0.90	0.90	0.92	0.93	0.92	0.89	0.92	0.91	0.94	0.91	0.92	0.93	0.95	0.89	0.93	0.96	0.93	0.90	0.91	0.93	0.92
T_c	0.71	0.03	0.82	0.78	0.53	0.69	0.21	0.61	0.74	0.07	0.72	0.11	0.70	0.56	0.64	0.76	0.54	0.66	0.74	0.53	0.62	0.56
6BWD	0.88	0.72	0.71	0.86	0.86	0.80	0.78	0.84	0.78	0.81	0.77	0.87	0.86	0.92	0.61	0.77	0.90	0.89	0.74	0.80	0.77	0.81
CB	0.94	0.56	0.91	0.89	0.94	0.92	0.85	0.87	0.92	0.74	0.90	0.82	0.92	0.90	0.91	0.90	0.87	0.89	0.92	0.90	0.84	0.87

Table 2.4. Table of coefficients of determination (R^2 values) between model-derived soundings and observed soundings for all parameters and stations analyzed in Gensini et al. (2014)

3. Results

3.1 Severe weather skill scores

The annual sum of severe reports collected by the NWS from 1980–2013 is presented in Fig. 3.1. The trend in annual reporting increases with time for both the national and Northeast domains for reasons hypothesized in chapter 2. Although the smaller Northeast domain exhibits more interannual variability than the CONUS domain, both domains vary considerably after 2005. The more restrictive 1-in (~2.5 cm) severe hail criterion, established 5 January 2010, does not prevent 2011 from having the highest number of severe weather reports of any year in the database for both regions. The annual sum of severe weather days across the study period is pictured in Fig. 3.2. The CONUS and the Northeast exhibit a marginal increase in the annual sum of severe weather days, likely due to the increase in reporting frequency discussed in chapter 2. However, comparing Figs 3.1 and 3.2 suggests the more numerous severe weather days cannot fully explain the rapid increase in annual severe report count.

The increase in severe reports with time, pictured in Fig. 3.1, is reflected in the annual distribution of severe reports per event (Fig. 3.3). An event must have at least 1 severe report occurring within the domain during the 1200–1200 UTC period. Medians for each year are plotted with interquartile ranges in whiskers. The variability of reports per event increases through the study period with the 75th percentile increasing substantially more than the median for both domains. The increasing report count of high-end events implies the reporting trend for prolific severe weather events increases more rapidly than the rest of the event distribution. The upward trend in reports per year and reports per event suggests a temporally dependent

threshold, such as that described in chapter 2, is necessary for discriminating high-impact events across both domains.

The annual POD scores for all slight risk events are depicted in Figure 3.4. Yearly medians are plotted with the 25th and 75th percentiles in whiskers. Over the study period, the Northeast displays better median POD scores than the CONUS for all but 3 years suggesting slight risk convective outlooks in the Northeast capture a higher frequency of severe reports than the CONUS. There is no significant trend in POD scores through the study period for either domain. Larger IQRs suggest more POD score variability for the Northeast than the steadier CONUS. The smaller Northeast domain has more volatile POD scores as a given slight risk contour centered in the Northeast domain covers a higher percentage of the total domain area than the same slight risk contour in the CONUS domain. Differences in event sample size likely contribute to the relatively higher variability of POD scores in the Northeast as well. The entire CONUS domain has at least 300% more slight risk days than the Northeast domain every year (Fig. 3.5).

The FAR medians and 25th and 75th percentiles are pictured in Fig. 3.6. Both domains show improvement with a downward trend from 1980–2013. The Northeast maintains lower median FAR scores than the CONUS throughout most of the study period. Larger IQRs and higher FAR score variability in the Northeast are evident throughout the study period, likely due to lower event sample size for Northeast events. Fig. 3.7 depicts the cumulative slight risk convective outlook area for each year in the study period. The national slight risk area increases from 1980–1996 and drops precipitously in the latter half of the 1990s. An increase in slight risk area occurs between the turn of the century and 2004 before declining through the end of the study period. These results across the national domain are congruent with Fig. 1.14. The

Northeast domain follows a similar, though more varied, trend. The reduction of slight risk outlook size partly contributes to the decline in FAR scores. However, the slight decline in FAR scores in the first half of the study period along with a continued, though muted, decline in the latter half suggests slight risk convective outlook placement has improved throughout the period.

The medians and 25th and 75th percentiles of TS are shown in Fig. 3.8. Similar to the POD and FAR scores, larger volatility is evident in the Northeast TS throughout the study period relative to the CONUS. Additionally, the range between the 75th percentile of TS in the Northeast from the median is higher than the same range for the CONUS domain while both domains have a similar range between their 25th percentile TS and their respective medians for most years in the period. This suggests the upper quartile of events in the Northeast benefit from higher TS than the upper quartile of CONUS events while the lower quartile events have similar TS in both domains. Both threat scores trend up with time, demonstrating gradual improvement in slight risk outlook placement and coverage. Over the 34-year period, the annual median Northeast TS fell below the national median on nine occasions, but remained above the national median for the remaining years of the study period. Therefore, the majority of Northeast slight risk outlooks have higher skill scores than CONUS slight risk outlooks.

3.2 High-impact, low-predictive skill event climatology

A climatology of high-impact, low-predictive skill severe weather events over the Northeast is constructed using the methods discussed in chapter 2. The annual frequencies of high-impact, type 1, type 2, and good events are shown in Fig. 3.9. Recall high-impact events are defined using a linear regression of the 55th percentile of area impacted by severe weather with a

slight risk contour present rather than using the raw 55th percentile for each year. Therefore, the results allow for some variability in the number of high-impact events from year to year instead of tracking events in the upper 45th percentile for a given year. A total of 825 (32%) of 2615 Northeast severe weather events are classified as high-impact events with an annual average of 24 events. A yearly maximum of 44 events occurred in 1994 and a yearly minimum of 10 events occurred in 1984. There is no discernable trend in high-impact events with time, but notable interannual variability exists through the period.

Type 1 (low POD) events composed 224 (27%) of all high-impact events through the period. Slightly more than 25% of high-impact events are classified as type 1 since the lowest 25th percentile POD score for all high-impact events is zero. A maximum of 16 type 1 events occurred in 1980 and a minimum of 1 type 1 event occurred in 2003 with an average of 7 events per year (Fig. 3.9). Type 1 events are a consistent phenomenon with no discernable trend in type 1 event occurrence through the study period. Type 2 (high FAR) events occur less frequently with a total of 42 events from 1980–2013. Before 1996, a total of 32 type 2 events occurred with only 10 events occurring thereafter (Fig. 3.9). An average of 1 type 2 event occurs a year, but type 2 occurrence frequency declines throughout the period with only 5 events occurring in the last decade of the study period. Lastly, 207 high-impact events are classified as good (upper quartile of TS) events with an average of 6 events a year. A maximum of 13 good events occurred in 2002, 2011, and 2012 while a minimum of zero events occurred from 1981–1986. Due in part to the scarcity of good events in the first decade of the study period, there is an upward trend in good event occurrence with time. Of the 9 years having ten or more good events, 8 of them occur in the last decade of the study period. The trend of good events supports

the positive TS trend (Fig 3.8) and further suggests slight risk placement and coverage has improved over time.

The monthly frequencies of high impact, type 1, type 2, and good events are presented in Fig. 3.10. High-impact events largely follow the climatology of severe reports in the northeast U.S. (Fig. 1.5) with a peak in the warm season and a minimum in the cool season. 70% of high-impact events occur in June, July, and August (JJA). April, May, and September account for an additional 23% suggesting high-impact events generally occur in boreal spring and summer over the Northeast. To first order, type 1, type 2, and good events follow the high-impact monthly climatology to within a couple percentage points with the exception of type 2 events in May and August. Type 2 events occur more frequently in May and less frequently in August relative to the high-impact event climatology; though, the small sample of type 2 events (N=42) relative to other event categories should be considered. Importantly, the type 1 and good event datasets are similar through all months aside from slight differences including a higher percentage of type 1 events in JJA. The overall likeness of type 1 and good events suggests little seasonal variability in the predictive skill of high impact weather over the Northeast.

The percent occurrence of high-impact, type 1, type 2, and good events by 1200 UTC 500-hPa flow direction is depicted in Fig. 3.11. 7 high-impact events occurred under a variation of easterly flow and are not shown. Most (83%) high-impact events occur under westerly and southwesterly flow regimes while 12% occur under northwesterly flow. Occurrence rates for type 1, type 2, and good events are generally within a few percentage points of the high-impact climatology however, there some notable differences. Type 2 events did not occur under northerly or southerly flow during the study period. Additionally, type 1 events occur at a higher frequency under northwesterly, northerly, and southerly flow than good events.

To investigate the differences between type 1 and good event flow regimes, Fig. 3.12 illustrates the percentage of high-impact events classified as type 1 or good events for each flow regime. The raw numbers of events are listed above the bars. High-impact events under westerly flow conditions result in the largest number of type 1 and good events. Notably, 24% of high-impact events under westerly flow are type 1 events and 26% of high-impact events under westerly flow are good events. These percentages indicate westerly flow events follow the high-impact event climatology and do not have a higher occurrence rate of poorly (well) forecasted events because both type 1 and good events are defined using the 25th percentile of POD and TS for high-impact events respectively. High-impact events under southwesterly flow have a similar distribution of type 1 and good events, implying southwesterly flow has little impact on the predictive skill of high-impact events.

High-impact events under northwesterly flow compose 12% of all high-impact events, however the occurrence rate of type 1 events per high-impact event is higher than either westerly or southwesterly flow regimes. 31 type 1 events occurred under northwesterly flow, accounting for 33% of all high-impact events under northwesterly flow. Good events compose 21 events representing 22% of all high-impact events under northwesterly flow. The southerly flow regime has similar percentages but sample size is limited as only 17 high-impact events occurred under southerly flow during the study period. High-impact events under northerly flow total 17 but 10 events (58%) are classified as type 1 while only 2 events (12%) are classified as good events. Therefore, type 1 events are most common during high-impact events under northerly flow. Threat scores are calculated for all high-impact events under each flow regime and while northerly and northwesterly flow regimes have the lowest TS, insufficient sample sizes preclude statistical significance. However, the high percentage of type 1 events under northerly flow and

the relative rarity of northerly flow severe events suggest forecasting high-impact severe weather under such flow regimes is difficult.

A composite of severe weather parameters of high-impact events is constructed for type 1 and good event categories centered at the point of maximum report density. 93% of high-impact events occur during the warm season (April–September, Fig. 3.10); as a result, cool season (October–March) events are omitted to focus the composites on environments producing the majority of high-impact events. Fig. 3.13 depicts the 1800 UTC MUCAPE and 1000–500-hPa wind shear magnitude for type 1 and good events. Variables are calculated with 0.5° CFSR data using an area average inside a 1.5° × 1.5° box centered on the point of maximum report density. The median MUCAPE (662 J kg^{-1}) and shear magnitude (31 kt) of the entire high-impact dataset are shown in horizontal and vertical black lines, respectively. The high-impact medians segregate the phase space into four quadrants consisting of Low Shear High MUCAPE (LSHC), High Shear High MUCAPE (HSHC), High Shear Low MUCAPE (HSLC), and Low Shear Low MUCAPE (LSLC) events. The median MUCAPE and shear magnitude for type 1 events are 667 J kg^{-1} and 29 kt respectively. The median MUCAPE and shear magnitude for good events are higher at 691 J kg^{-1} and 35 kt respectively. Both event types have higher MUCAPE medians than the median for all high-impact events; however, the type 1 shear magnitude median is less than both the good event median shear and the total high-impact event median shear values indicating most type 1 events occur under lower shear conditions.

Fig. 3.14 illustrates the total number of type 1 and good events in each quadrant of the MUCAPE-shear phase space. Good events outnumber type 1 events under HSLC and HSHC conditions while type 1 events outnumber good events under LSLC and LSHC conditions, indicating less than 31 knots of 1000–500-hPa shear (low-shear) conditions are associated with

more type 1 events and fewer good events. To further explore the relationship between high-impact event type and the MUCAPE-shear phase space we segregate events by 1200 UTC 500-hPa flow over the point of maximum report density. Fig. 3.15 illustrates the number of type 1 and good events under westerly 500-hPa flow corresponding to each quadrant of the MUCAPE-shear phase space. For westerly flow events, good events outnumber type 1 events when 31 kt or greater of 1000–500-hPa shear (high-shear) is present whereas type 1 events outnumber good events under low-shear conditions. No strong correlation to MUCAPE is found for westerly flow events. Fig. 3.16 is the same as Fig. 3.15, but for southwesterly 500-hPa flow. For events under southwesterly flow regimes, a larger number of good events occur under high-shear conditions than type 1 events. Type 1 events occurred 19 times under LSLC conditions, eclipsing the 5 good events under the same conditions. LSHC conditions have a similar number of type 1 and good events. High-impact events under northwesterly 500-hPa flow have a larger number of type 1 events than good events overall and type 1 events equal or outnumber good events in every category (Fig. 3.17). Similar to other flow regimes, low-shear conditions produce the most type 1 events under northwesterly flow. However, good events under low-shear conditions are more common than good events under high-shear in contrast to the other flow regimes. 16 good events occurred under low-shear conditions while only 4 good events occurred under high-shear conditions.

Analysis suggests type 1 events have a higher rate of occurrence under low-shear conditions than good events. Moreover, average threat scores for all high-impact events are shown in Fig. 3.18. High-impact events under low-shear conditions have a significantly (99% confidence level) lower threat scores than high-impact events under high shear conditions. Additionally, the median TS of low-shear high-impact events is significantly lower (99%

confidence level) than the median TS of high-shear high-impact events (not shown). However, only 4 good events occurred under high-shear conditions in northwesterly flow regimes suggesting that while type 1 events are most common under low-shear conditions, high-impact events under northwesterly 500-hPa flow with high deep-layer shear are rarely classified as a good events. This suggests high-shear events can have low predictive skill even though low-shear events are more likely to be associated with lower threat scores, Aside from 1000-500-hPa shear, no other convective parameters were found to be significant in discriminating threat scores of high-impact events in the Northeast.

3.3 Composite analysis

3.3.1 Northwesterly composite

As discussed in section 3.2, only high-impact type 1 and good events occurring from April–September are included in the event-centered composite calculations. Composite 250-hPa geopotential height and wind are shown in Figs. 3.19a, b. The point of maximum report density for type 1 and good events is found beneath the equatorward exit region of a zonally oriented 50–60-kt upper-level jet streak (Figs. 3.19a, b). The good composite exhibits stronger wind speeds within the jet and a more zonally oriented jet axis than the type 1 composite. Both event centers lie beneath a mean equatorward jet exit region however the weak horizontal wind speed gradient limits the strength of the mean secondary ageostrophic circulation and associated vertical motion over the event centers. The upstream ridge exhibits more pronounced anticyclonic curvature in the type 1 composite than the good composite likely contributing to the reduced ascent at 500 hPa (Fig. 3.19b). At 500 hPa, a ridge lies upstream of the event centers

while a plume of enhanced 700–500-hPa lapse rates advects around the ridge and toward the point of maximum report density from the west (Figs. 3.20a, b). The good composite depicts stronger 35–40-kt wind speeds and steeper lapse rates upstream of the event center than the type 1 composite. Additionally, the tightened geopotential height gradient and enhanced ascent directly upstream of the event center (Figs. 1.19a and 3.20a) suggest a mean shortwave trough may exist ~1000 km west-northwest of the event center. However, the compositing technique likely dampens the shortwave signal due to variability in the strength and location of the trough relative to the point of maximum report density. The approaching type 1 midlevel ridge displays enhanced anticyclonic curvature relative to the upstream ridge in a similar fashion to the 250-hPa height field. The mean sea level pressure (MSLP) field is relatively diffuse in the type 1 composite depicting westerly geostrophic winds and weak warm air advection over the region (Fig. 3.21b). The good composite displays stronger westerly geostrophic winds over the event center under a similar warm air advection regime (Fig. 3.21a). The good composite also depicts enhanced baroclinicity beneath the upper-level jet, reflected in the stronger 1000–500-hPa thickness gradient, as well as higher thickness values over and upstream of the event center. Additionally, an area of 35–40-mm precipitable water (PW) values lies to the west of the good composite event center ahead of a southwest to northeast oriented surface trough. The enhanced PW zone west of the event center coincides with an area of larger 500–1000 J kg^{-1} MUCAPE and >6.5 K km^{-1} 850–500-hPa lapse rates within the good composite (Figs. 3.21a and 3.22a). The type 1 events, by contrast, have weaker lapse rates and between 250–500 J kg^{-1} of MUCAPE across much of the domain ~1000 km west of the event center (Fig. 3.22b). Additionally, the enhanced baroclinicity and faster flow aloft contribute to higher deep-layer shear values of 35–45 kt to the west-northwest of the event center in the good cases (Figs. 3.22a,

b). The steeper lapse rates, accelerated flow aloft, and enhanced instability are likely responsible for the improved forecast performance in the good cases despite the lack of strong synoptic forcing. However, upstream 250–500 J kg^{-1} 1200 UTC MUCAPE values, >6 K km^{-1} lapse rates to the west of the event center, and 30–35-kt deep-layer shear to the west-northwest of the event center indicate the more modest convective parameters of the type 1 cases, relative to the good cases, remain supportive of high-impact severe weather in the Northeast.

3.3.2 Southwesterly composite

The point of maximum report density for southwesterly flow regimes lies beneath the equatorward jet entrance region of an upper-level jet streak (Figs. 3.23a, b). A 70-kt mean jet maximum north of the event center highlights the good composite whereas a weaker 50-kt jet streak is found to the north of the type 1 event center. The good composite depicts the 50-kt isotach extending into the base of an approaching upper-level trough ~800 km west of the event center while type 1 cases have plus-50 kt flow restricted to the north of the event center. Good cases have a more amplified 250-hPa trough and a stronger equatorward entrance region over the event center providing favorable deep-layer ascent; type 1 cases have a less amplified trough in a similar location, providing more modest forcing for ascent.

At 500-hPa, the amplified trough axis of the good composite lags the more progressive type 1 trough axis located ~200km further east (Figs. 3.24a, b). Midlevel lapse rates are generally under 6 K km^{-1} over and upstream of the event center in both composites suggesting advection of steep 700–500-hPa lapse rates is not a prominent process in type 1 or good high-impact events under southwesterly flow. A closed 1008-hPa surface low lies ~350 km west-

northwest of the good composite event center (Fig. 3.25a). The surface cyclone is ahead of a 1000–500-hPa thickness trough to the west and is in a favorable position to strengthen under positive 1000–500-hPa thermal vorticity advection by the 1000–500-hPa thermal wind. The thermal trough in the type 1 composite is weaker and more progressive with a broader trough axis ~200 km east of the thermal trough in the good composite (Figs. 25a, b).

Deep-layer shear values around southwest of the good composite event center range from 30–35 kt while type 1 events average ~25 kt (Figs. 26a, b). 850–500-hPa lapse rates are weak with slightly stronger lapse rates ~6 K km^{-1} southwest of the type 1 and good event centers. The good cases depict MUCAPE exceeding 250 J kg^{-1} over a larger area as well as ~6 K km^{-1} lapse rates over a broader area upstream of the event center than the type 1 cases; though, MUCAPE at 1200 UTC remains low for both events, suggesting instability develops predominantly in-situ rather than by advection. However, errors in the CFSR MUCAPE field may contribute the low instability depicted in Figs. 26a, b.

3.3.3 Westerly composite

The point of maximum report density for westerly flow regimes lies to the south of a zonal jet streak for both composites (Figs. 3.27a, b). On average, the event center does not lie under a prominent jet entrance or exit quadrant, preventing robust conclusions concerning jet forcing over the event center. However, an area of midlevel ascent coincides with a weak upstream trough at 250 hPa ~1000 km west of the event center (Fig. 3.27a). The 60–70-kt jet north of the good composite event center is stronger and elongated relative to the 50–60-kt jet in the type 1 composite. The geopotential height field at 500-hPa depicts a diffuse shortwave

trough approaching both event centers from the west-northwest attendant with accelerated flow around the trough axis (Figs. 28a, b). The good cases average wind speeds around 35–40 kt at the trough axis while the type 1 cases average speeds around 30–35 kt in the trough axis. Both composites depict ~6 K km^{-1} 700–500-hPa lapse rates to the west-southwest of the event center with marginal differences in the location of the lapse rate plume.

Areas of 30–40-mm PW lie around and west of the good composite event center, indicating higher moisture content than type 1 events which average 30–35-mm PW to the south of the event center (Figs. 3.29a, b). A weak 1000–500-hPa thickness ridge approaches the good composite event center from the west and the 564-dam thickness isopleth lies north of the event center. Conversely, the type 1 composite lacks the thickness ridge signature and the 564-dam thickness isopleth lies south of the event center, indicating a cooler airmass over the type 1 event center at 1200 UTC relative to the good composite. Additionally, the meridional thickness gradient to the northwest of the event center is stronger in the good composite, driving stronger flow aloft and contributing to higher vertical wind shear values than the type 1 composite. Figs. 3.30a and 3.30b depicts 35–40 kt of deep-layer shear to the west-northwest of the good composite event center while ~30 kt of shear dominates the area around and west-northwest of the type 1 event center. 500–750 J kg^{-1} MUCAPE west-southwest of the good composite event center indicate higher instability upstream than the type 1 composite. The area of enhanced instability corresponds with the area of 35–40-mm PW to the west-southwest of the good composite event center (Figs. 3.29a and 3.30a). Type 1 and good event composites have a plume of plus-6 K km^{-1} 850–500-hPa lapse rates approaching from the west-southwest, however the differences in strength and spatial extent of the plume are marginal.

In general, the type 1 composites have similar, though less amplified patterns than the good composites. Relative to the type 1 events, good events tend to have stronger flow aloft, steeper lapse rates, and a mean surface trough upstream of the event center under northwesterly flow. Southwesterly good events contained a more amplified upstream trough, faster upper-level winds, a pronounced thickness ridge over the event center, and a mean closed surface cyclone ~350 km northwest of the event center relative to the type 1 composites. Lastly, good cases under westerly flow exhibit enhanced ascent at 500 hPa in response to a slightly more amplified upper level shortwave trough, faster geostrophic westerly flow at the surface, and enhanced moisture and a thickness ridge approaching the event center from the west.

3.4 Case studies

3.4.1 18–19 August 2009 event: type 1 LSHC westerly flow

The 0600 UTZ SPC severe wind convective outlook valid 1200 UTC 18 August 2009 to 1200 UTC 19 August 2009 and accompanying storm reports are shown in Figs. 3.31 and 3.32. A 5% severe wind and severe hail (not shown) probability corridor extends up the Ohio River valley into eastern NY encompassing the southeastern Great Lakes region (Fig. 3.31). 7 severe wind reports spanned east and central New York while a large group of wind reports, including 5 severe hail reports and one 77-kt wind report, extend southeast from central PA to portions of MD, DE, NJ, and extreme southern NY (Fig. 3.32). The majority of severe reports occur further downstream and closer to the Atlantic coast than the convective outlook corridor suggests and the severe report coverage area ranks in the top 32nd percentile of all Northeast high-impact events. Fig. 3.33 depicts a radar mosaic at 2154 UTC 18 August while severe storms

were ongoing over portions of NY, PA, and MD. Storm initiation occurs ~1600 UTC along the southeast coast of Lake Erie and within the higher terrain of western PA and WV. After convective initiation, storms consolidate into small and broken line segments with bowing elements through the duration of the event.

The synoptic environment at the time of convective initiation is shown in Figs 3.34–3.36. At 250-hPa, a 145-kt jet streak streams across the Great Lakes at the base of an upper-level trough over Ontario. An upper-level ridge axis extends from TN to central PA with an upper-level closed low off the east coast of the Delmarva peninsula (Fig. 3.34). The aggregate synoptic forcing over the southeastern Lake Erie coastline, from the equatorward exit region of the jet to the north and the departing ridge axis over PA to the west, is weak as upper-level divergence is minimal. 500-hPa vorticity suggests the Canadian trough is too far removed from the Northeast to force ascent over the area through vorticity advection aloft; however, a region of enhanced relative vorticity associated with the departing offshore upper-level low provides forcing for descent over NJ, DE and southeastern PA (Fig. 3.35). Wind speeds of 10–25 kt from western VA north to Lake Erie and east across New England provide little deep-layer shear in the wake of the offshore trough. Furthermore, deep-layer shear values are no higher than 20 kt across the entire eastern seaboard with higher shear values remaining over Canada at 1600 UTC (Fig. 3.36). Surface-based CAPE values along the southern Lake Erie coast of 500–1000 J kg^{-1} indicate the potential for convection and higher CAPE values in excess of 2000 J kg^{-1} to the southeast provide ample instability for further convective development after initiation. Poor 850–500-hPa lapse rates of ~6 K km^{-1} or less limit convective potential across much of New England.

Observed 1200 UTC soundings from Pittsburg, PA (PIT) and Wallops Flight Facility (WAL), VA are shown in Figs. 3.37 and 3.38. The PIT sounding is similar to the BUF profile (not shown) and represents the convective initiation environment near Lake Erie at 1200 UTC, depicting a moist profile through the lowest ~400 hPa (Fig. 3.37). Mixed-layer CAPE (MLCAPE) of 1948 J kg^{-1} suggests potential for strong convection provided diurnal heating forces mixing of the boundary layer during the morning and early afternoon hours. Deep-layer shear is weak at 12 kt; however, stronger shear values exist in the lower levels where observed 700-hPa wind speeds reach 30 kt. Downdraft CAPE (DCAPE) is calculated using the minimum equivalent potential temperature in the lowest 400 hPa and represents the energy available to a saturated downdraft parcel descending to the surface. 510 J kg^{-1} of DCAPE suggests a reduced threat of strong downdrafts in the vicinity of PIT.

The 1200 UTC profile at WAL is similar to the sounding at Washington Dulles airport (IAD; not shown) and represents the 1200 UTC environment where severe weather occurs later in the day. WAL depicts similar instability to the upstream PIT sounding with 2192 J kg^{-1} MLCAPE (Fig. 3.38). Shear throughout the depth of the troposphere is weak; wind speeds do not rise above 15 kt below 400 hPa. DCAPE of 1294 J kg^{-1} is substantially higher than PIT due to an intrusion of dry air around 600-hPa. Fig. 3.39 illustrates the monthly climatology of DCAPE values for WAL soundings. 1294 J kg^{-1} of DCAPE is above the maximum 90-day moving average for the month of August, suggesting unusually high DCAPE values are in place prior to convective passage. As a result, rain-cooled, saturated parcels around 600-hPa would become strongly negatively buoyant and accelerate toward the ground, providing an enhanced risk of damaging winds at the surface.

As the day progresses, solar insolation heats the surface, leading to a well-mixed boundary layer in the afternoon. An aircraft descending into IAD at 2002 UTC 18 August records an atmospheric temperature profile 30–90 minutes prior to convective passage and a severe storm report 80 km to the northeast of the airport (Fig. 3.40). The 1953 UTC IAD surface observation of 36 °C air temperature and 17 °C dewpoint temperature yield a surface-based lifting condensation level height (LCL) of 818 hPa. The dry boundary layer and high LCL heights contribute to the potential of enhanced evaporative cooling of parcels within the approaching storms, increasing the threat for severe wind damage at the surface.

3.4.2 4–5 May 2010 event: type 1 HSLC westerly flow

The 0600 UTC SPC convective outlook valid 1200 UTC 4 May 2010 to 1200 UTC 5 May 2010 and accompanying storm reports are shown in Figs. 3.41 and 3.42. A 5% severe wind and severe hail (not shown) probability corridor covers New England, NY, and portions of northern PA and NJ (Fig. 3.41). 3 severe hail reports occur along with a widespread and prolific windstorm that sweeps east through the Mohawk valley and into New England (Fig. 3.42). The severe report area associated with the storm ranks within the top 25th percentile of all Northeast high-impact events, suggesting the event deserved a higher severe wind threat outlook category than the 5% category issued at 0600Z. Furthermore, SPC issued a 15% severe wind outlook over portions of eastern NY, NH, VT, and MA during the 1630 UTC convective outlook update. The radar is depicted in Fig. 3.43 at 1857 UTC 4 May while severe storms are ongoing over eastern NY. Convective initiation occurs at ~1400 UTC along the eastern and southern shores of Lake

Erie and Lake Ontario, respectively. Convection grows upscale, forming small lines and bowing segments producing severe wind for the duration of the event (Fig. 3.43).

Strong flow dominates the 250-hPa-wind field over the northeast with a 165-kt jet streak spanning WV through New England and Maine (Fig. 3.44). Additionally, an upper-level trough axis exits the Great Lakes region heading towards the Northeast. Despite, the approaching trough, the poleward entrance region of the jet and its concomitant forcing for descent limit upper-level divergence over the eastern Great Lakes (Fig. 3.44). 500-hPa relative vorticity accompanies the prominent 75-kt 500-hPa jet streak stretching across the Northeast (Fig. 3.45). A negatively tilted trough with attendant implied cyclonic vorticity maxima stretches from Ontario to northwestern PA, providing differential cyclonic relative vorticity advection and forcing for ascent over the area of convective initiation.

At the surface, SBCAPE remains below 250 J kg^{-1} over a large portion of the Northeast with small pockets of 250–500 J kg^{-1} SBCAPE on the western shore of Lake Ontario and south of Lake Erie (Fig. 3.46). An area of plus-7 K km^{-1} 850–500-hPa lapse rates spans across the eastern Great Lakes, western NY, and southern Ontario supporting the fledgling convective cells in the area at ~1400 UTC. Deep-layer shear values between 30–35 kt directly surround the southern shore of Lake Ontario. Higher shear values in excess of 50 kt are found downstream across central NY providing convective cells a favorable environment for upscale growth. Fig. 3.47 depicts the surface equivalent potential temperature and MSLP field at the time of convective initiation over extreme western NY. Low-level baroclinic zones along the boundaries of Lake Ontario and Lake Erie coincide with a weak surface trough extending from southern Quebec toward Lake Ontario, providing a focus for convective activity. By 1400 UTC, surface

equivalent potential temperatures have warmed to 320–330 K across New England and the Northeast coast, increasing instability ahead of the nascent system.

1200 UTC sounding data over Buffalo, NY (BUF) indicates strong, unidirectional tropospheric flow and 37 kt of 0–6-km wind shear, providing favorable dynamic conditions for multicellular storms in the convective initiation environment (Fig. 3.48). An elevated mixed layer (EML) between 600–500 hPa contributes to the 7.2 K km^{-1} 3–6-km lapse rate and the potential for instability provided sufficient diabatic heating in the boundary layer. Importantly, ~40 kt westerly flow through the elevated mixed layer provides strong lapse rate advection downstream toward New England. Moist low-level conditions favor cloud development, but MLCAPE of 362 J kg^{-1} suggests minimal potential energy available for convective cells at 1200 UTC and subdued updraft speeds. Sounding data from Albany, NY (ALB) indicates a substantially drier lower troposphere under similarly strong westerly flow aloft (Fig. 3.49) that is too stable at the surface to support convection at 1200 UTC. However, deep-layer shear between 60–70 kt suggests a favorable dynamic conditions for upscale growth of convection. Steep low-level lapse rates above the surface inversion indicate the potential for afternoon instability beyond what is implied by the meager 29 J kg^{-1} of MLCAPE at 1200 UTC. The steep low-level lapse rates within accelerated tropospheric flow enhance the vertical transport of horizontal momentum down to the surface, exacerbating the severe wind theat. Lastly, subtle backing winds ~500 hPa indicate cold air advection aloft and suggest steepening mid-level lapse rates as the day progresses.

Visible satellite imagery at 1415 UTC 4 May depicts a line of incipient convection in extreme western NY ahead of the surface trough (Figs. 3.47 and 3.50). A corridor of clearer skies spanning northern NJ into New England allows substantial diabatic heating through solar

insolation ahead of the growing system. The Bradley International Airport (BDL) meteogram valid for 4 May 2010 provides surface observations within the clear sky corridor (Fig. 3.51). Temperatures rise during the morning under calm conditions between 1000–1400 UTC, reaching a peak of 80 °F (~27 °C) at 1800 UTC. Low dew point temperatures through the afternoon ~48 °F (~9 °C) contribute to high cloud bases above 6,500 ft (~2000 m) throughout the day. Gusty conditions starting at 1800 UTC suggest vertical mixing of horizontal momentum under steep low-level lapse rates. A departing aircraft sounding from BDL valid at 1617 UTC depicts nearly dry-adiabatic conditions in the lowest 200-hPa (Fig. 3.52). Surface-based LCL and level of free convection (LFC) height of 770 hPa is consistent with the large dew point spread in the BDL surface observations. The aircraft samples a well-mixed, dry boundary layer indicating low relative humidity below the cloud base favorable for vertical mixing and enhanced evaporative cooling of descending saturated parcels. The steep low-level lapse rates and dry boundary layer likely contribute to the 38-kt wind gust at BDL, coinciding with convective passage at 2100 UTC (Fig. 3.51).

3.4.3 4–5 July 2012 event: type 1 LSHC northwesterly flow

The 0600 UTC SPC convective outlook valid 1200 UTC 4 July 2012 to 1200 UTC 5 July 2012 and accompanying storm reports are shown in Fig. 3.53. The SEE TEXT region consists of a 5% severe wind and severe hail probability outlook (not shown) spanning the Mississippi River valley east across the entire U.S. East Coast. A swath of hail and wind reports blanket central MI and continue across Lake Erie into OH, PA, WV, MD, and VA. A second swath of hail and wind reports span extreme northern NY into VT, NH, MA and ME. The severe report area associated

with the event ranks within the top 9th percentile of all Northeast high-impact events, suggesting the event deserved a higher severe weather outlook category than the 5% category issued at 0600Z. Furthermore, SPC issued a 15% severe wind outlook along the southeast shore of Lake Erie into Ohio and extreme northwestern PA during the 1300 UTC convective outlook update. After a moderate expansion of the Lake Erie slight risk east into the D.C. metro area and west across MI during the 1630 UTC convective outlook update, the 2000 UTC update included the storms occurring in northern New England (Fig. 3.54). The first round of severe weather during the event is depicted in Fig. 3.55 as storms progress out of southern Quebec and into northern New England while convective cells are ongoing in southern PA. The cluster of cells in southeast PA track southeast, producing severe hail and wind reports while discreet cells and small lines with bowing segments in New England produce mostly severe wind and a few hail reports. Both groups of storms produce at least one report of ≥ 2-in hail and one ≥ 65-kt wind gust in NY and VT. A secondary round of storms initiates along the southern shore of Lake Erie and grows upscale into small line segments (Fig. 3.56) displaying bowing behavior as convection progresses into southeastern Ohio, southwestern PA, and WV. The evening convection produces severe hail and wind reports as well as one 2-in hail report in Ohio.

The event has origins in the upper Great Plains, Saskatchewan, and Manitoba the day before. Convection initiates ahead of a midlevel trough in British Columbia ~2030 UTC 3 July and grows upscale into a linear MCS system (Fig. 3.57). The system persists over the next 24 hours, crossing ND and into MN and the upper peninsula of Michigan at 2215 UTC 4 July (Fig. 3.58). Tropospheric diabatic heating associated with latent heat release increases potential temperature on the dynamic tropopause (DT) and can have downstream impacts on the mass field. Fig. 3.59 depicts potential temperature and wind on the DT and low-level relative vorticity

from the Global Forecast System model (GFS) analysis at 0000 UTC 4 July 2012. A strip of low-level vorticity represents a front over eastern Montana and southern Saskatchewan concomitant with the ongoing MCS system and a ridge of high potential temperature air between 336–348 K on the DT lies to the northeast of the MCS. A trough of potential temperature between 324–330 K on the DT is present east of the aforementioned ridge. Over the next 18 hours, convection strengthens the ridge and raises potential temperature on the DT above and ahead of the MCS system until an area of 348–366 K potential temperature on the DT spans southern Manitoba, Ontario, and the northern Great Lakes (Fig. 3.60). The elevated area of potential temperature on the DT forces a kinematic response in the wind field, producing stronger anticyclonic curvature as well as strengthening wind speeds along the now-enhanced zonal gradient in potential temperature on the DT between the ridge and the trough to the east. The tightened zonal potential temperature gradient increases northerly flow on the eastern side of the ridge, forcing the trough of lower potential temperature on the DT further to the south. The attendant implied quasigeostrophic forcing through differential advection of cyclonic relative vorticity as well as cooler air below the cyclonic PV feature enhance the risk of convection in southern Quebec, eastern Ontario, and the northern Northeast states.

Convective initiation occurs around 1745 UTC over southern Quebec (Fig. 3.61). A northwesterly jet streak over southern Ontario approaches northwestern NY as the jet corridor rounds the base of a 250-hPa trough over southern Quebec at 1800 UTC 4 July (Fig. 3.62). The poleward exit region of the jet streak, along with differential advection of cyclonic relative vorticity on the poleward side of the jet, provide forcing for ascent in extreme southern Quebec. At 500-hPa, a prominent shortwave rotates around the base of the trough, providing deep-layer ascent into southern Quebec and northern New England while enhancing wind speeds to 50 kt in

the base of the cyclonic relative vorticity maximum (Fig. 3.63). SBCAPE values swell in excess of 2000 J kg^{-1} in southern Quebec, northern NY, and northern New England by 1800 UTC (Fig. 3.64). 1000–500-hPa shear between 35–45 kt is supportive of upscale growth of convection and a multicellular storm mode in the region. The 1200 UTC sounding at Maniwaki, QC (WMW) depicts an EML above 500 hPa with a moist boundary layer and 42 kt of 0–6-km shear (Fig. 3.65). The surface inversion prevents any SBCAPE in the morning, but diurnal heating of the boundary layer will result in SBCAPE values well in excess of the 722 J kg^{-1} MLCAPE calculated at 1200 UTC and similar to those depicted in the RAP analyses at (Fig. 3.64). Notably, the 906 J kg^{-1} of DCAPE calculated at WMW is in the highest 10^{th} percentile of DCAPE climatologies for radiosonde sites at a similar latitude (e.g. INL, GYX, and CAR).

The severe storms in western PA occur under much more subtle forcing. The upper-level trough, jet, and cyclonic relative vorticity maximum associated with the convection in southern Quebec and northern New England do not provide deep-layer forcing in southwestern PA (Figs. 3.62 and 3.63). The lack of strong forcing allows extended diurnal heating and destabilization before convective initiation ~1930 UTC. The 1200 UTC sounding from PIT displays 1214 J kg^{-1} MLCAPE, 29 kt of 0–6-km shear and a steep lapse rate above the surface inversion to ~650 hPa (Fig. 3.66). DCAPE, calculated at 1420 J kg^{-1}, is highly anomalous, ranking higher than the 90-day maximum moving average for all months in PIT (Fig. 3.67).

Diurnal heating enhances thermal instability into the afternoon with SBCAPE rising in excess of 3500 J kg^{-1} around the southern Great Lakes; however, by 1800 UTC, deep-layer shear remains between 20–30 kt across western PA (Fig. 3.64) and does not increase substantially for the duration of the event. Around the time of convective initiation in southern Quebec, remnant clouds from an early-morning MSC persist across western PA (Fig. 3.61). The gradient in

insolation associated with the MCS cloud cover as well as the cold pool generated from the early morning convection establish local thermal boundaries in southwest PA. Fig. 3.68 illustrates the thermal gradient present over western PA in the 1800 UTC surface observations. Additionally, a dew point maximum of 75°F (~24°C) in the vicinity of the thermal boundary suggests surface parcels have ample moisture for strong deep convection. At convective initiation around ~1930 UTC, cells preferentially form along the southern edge of the surface baroclinic zone. A partial profile from an aircraft sounding at PIT illustrates the LCL height and low-level lapse rate before convective initiation (Fig. 3.69). The 1800 UTC surface observation at PIT of 32 °C air temperature and 22 °C dewpoint temperature results in 539 J kg^{-1} of CAPE below 500 hPa and an LCL height at 827 hPa. The temperature profile is dry adiabatic and well mixed below 800 hPa, supporting acceleration of descending saturated parcels through evaporative cooling.

The second round of storms in OH and PA initiate around 0030 UTC 5 July off the southern shore of Lake Erie. At 0000 UTC, RAP analyses suggest 850–500-hPa lapse rates strengthened to 6.5–7 K km^{-1} across Lake Erie, western PA, and OH with steeper lapse rates to the west (Fig. 3.70). Deep-layer shear between 10–25 kt dominates the region however SBCAPE remains above 3000 J kg^{-1} in the RAP analysis. 0000 UTC sounding data from PIT depicts a similarly unstable environment to the model data, indicating 3203 J kg^{-1} SBCAPE, a 7.5 K km^{-1} 850–500-hPa lapse rate, and –3 J kg^{-1} of surface-based convective inhibition. 24 kt of 0–3-km shear provides some support for multicellular convection while 1599 J kg^{-1} DCAPE suggests anomalously high negative buoyancy available to saturated descending parcels (Fig. 3.71). Upper-level forcing for the second round of convection is lacking; however, similar to earlier convection in southwestern PA, a low-level temperature gradient is evident in the surface observations before convective initiation (Fig. 3.72). The boundary between CLE and HZY,

along with the lake-land interface, provides weak low-level forcing for ascent and focus convection in the weakly inhibited environment. Convection grows upscale after 0200 UTC (Fig. 3.56) and evolves into a bowing line after 0500 UTC propagating into northern WV.

3.4.4 24–25 May 2011 event: type 2 HSLC westerly flow

The 0600 UTC SPC convective outlook valid 1200 UTC 24 May 2011 to 1200 UTC 25 May 2011 and accompanying storm reports are shown in Fig. 3.73. A severe weather outbreak occurs in the central Great Plains along with a series of severe MCSs over TN, KY, NC, and VA. Much of the Northeast is under a slight risk for severe weather with a 15% chance of severe wind and hail (not shown). The day 2 and day 1 SPC convective outlooks at 1730 UTC 23 May and 0600 UTC 24 May respectively, mention a weak shortwave ejecting eastward into the Ohio valley, a cold front advancing into New England, and boundary layer destabilization through diurnal heating ahead of the front as contributing factors of severe weather in the Northeast. However, despite the slight risk outlook ranking in the highest 12^{th} percentile of slight risk area of all slight risk events in the Northeast, only 2 severe reports occur within the Northeast domain. At the peak of the event, storms are small and disorganized; upscale growth is limited, with a couple small, nonsevere line segments in New England and weak cellular systems across NY, PA, and OH (Fig. 3.74).

A 250-hPa jet corridor with winds upward of 90 kt spans OH, PA, NY, and into southern Quebec (Fig. 3.75). Broad cyclonic flow aloft dominates the pattern with a shortwave trough approaching extreme northern ME with attendant upper-level divergence downstream. The diffuse jet lacks strong horizontal wind speed gradients over the Northeast, leading to weak

induced secondary ageostrophic circulations. Therefore, upward vertical motion on the equatorward entrance region of the embedded jet streaks is reduced (Fig. 3.75). At 500-hPa, an area of 22×10^{-5} s^{-1} cyclonic relative vorticity approaches ME while disjointed strips of shear vorticity overspread the spine of the Appalachians and west across the southern tier of the Great Lakes (Fig. 3.76). Weakly confluent flow dominates the eastern region of the U.S. with a 50 kt jet maximum over VA, KY, and TN.

The morning sounding at PIT depicts a moist boundary layer and modest MLCAPE of 483 J kg^{-1} (Fig. 3.77). 34 kt of 0–6-km unidirectional shear, ample low-level moisture and modest midlevel lapse rates indicate the potential for severe convection if more instability can develop into the afternoon. Similar profiles were sampled over BUF and ALB (not shown). The 1200 UTC IAD sounding contains 784 J kg^{-1} of MLCAPE and 48 kt of 0–6-km shear with higher amounts in lower layers (Fig. 3.78). The profile is potentially supportive of severe weather as vertical advection of strong tropospheric flow is enhanced by steep low-level lapse rates provided diurnal heating removes the surface inversion. Drier boundary layer conditions inhibit cloud growth relative to profiles further west and north, decreasing the probability of convective initiation around IAD.

At the peak of the event, a cold front draped across the Northeast and the southern Great Lakes propagates slowly towards the southeast (Fig. 3.79). Ahead of the front, SBCAPE is marginal with values ranging from 500–1000 J kg^{-1} and higher values in Ohio and Indiana (Fig. 3.80). Midlevel lapse rates between 6–6.5 K km^{-1} lie ahead of the front and deep-layer shear values range from 20–30 kt in the Northeast with higher values south of MD.

The lack of CAPE and instability is attributable to cloud cover from upstream convection in the Ohio River valley during the previous day. A large MCS moved through the valley with

storms spanning from western OH to TN (Fig. 3.81). The system dissipated on the western slopes of the Appalachians during the overnight and early morning hours of 23–24 May. The convection generated substantial cloud cover (Fig. 3.82), which advected towards the Northeast under west-southwesterly flow conditions. By 1215 UTC, clouds blanketed most of the Northeast, preventing strong diurnal heating (Fig. 3.83). The broad cyclonic flow aloft and weak synoptic ascent provide a favorable environment for cloud persistence and, at 1815 UTC, the cloud field remains a robust feature over the northeast U.S. (Fig. 3.84) Surface observations of cloud cover confirm overcast and mostly cloudy conditions persist over the majority of the slight risk region in the Northeast (Fig. 3.85).

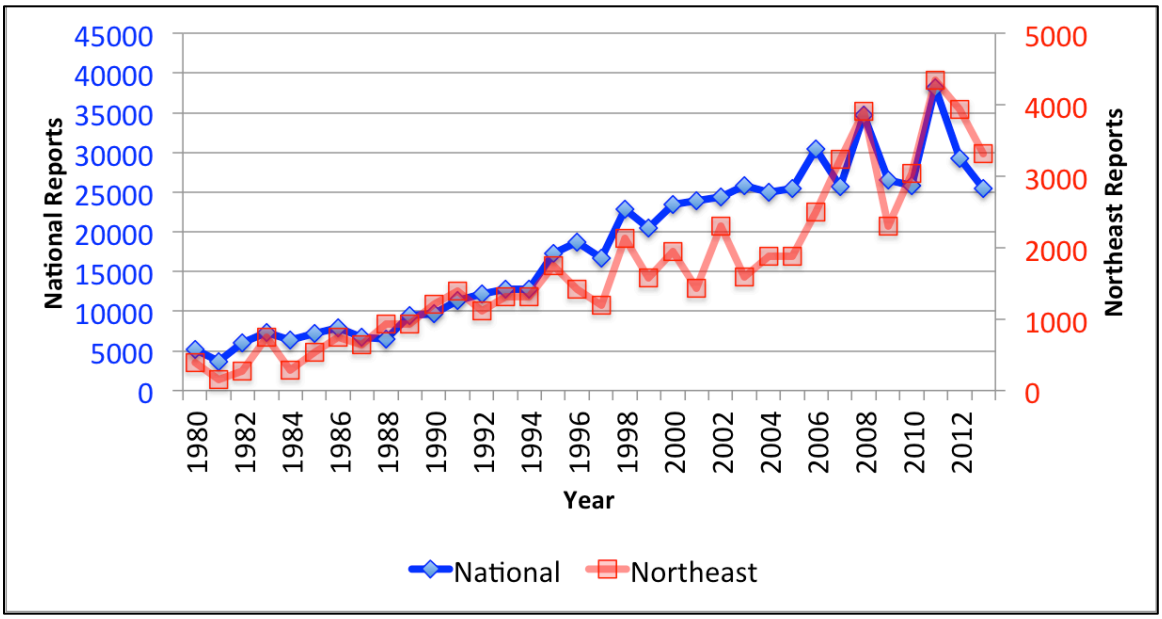

Figure 3.1. Annual sum of severe reports from 1980–2013 for the Northeast domain (red) and the entire U.S. domain (blue).

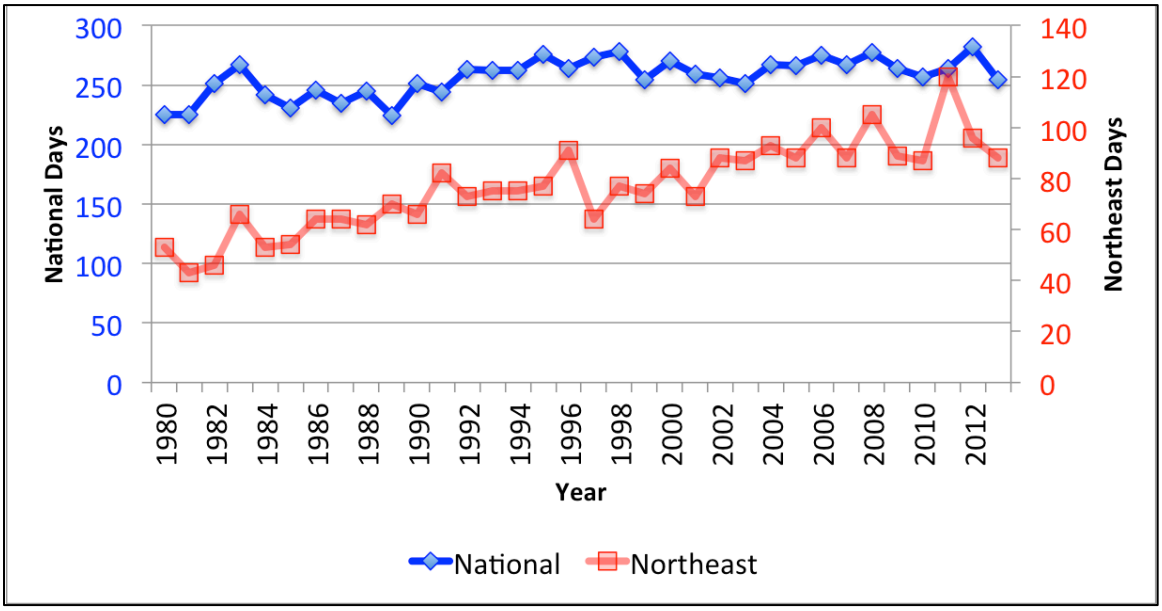

Figure 3.2. . Annual number of days with at least 1 severe report from 1980–2013 for the Northeast domain (red) and the entire U.S. domain (blue).

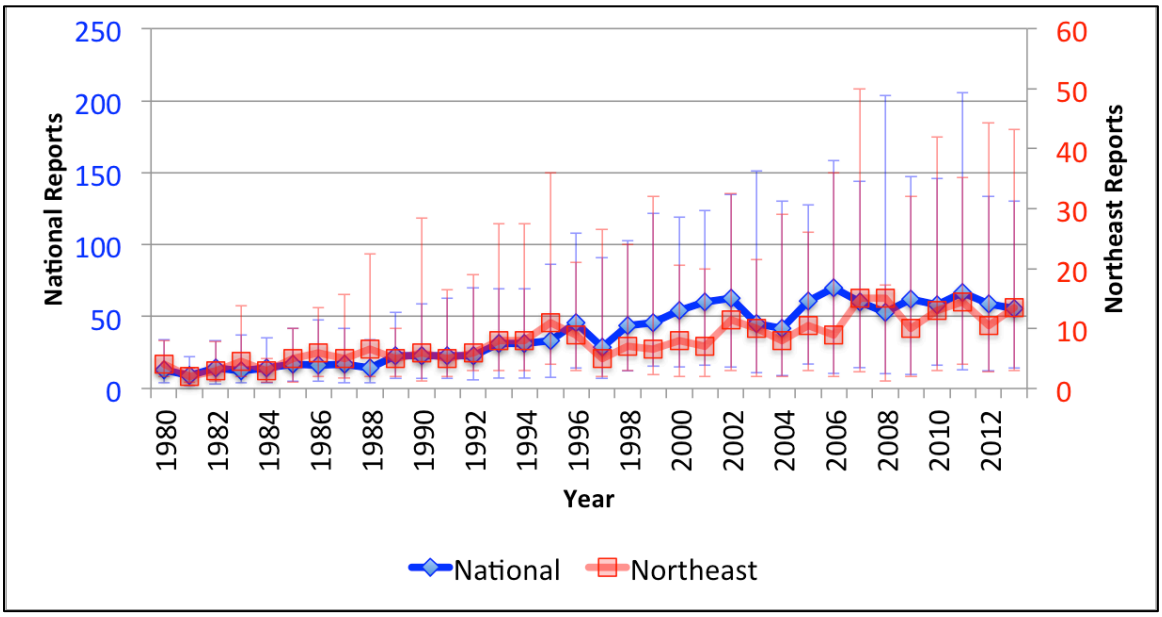

Figure 3.3. Annual distribution of reports per severe event from 1980–2013 for the Northeast domain (red) and the entire U.S. domain (blue). The median is plotted with the 25th and 75th percentiles in the whiskers.

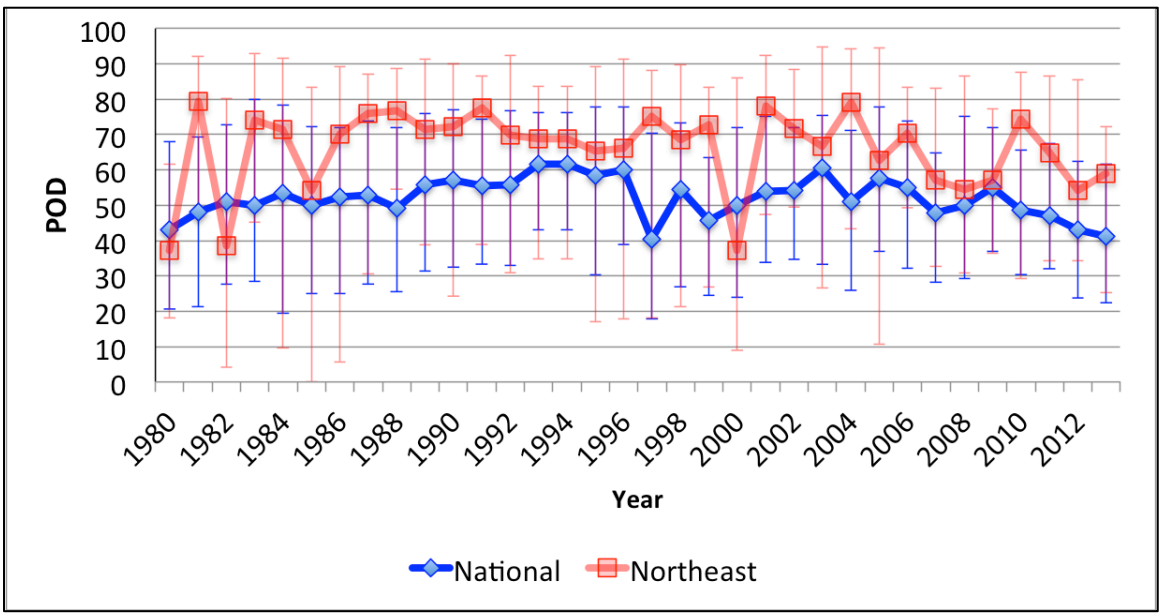

Figure 3.4. Annual distribution of POD scores from 1980–2013 for the Northeast domain (red) and the entire U.S. domain (blue). The median is plotted with the 25th and 75th percentiles in the whiskers.

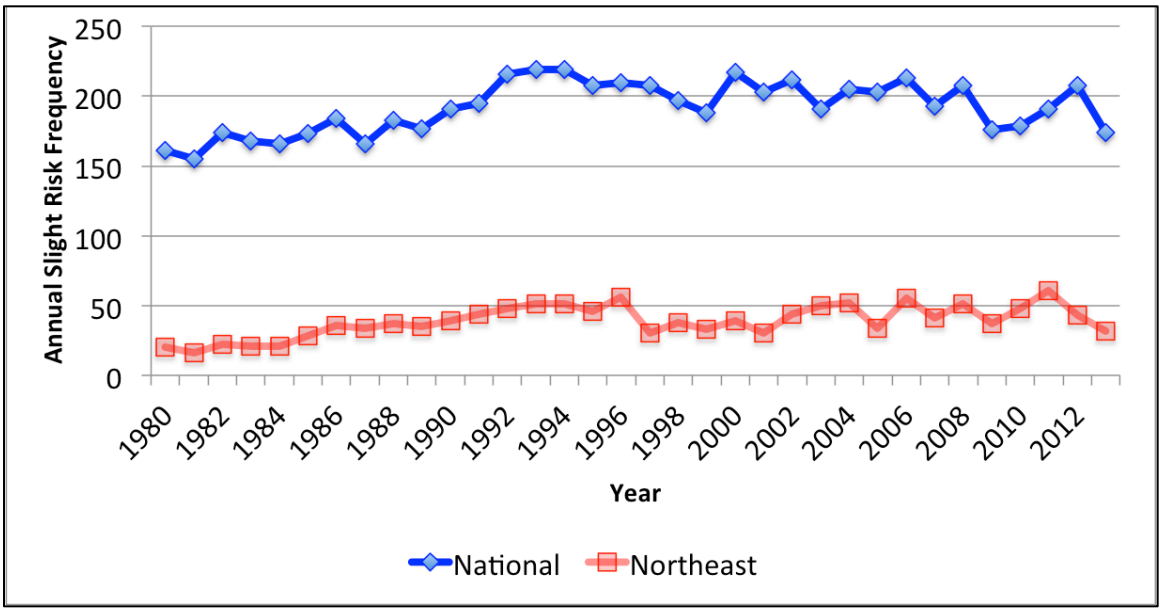

Figure 3.5. Annual number of days with a slight risk outlook covering a portion of the domain from 1980–2013 for the Northeast domain (red) and the entire U.S. domain (blue).

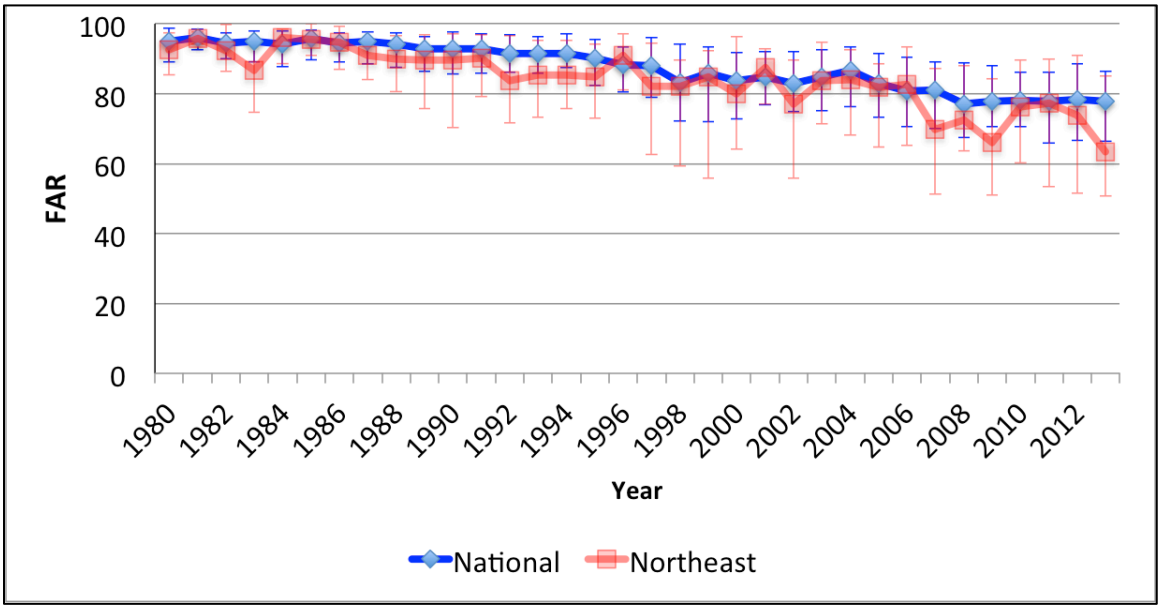

Figure 3.6. Annual distribution of FAR scores from 1980–2013 for the Northeast domain (red) and the entire U.S. domain (blue). The median is plotted with the 25th and 75th percentiles in the whiskers.

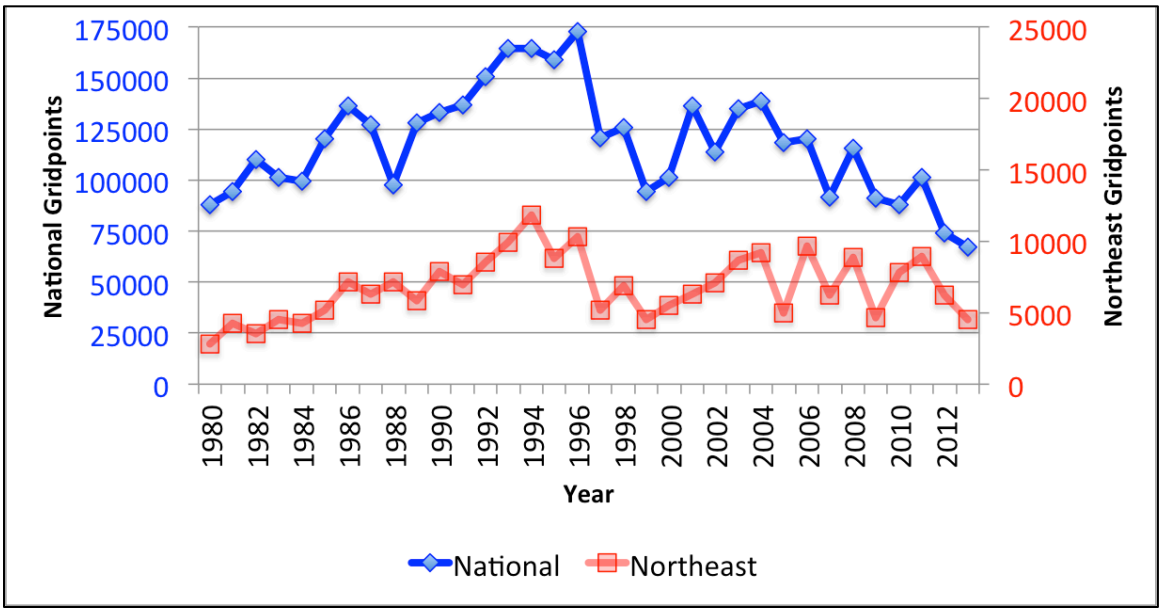

Figure 3.7. Annual sums of slight risk convective outlook area from 1980–2013 for the Northeast domain (red) and the entire U.S. domain (blue).

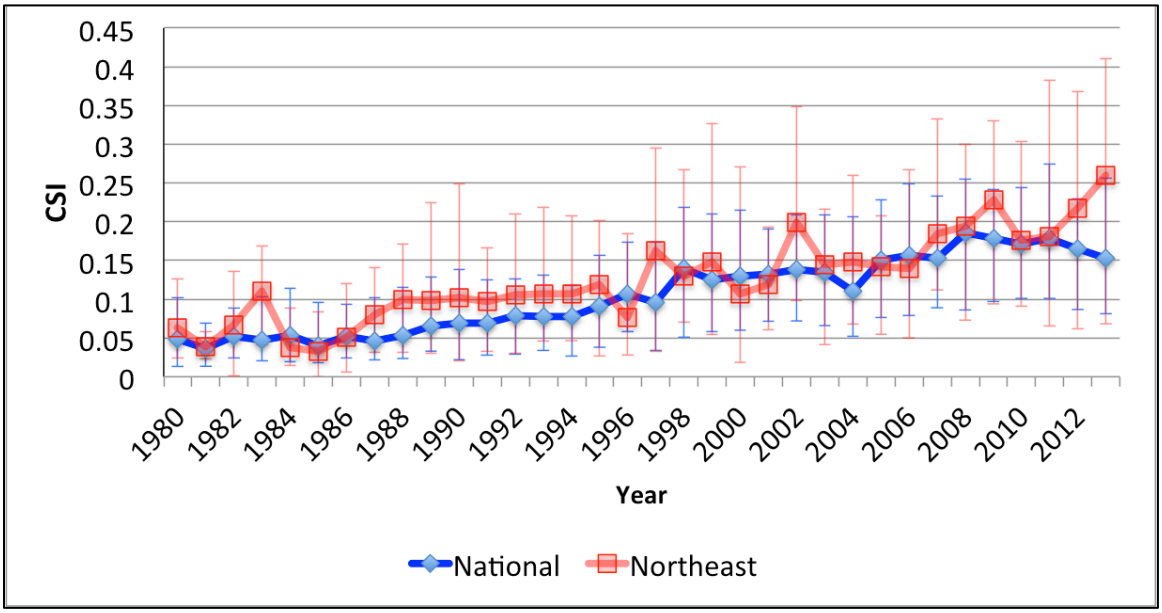

Figure 3.8. Annual distribution of threat scores from 1980–2013 for the Northeast domain (red) and the entire U.S. domain (blue). The median is plotted with the 25th and 75th percentiles in the whiskers.

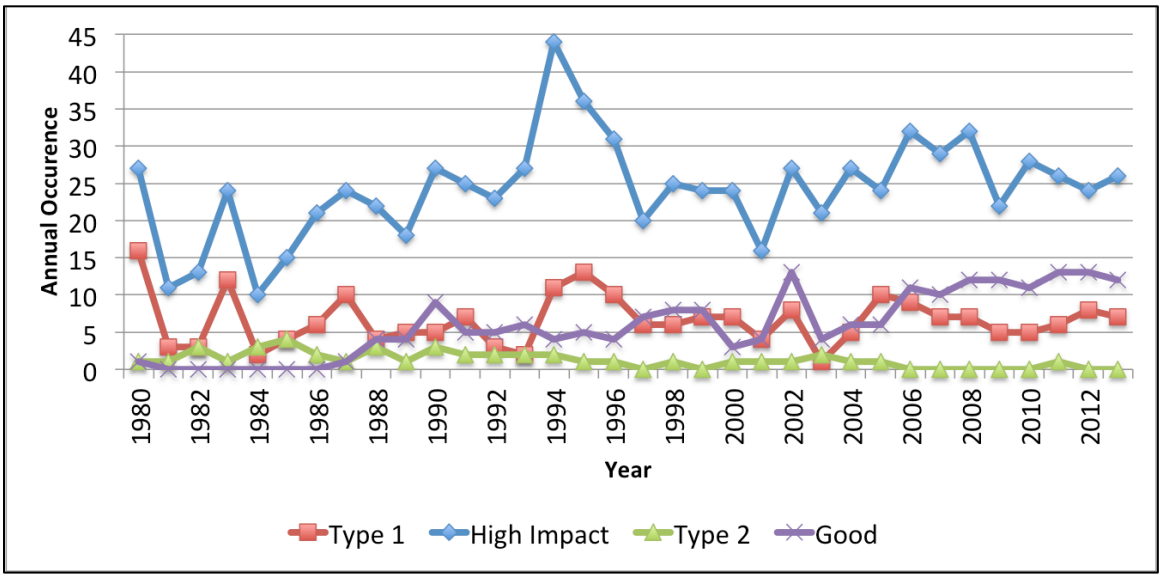

Figure 3.9. Annual frequency of high-impact (blue), type 1 (red), type 2 (green), and good (purple) events from 1980–2013 for the Northeast domain.

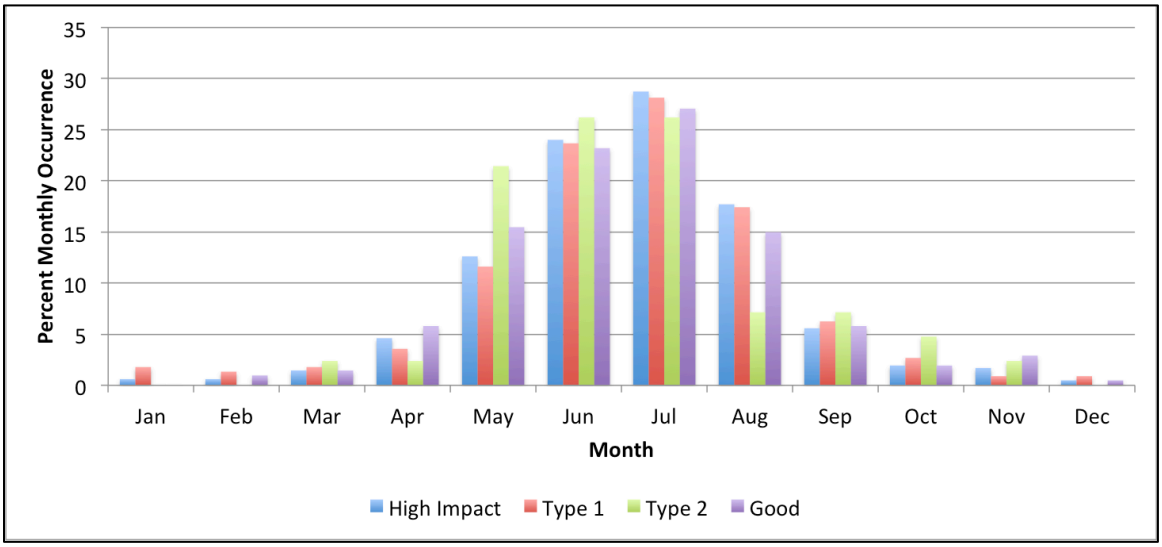

Figure 3.10. Percent occurrence of high-impact (blue), type 1 (red), type 2 (green), and good (purple) events per month from 1980–2013 for the Northeast domain.

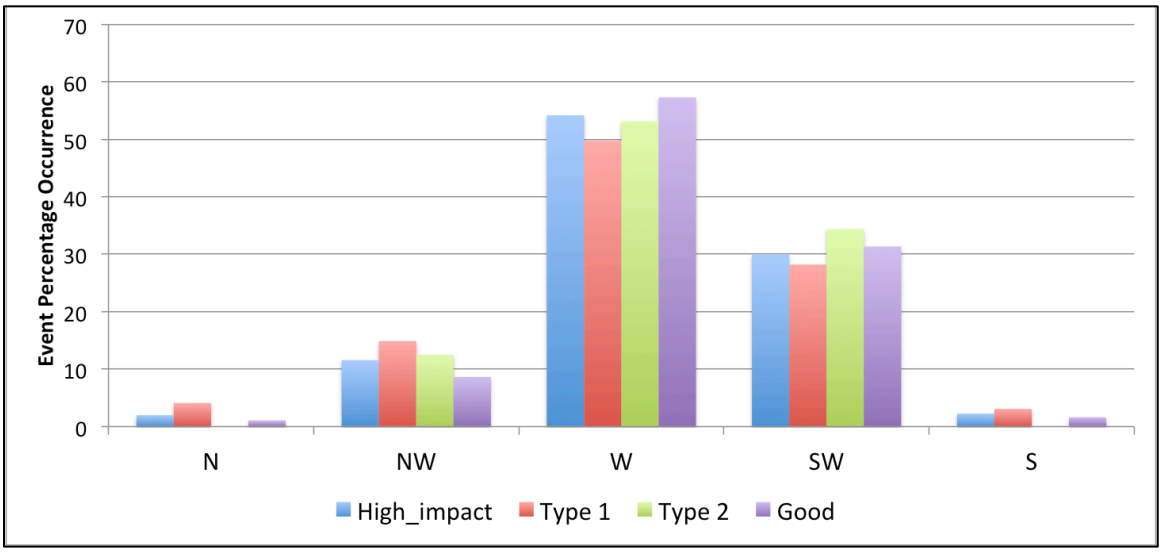

Figure 3.11. Percent occurrence of high-impact (blue), type 1 (red), type 2 (green), and good (purple) events for northerly, northwesterly, westerly, southwesterly, and southerly 500-hPa flow directions from 1980–2013. Wind values are derived from 1200 UTC CFSR data.

Figure 3.12. Percent of high-impact events classified as type 1 (red) and good (purple) events for northerly, northwesterly, westerly, southwesterly, and southerly 500-hPa flow directions from 1980–2013. Raw numbers of type 1 and good events in each 500-hPa flow category are listed above their respective bars. Wind values are derived from 1200 UTC CFSR data.

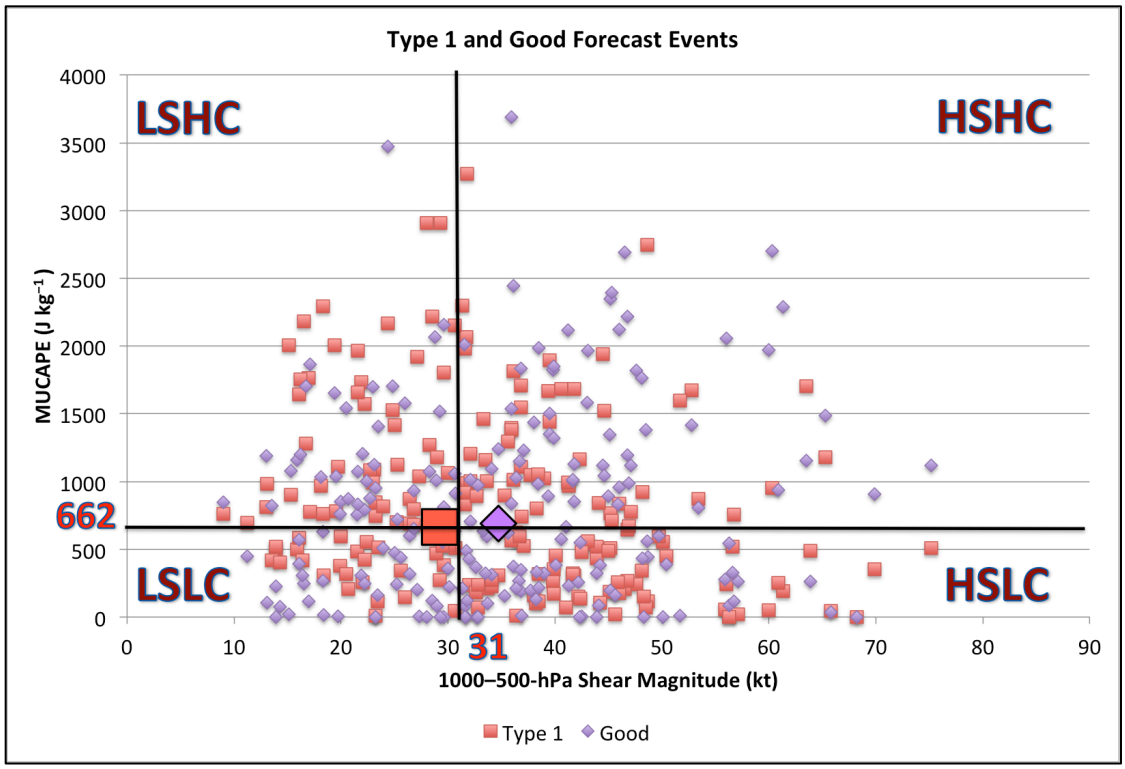

Figure 3.13. Phase space diagram of MUCAPE (J kg^{-1}) and 1000–500-hPa shear magnitude (kt) for all type 1 (red) and good (purple) events from 1980–2013. High-impact dataset medians of MUCAPE (662 J kg^{-1}) and shear (31 kt) are overlaid as black lines. From the top left going clockwise, quadrants are labeled: Low Shear High MUCAPE (LSHC), High Shear High MUCAPE (HSHC), High Shear Low MUCAPE (HSLC), and Low Shear Low MUCAPE (LSLC). The bold red square and bold purple diamond denote the median MUCAPE and shear values for type 1 and good events respectively. Values are derived from 1800 UTC CFSR data.

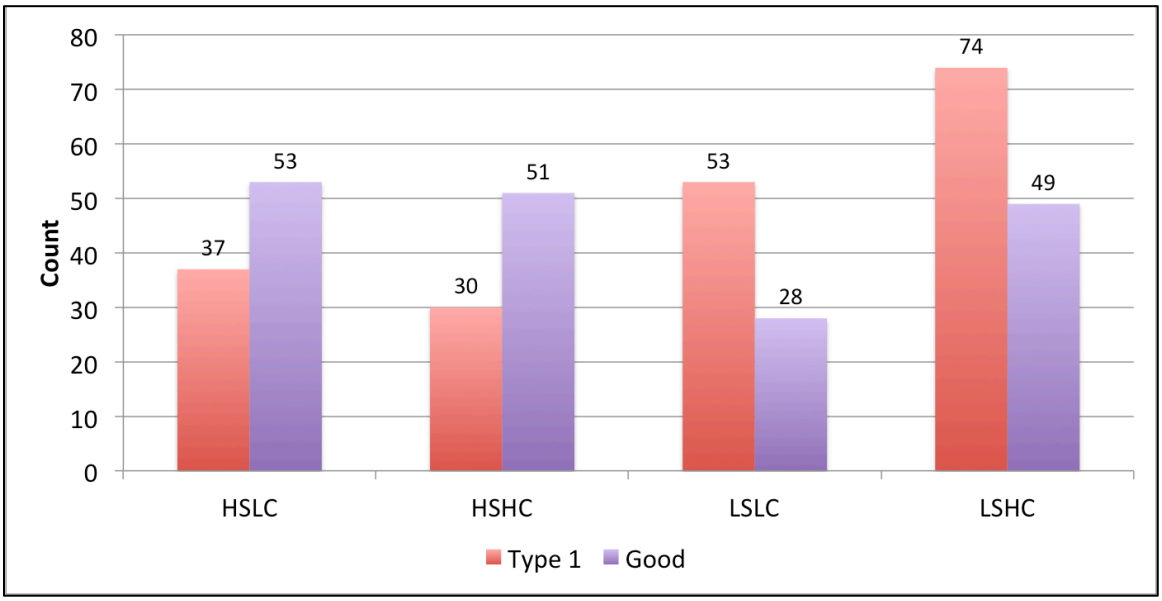

Figure 3.14. Number of type 1 and good events binned in each MUCAPE-shear phase space category from 1980–2013. Phase space categories include: Low Shear High MUCAPE (LSHC), High Shear High MUCAPE (HSHC), High Shear Low MUCAPE (HSLC), and Low Shear Low MUCAPE (LSLC). Values are derived from 1800 UTC CFSR data.

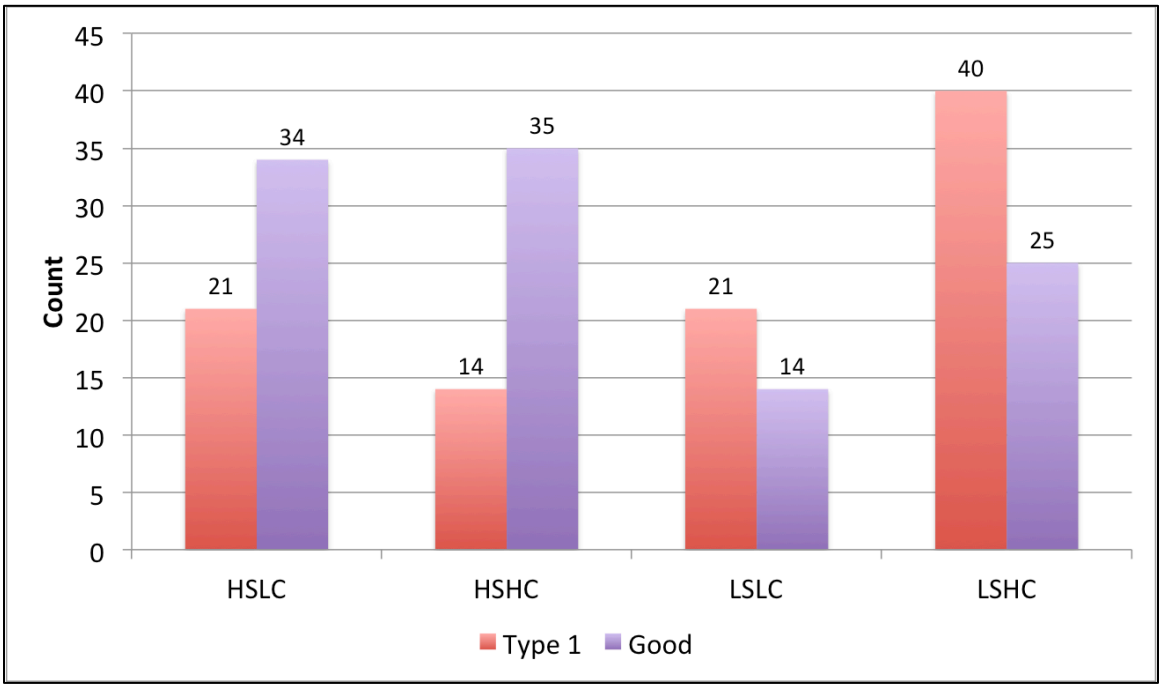

Figure 3.15. Same as Fig. 3.14 but for westerly 500-hPa flow cases

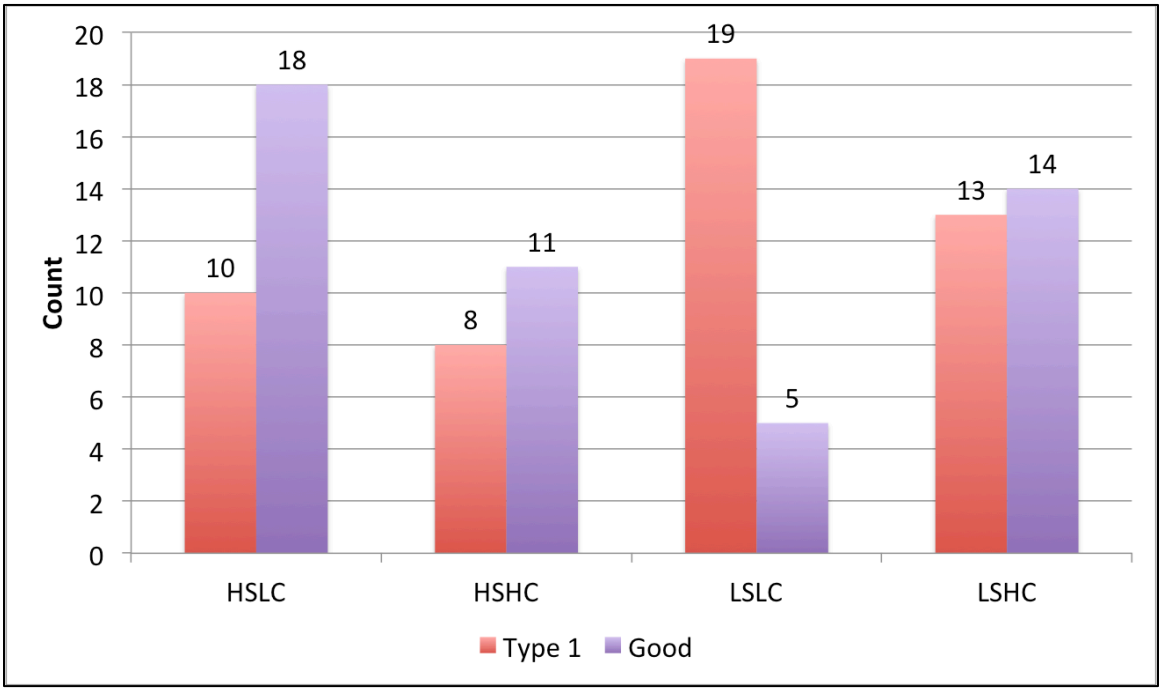

Figure 3.16. Same as Fig. 3.14 but for southwesterly 500-hPa flow cases

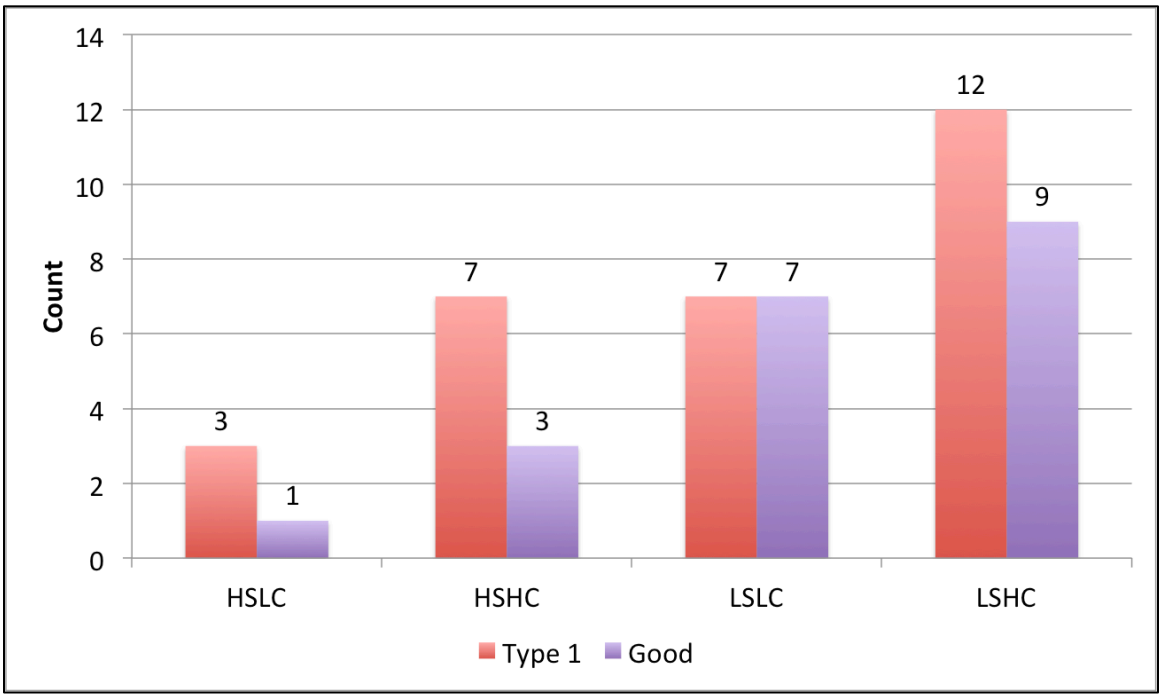

Figure 3.17. Same as Fig. 3.14 but for northwesterly 500-hPa flow cases

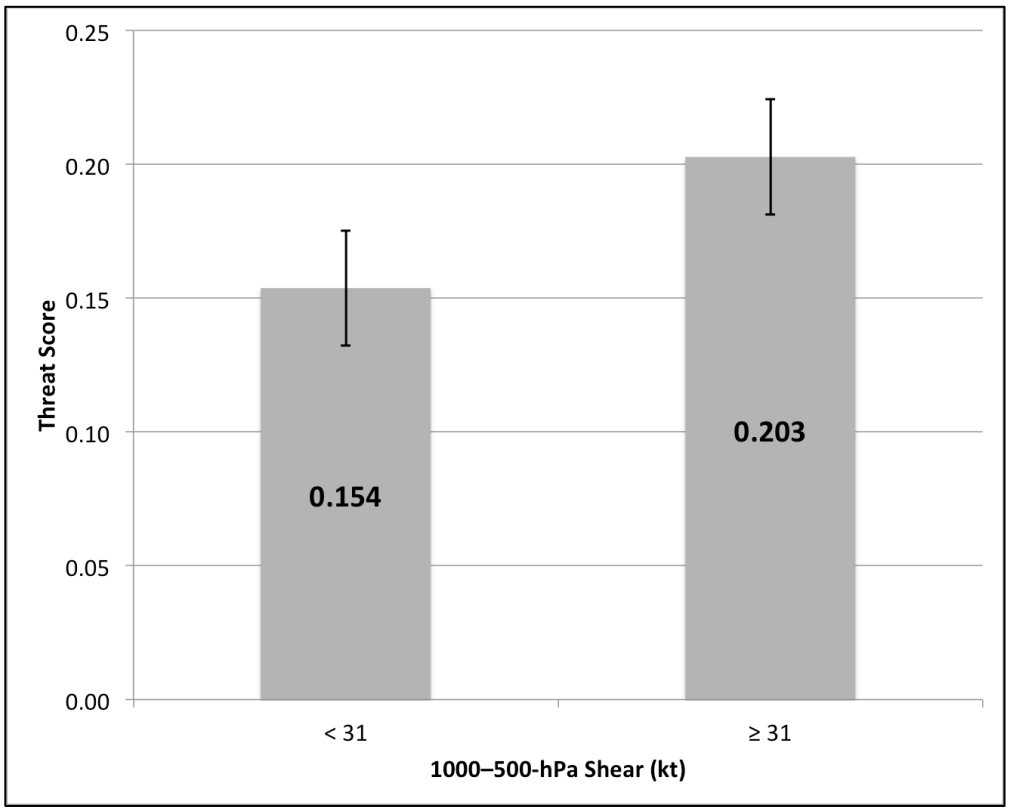

Figure 3.18. Average threat scores of high-impact events occurring under low (< 31 kt) and high (≥ 31 kt) 1000–500-hPa shear. Whiskers are confidence intervals at the 99% level.

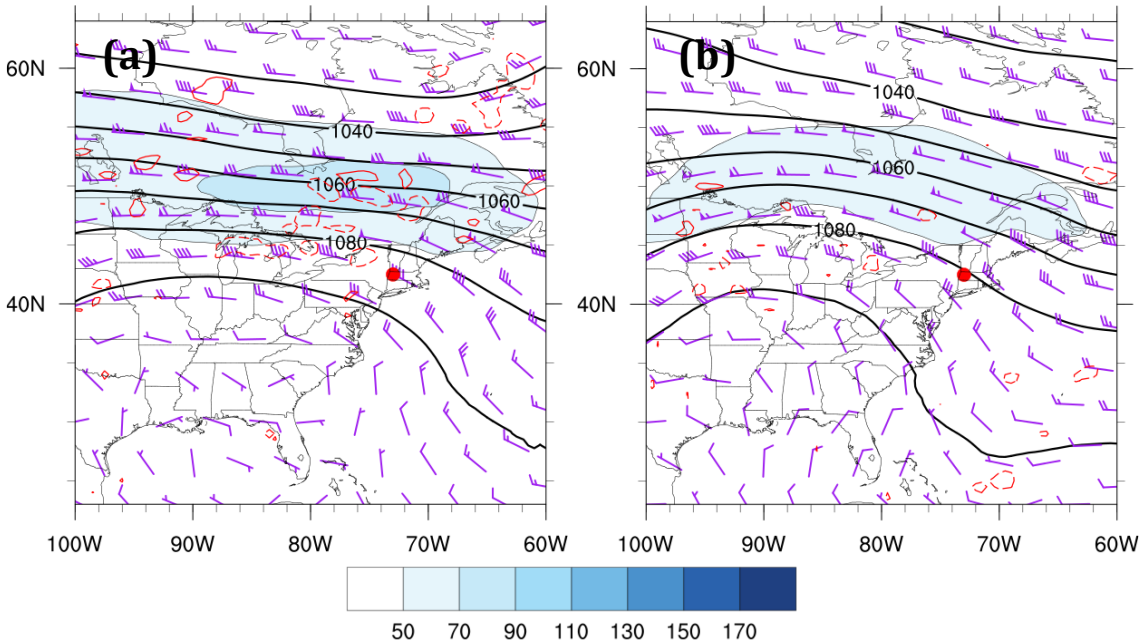

Figure 3.19. Northwesterly flow category composite 250-hPa geopotential height (black contours, dam), wind speed (fills, kt), wind barbs (kt), and 500-hPa omega (red dashed contours are negative, red solid contours are positive, contoured every 3×10^{-3} hPa s^{-1}) for good (a) events (N = 20) and type 1 (b) events (N = 29). Heavy red dot represents composite center at point of maximum report density.

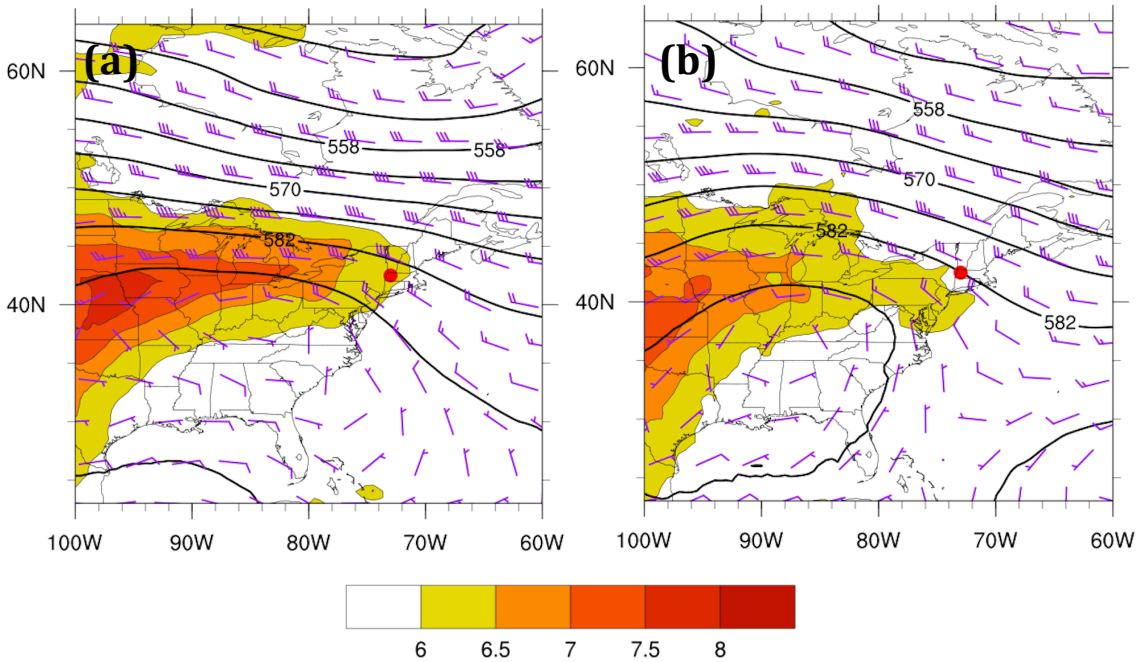

Figure 3.20. Northwesterly flow category composite 500-hPa geopotential height (black contours, dam), wind barbs (kt), and 700–500-hPa lapse rate (fills, K km^{-1}), for good (a) events (N = 20) and type 1 (b) events (N = 29). Heavy red dot represents composite center at point of maximum report density.

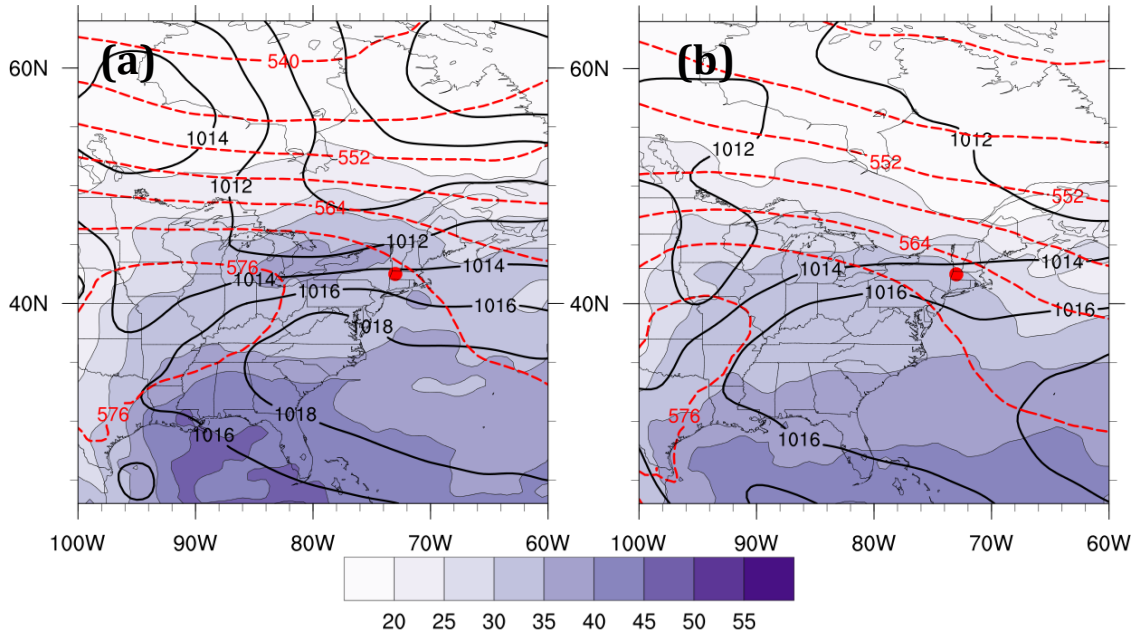

Figure 3.21. Northwesterly flow category composite mean sea level pressure (black contours, every 2 hPa), 1000–500-hPa thickness (dashed, every 6 dam), and total columnar precipitable water (fills, mm), for good (a) events (N = 20) and type 1 (b) events (N=29). Heavy red dot represents composite center at point of maximum report density.

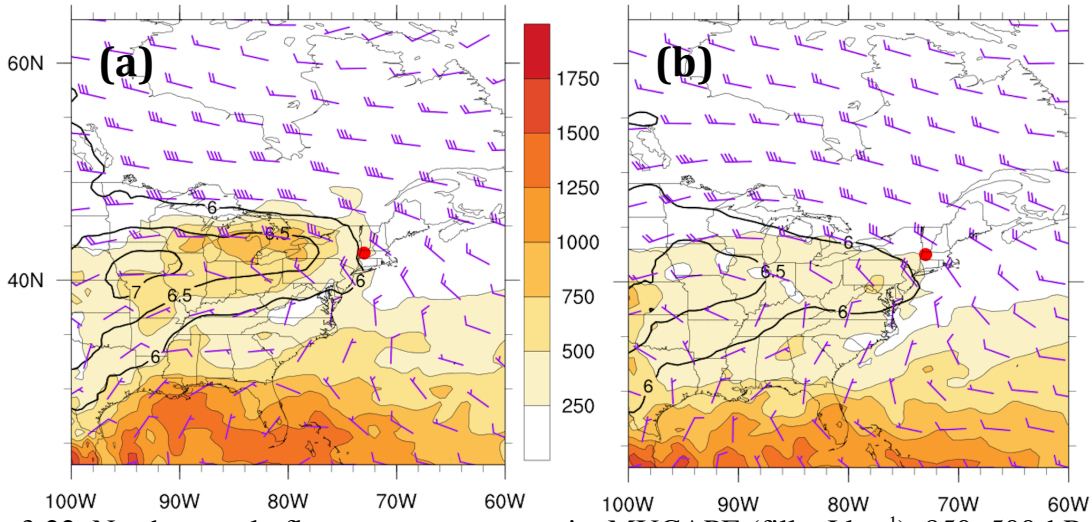

Figure 3.22. Northwesterly flow category composite MUCAPE (fills, J kg^{-1}), 850–500-hPa lapse rate (black contours, K km^{-1}), and 1000–500-hPa wind shear (barbed, kt), for good (a) events (N = 20) and type 1 (b) events (N=29). Heavy red dot represents composite center at point of maximum report density.

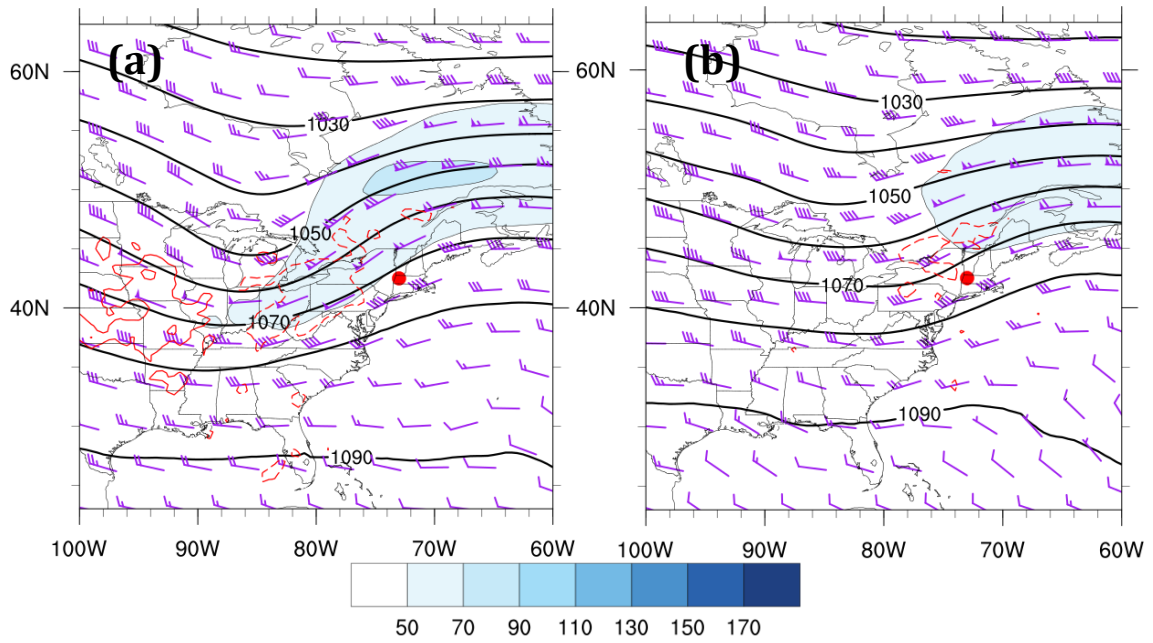

Figure 3.23. As in Fig. 3.19 except for the southwesterly flow category composite for good (a) events (N = 48) and type 1 (b) events (N = 50). Heavy red dot represents composite center at point of maximum report density.

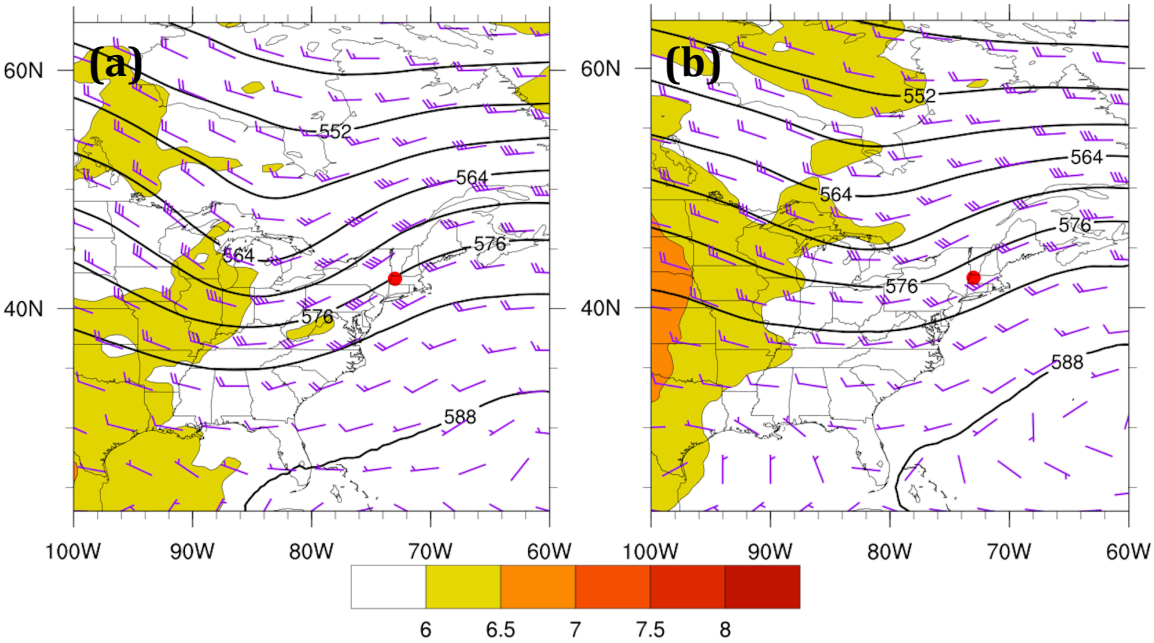

Figure 3.24. As in Fig. 3.20 except for the southwesterly flow category composite for good (a) events (N = 48) and type 1 (b) events (N = 50). Heavy red dot represents composite center at point of maximum report density.

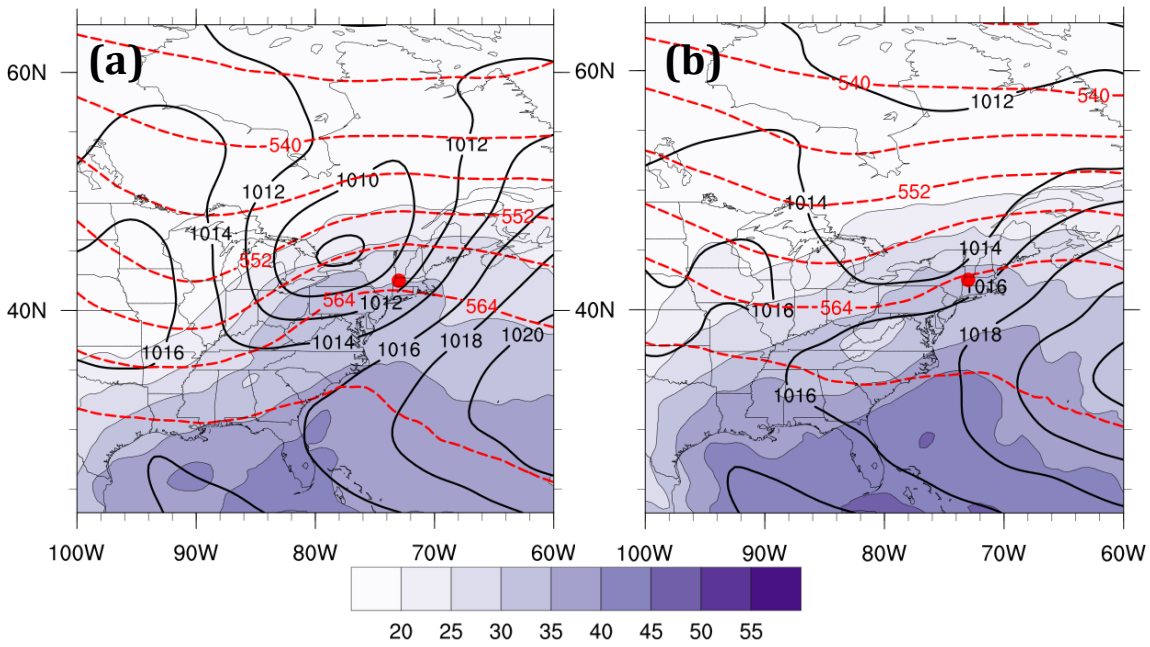

Figure 3.25. As in Fig. 3.21 except for the southwesterly flow category composite for good (a) events (N = 48) and type 1 (b) events (N = 50). Heavy red dot represents composite center at point of maximum report density.

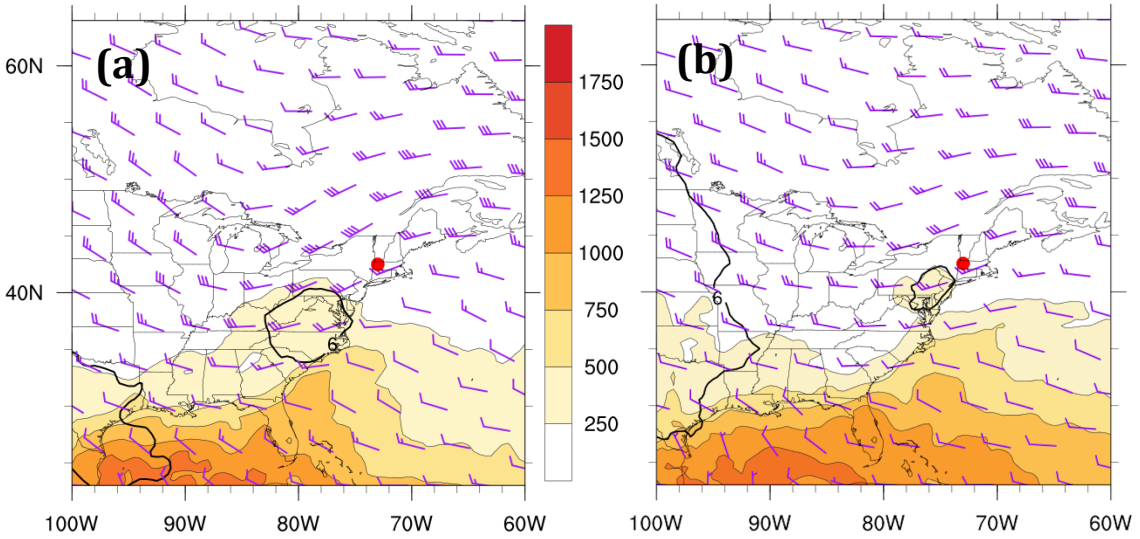

Figure 3.26. As in Fig. 3.22 except for the southwesterly flow category composite for good (a) events (N = 48) and type 1 (b) events (N = 50). Heavy red dot represents composite center at point of maximum report density.

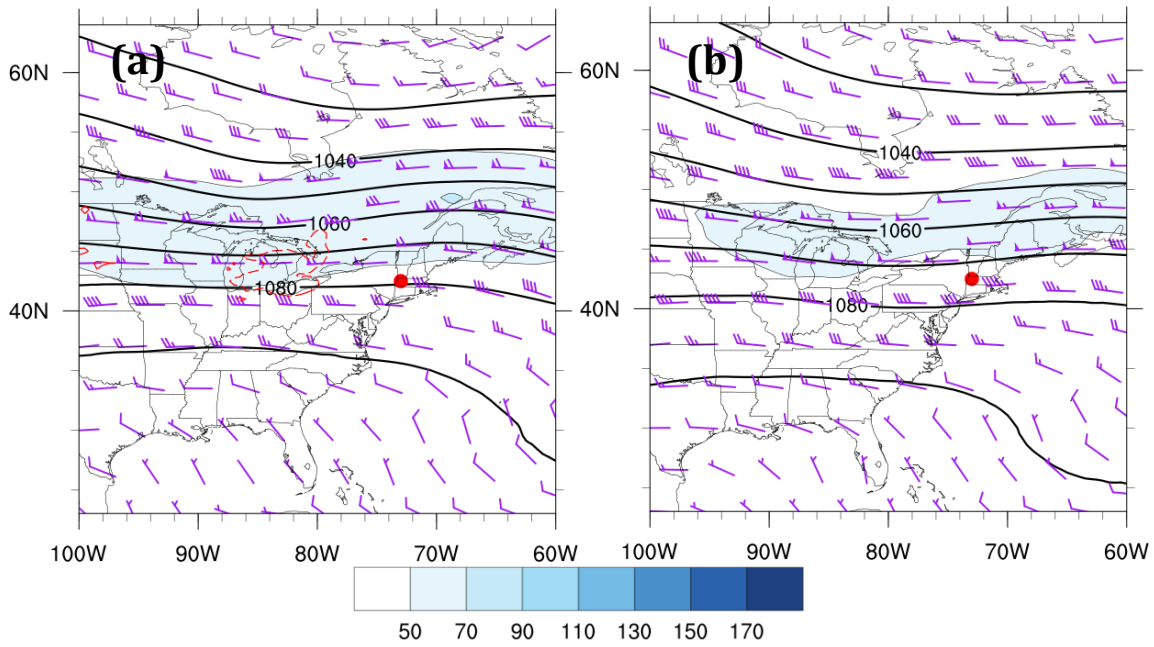

Figure 3.27. As in Fig. 3.19 except for the westerly flow category composite for good (a) events (N = 108) and type 1 (b) events (N = 96). Heavy red dot represents composite center at point of maximum report density.

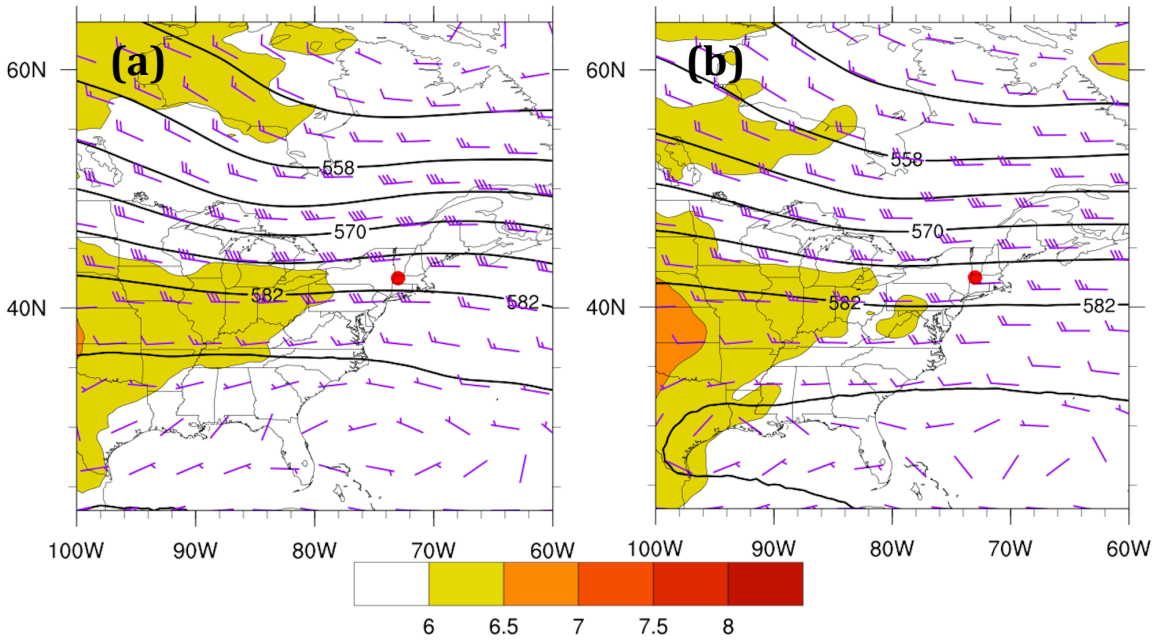

Figure 3.28. As in Fig. 3.20 except for the westerly flow category composite for good (a) events (N = 108) and type 1 (b) events (N = 96). Heavy red dot represents composite center at point of maximum report density.

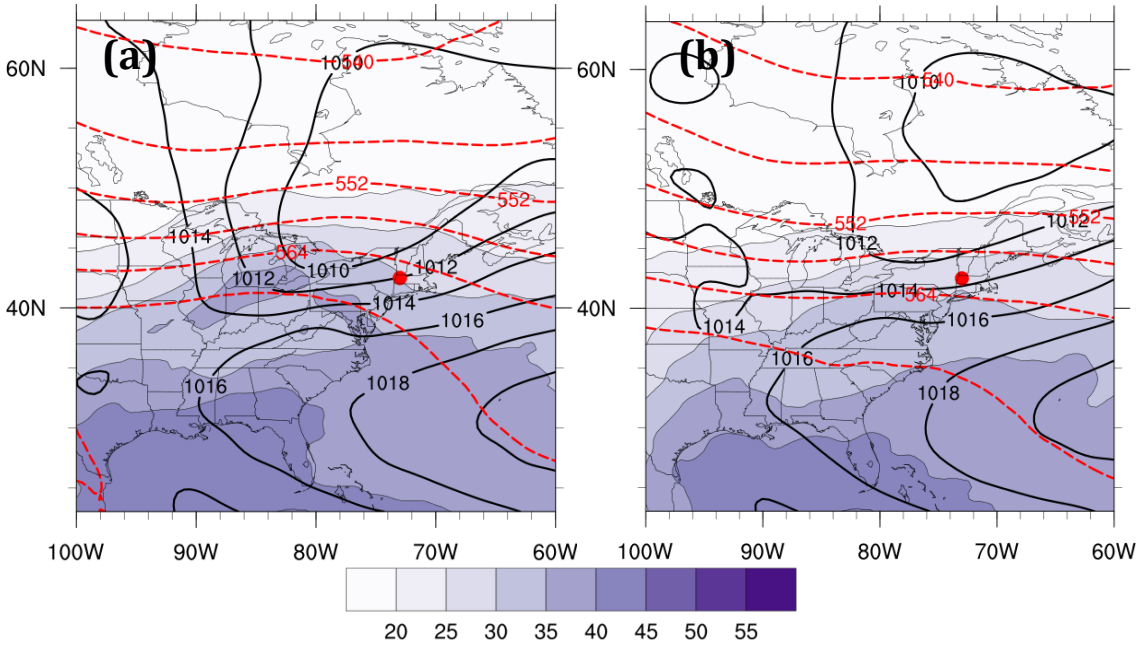

Figure 3.29. As in Fig. 3.21 except for the westerly flow category composite for good (a) events (N = 108) and type 1 (b) events (N = 96). Heavy red dot represents composite center at point of maximum report density.

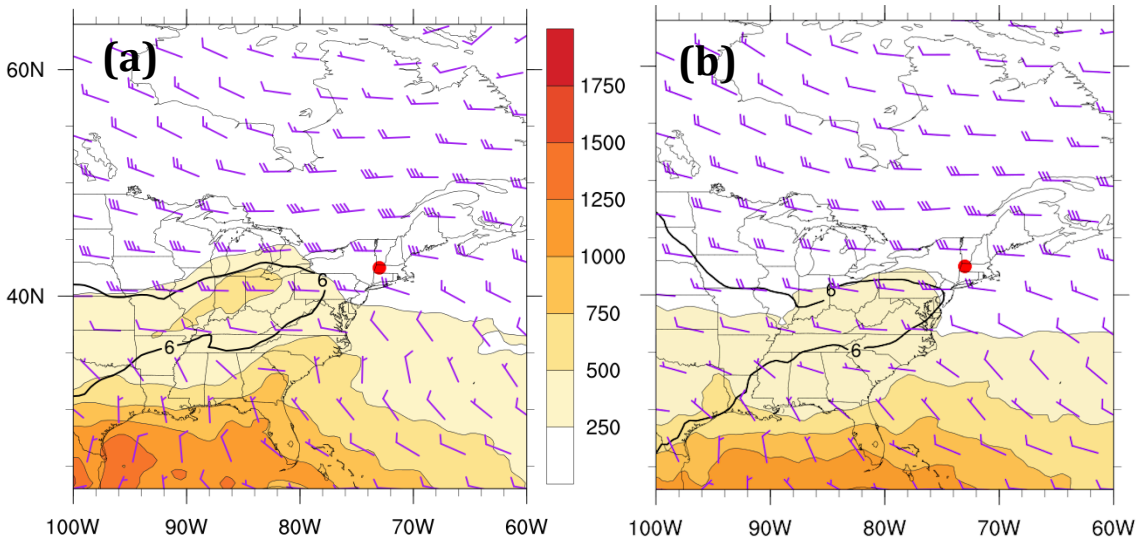

Figure 3.30. As in Fig. 3.22 except for the westerly flow category composite for good (a) events (N = 108) and type 1 (b) events (N = 96). Heavy red dot represents composite center at point of maximum report density.

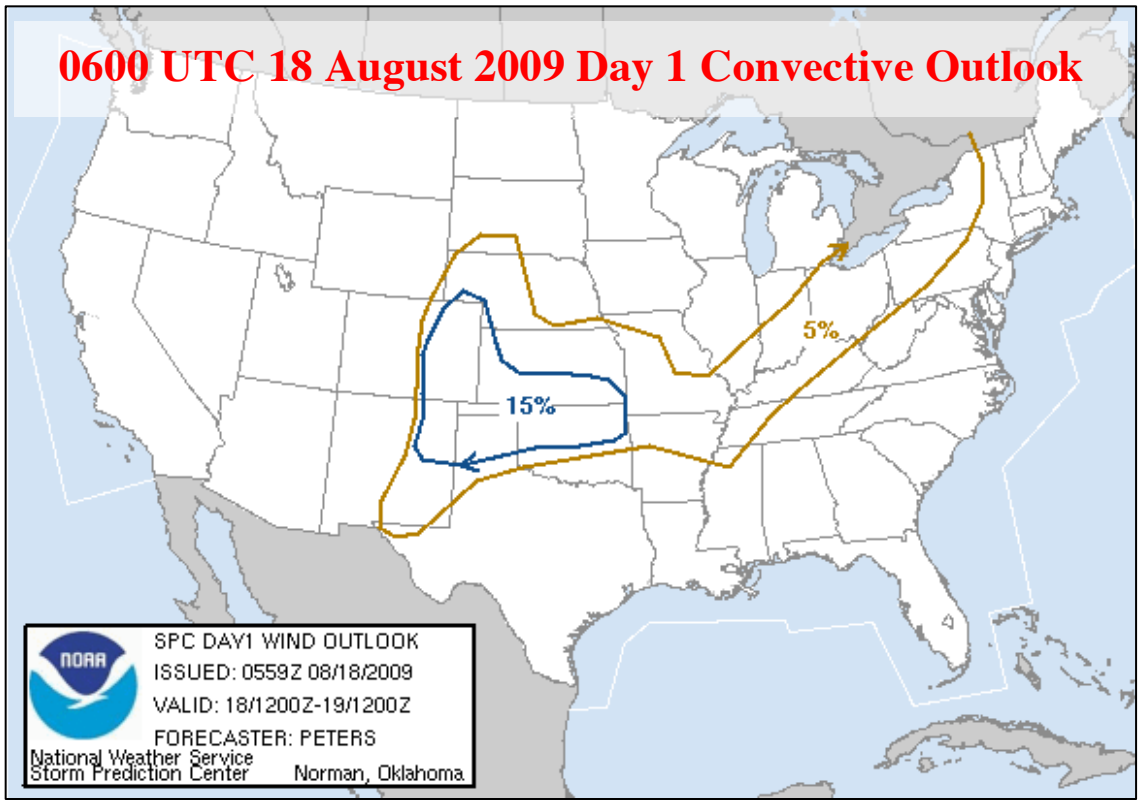

Figure 3.31. SPC 0600 UTC 18 August 2009 severe wind convective outlook valid 1200 UTC 18 August 2009 to 1200 UTC 19 August 2009.

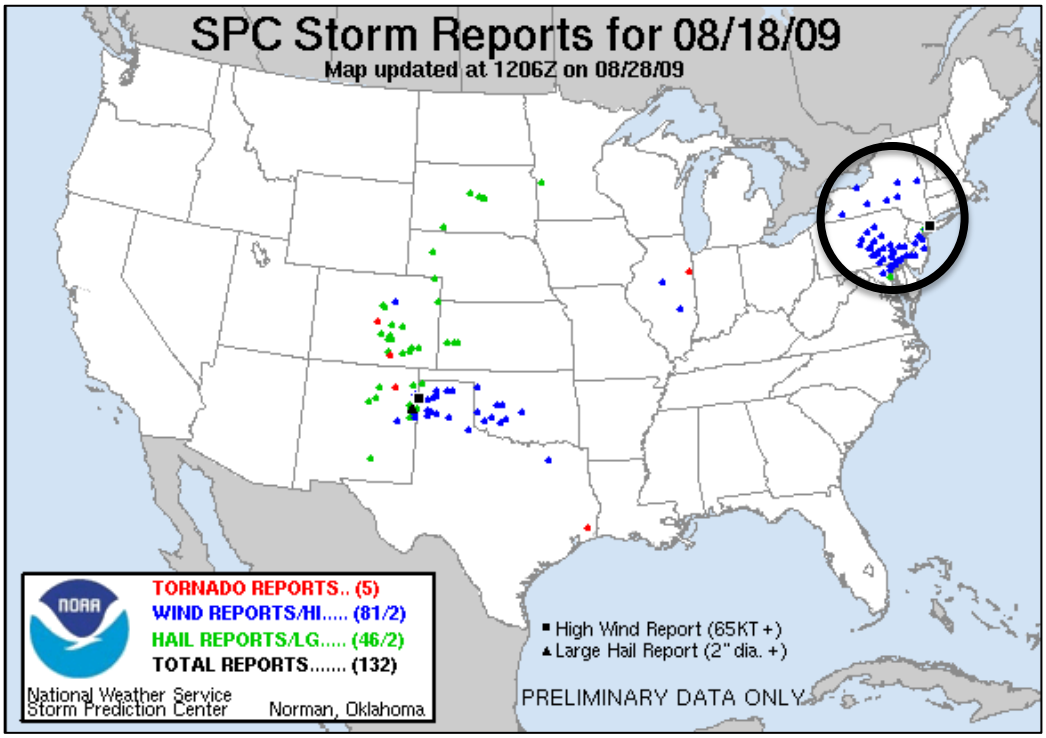

Figure 3.32. Storm reports valid from 1200 UTC 18 August 2010 to 1200 UTC 19 August 2009. Black circle represents area of interest.

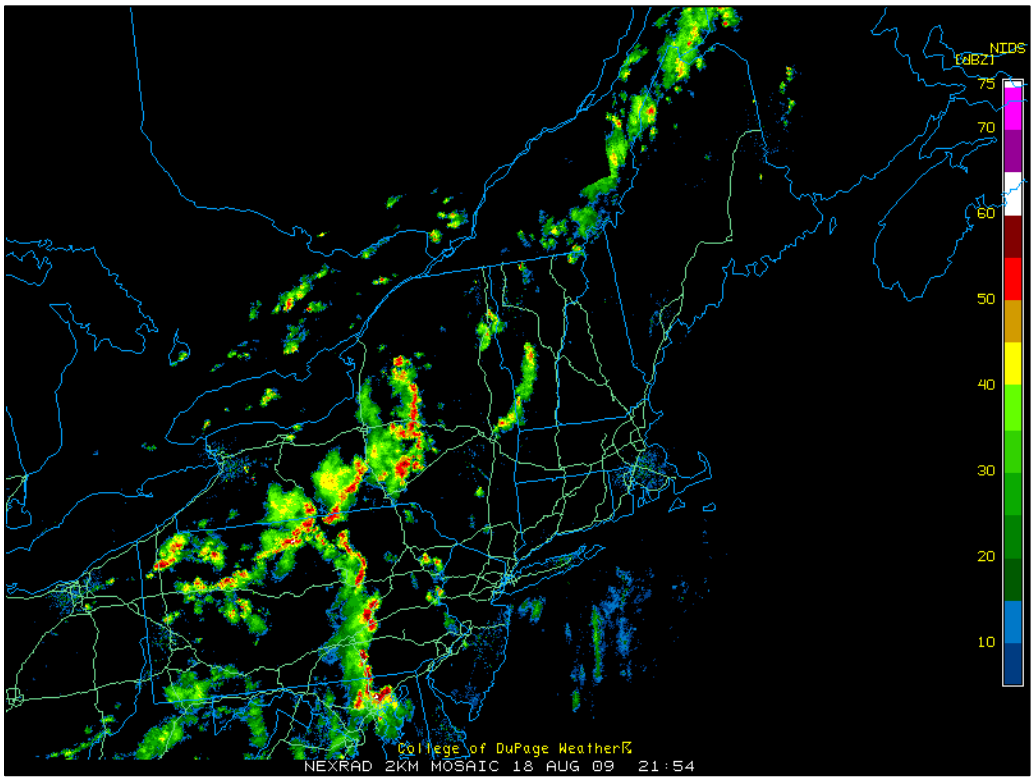

Figure 3.33. Radar reflectivity valid at 2154 UTC 18 August 2009 (source: College of DuPage).

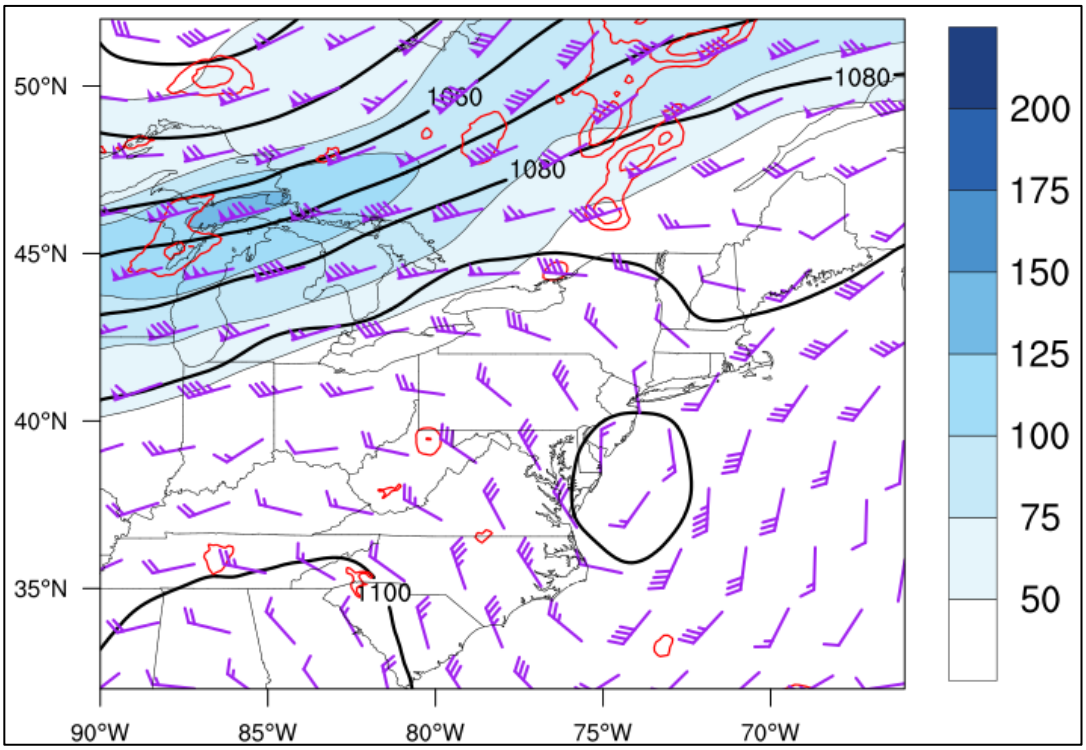

Figure 3.34. 250-hPa geopotential height (black contours, dam), divergence (red contours every 5×10^{-5} s^{-1} starting at 10×10^{-5} s^{-1}), wind speed (fills, kt), and wind barbs (kt) at 1600 UTC 18 August 2009 using RUC model analysis data.

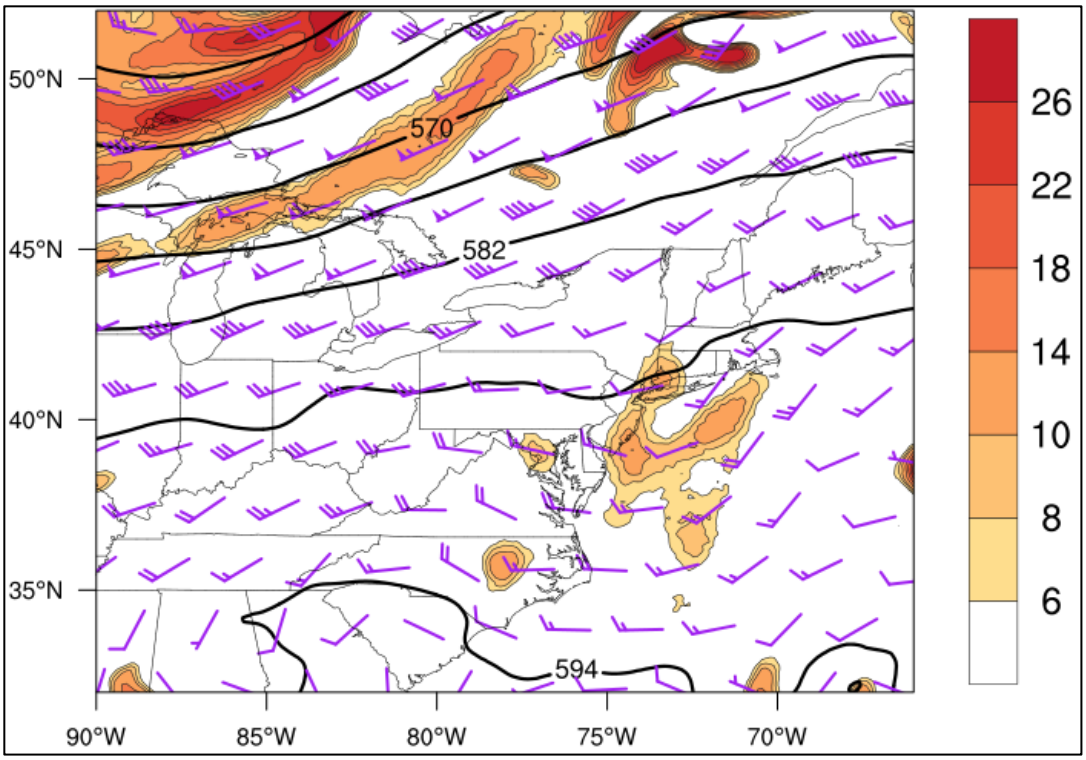

Figure 3.35. 500-hPa geopotential height (black contours, dam), relative vorticity (fills, $\times 10^{-5}$ s^{-1}), and wind barbs (kt) at 1600 UTC 18 August 2009 using RUC model analysis data.

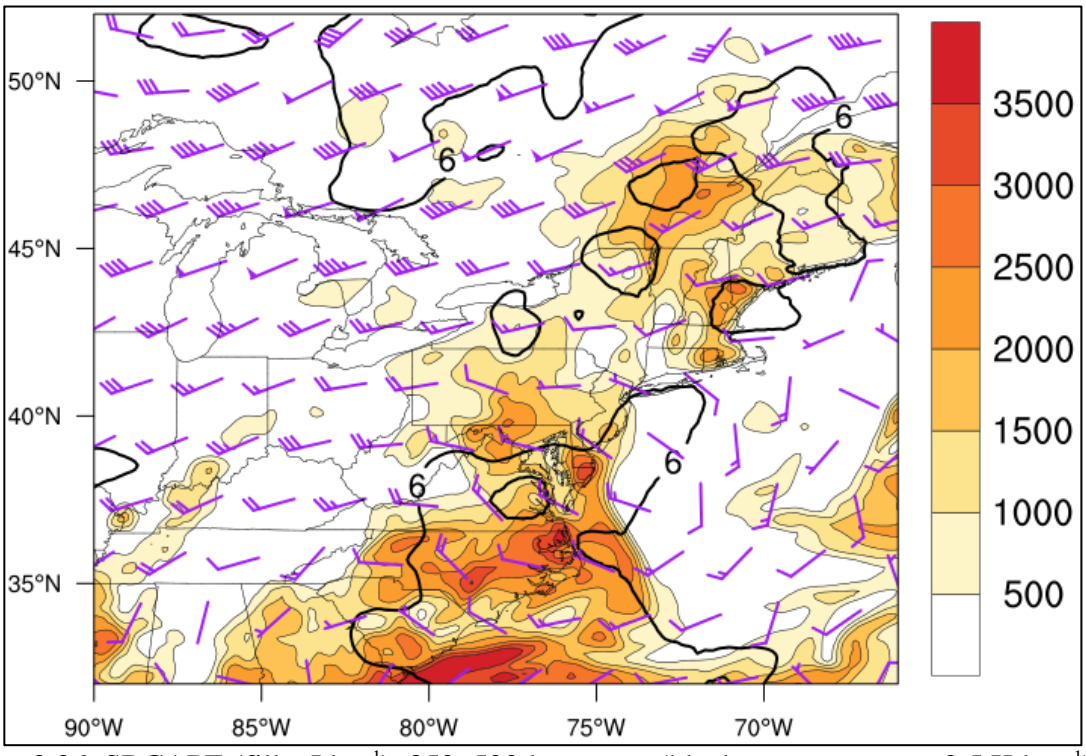

Figure 3.36. SBCAPE (fills, J kg^{-1}), 850–500 lapse rate (black contours every 0.5 K km^{-1}) and 1000–500-hPa shear (barbed, kt) at 1600 UTC 18 August 2009 using RUC model analysis data.

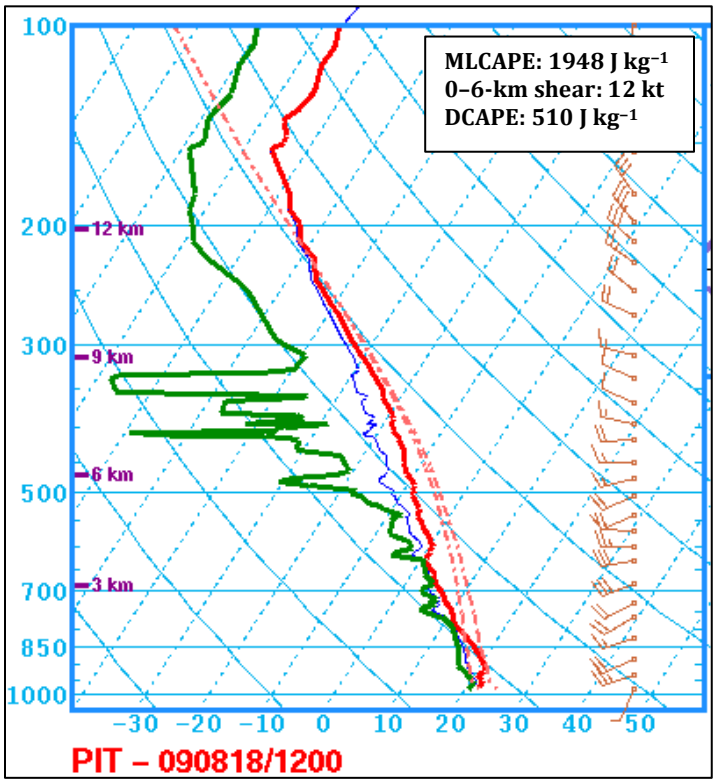

Figure 3.37. Sounding at PIT valid at 1200 UTC 18 August 2009 (source: SPC).

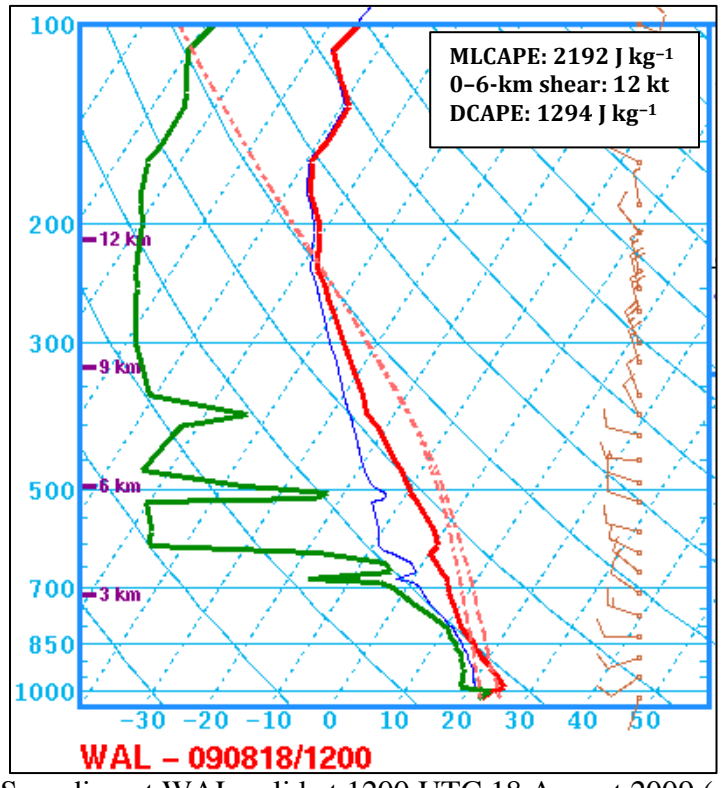

Figure 3.38. Sounding at WAL valid at 1200 UTC 18 August 2009 (source: SPC).

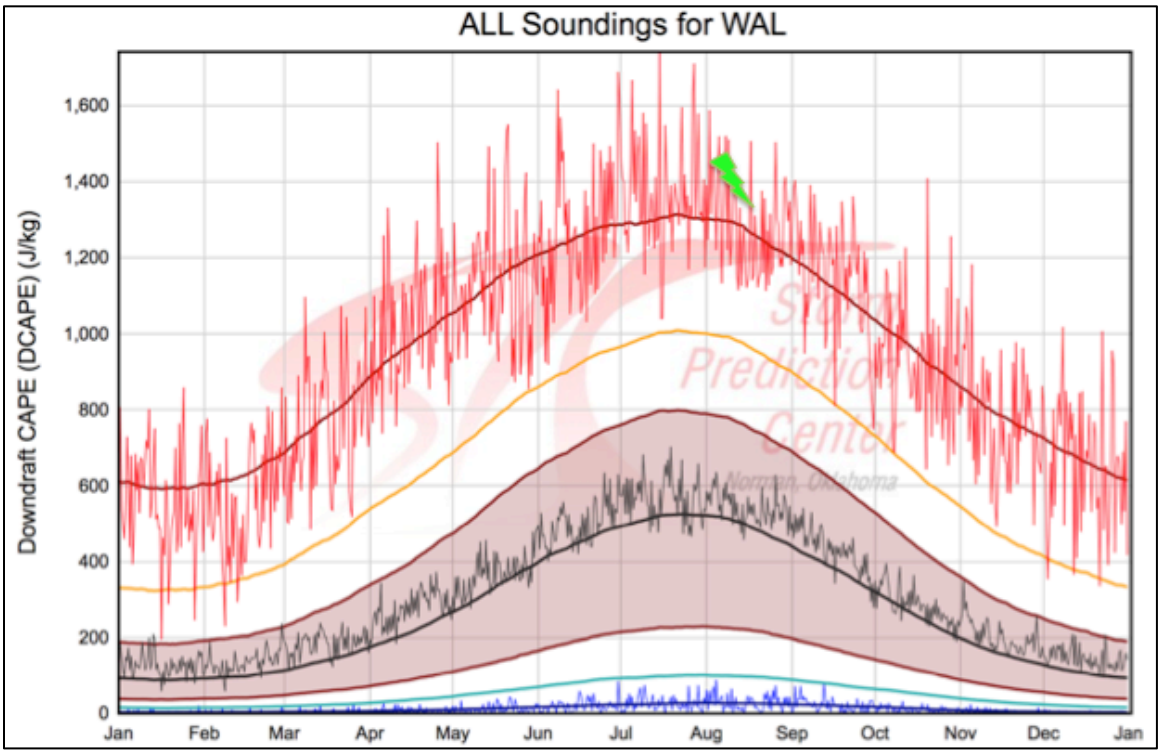

Figure 3.39. DCAPE climatology at WAL. Dark red line represents the maximum 91-day moving average while the thin red line is the daily maximum. Green bolt represents the observed value at 1200 UTC 18 August 2009 (source: SPC).

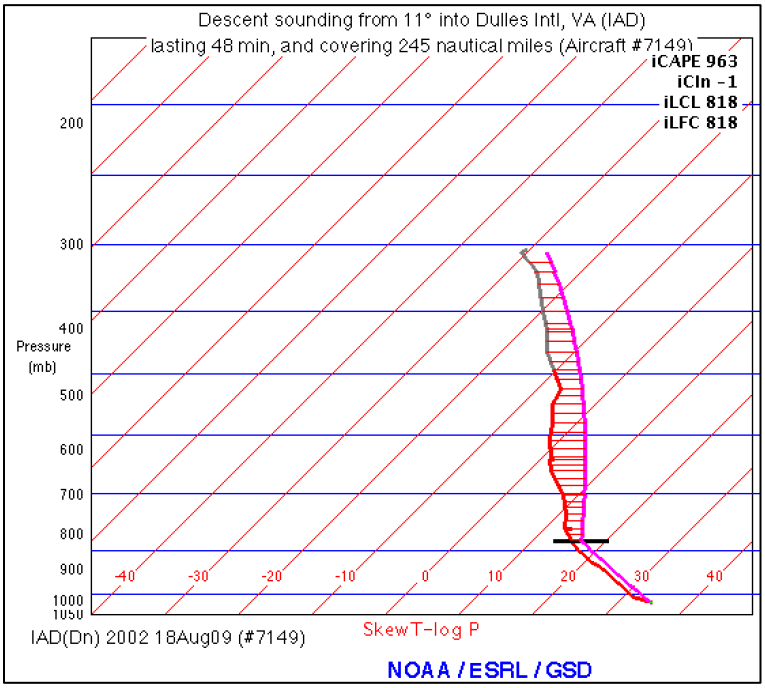

Figure 3.40. Aircraft sounding and computed parcel path using METAR data valid at 2002 UTC 18 August 2009. Sounding is located at IAD.

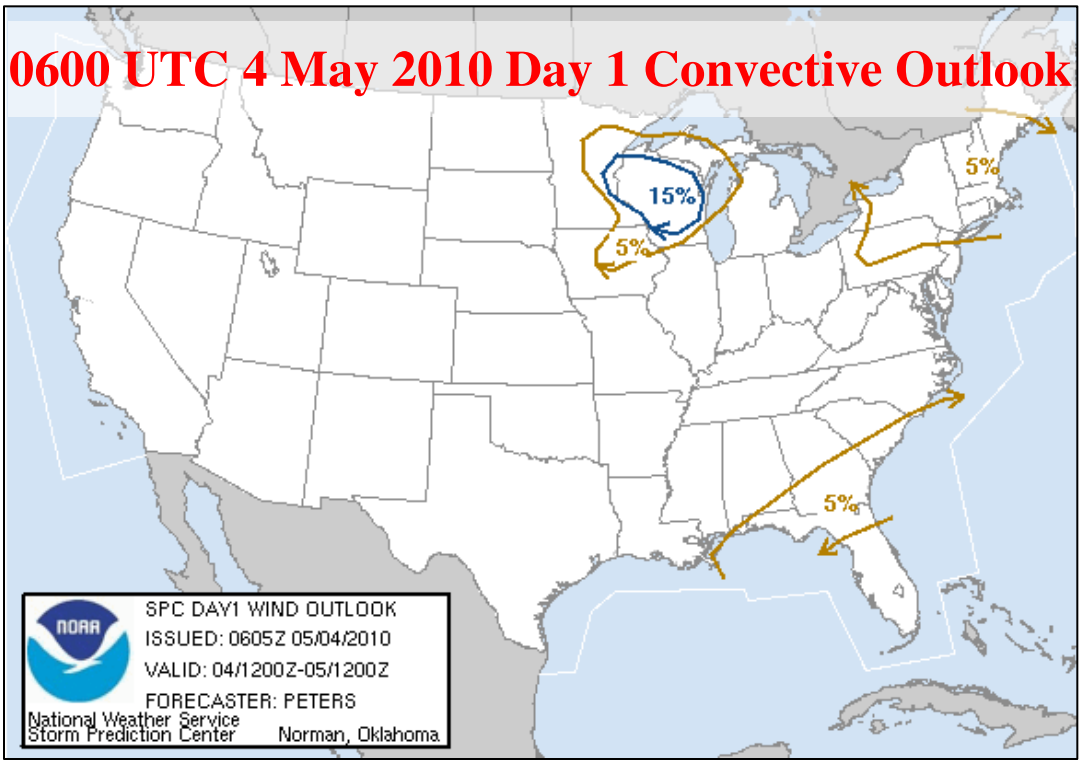

Figure 3.41. SPC 0600 UTC 4 May 2010 severe wind convective outlook valid 1200 UTC 4 May 2010 to 1200 UTC 5 May 2010.

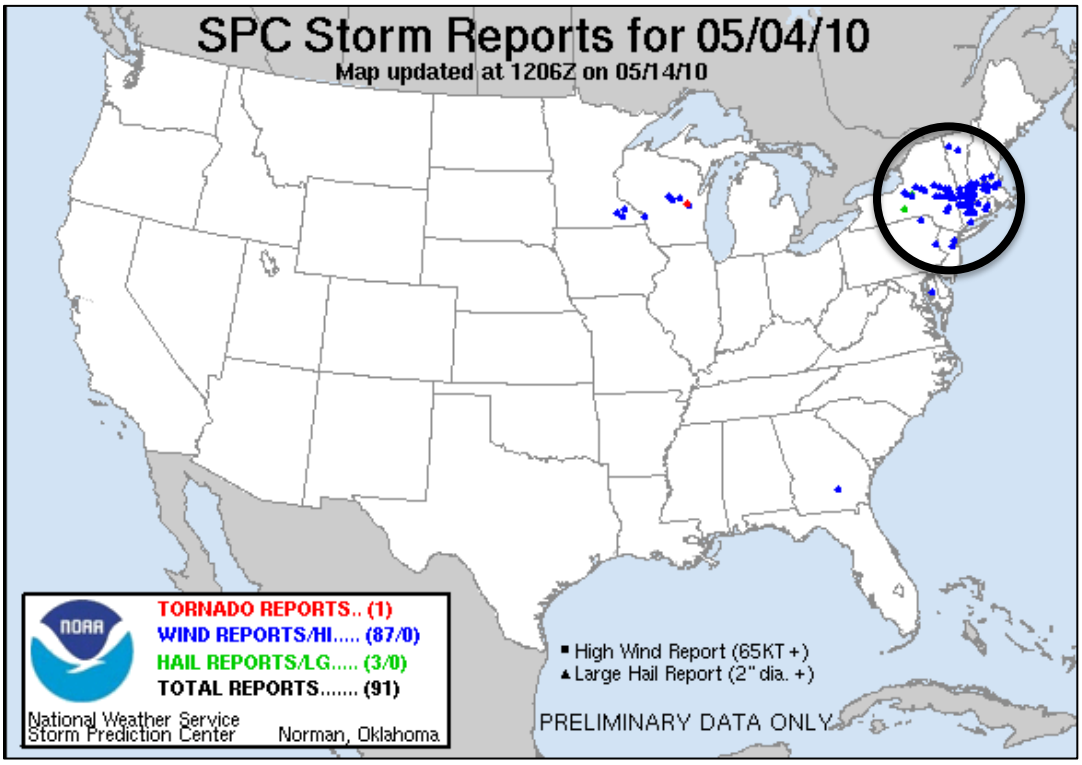

Figure 3.42. Storm reports valid 1200 UTC 4 May 2010 to 1200 UTC 5 May 2010. Black circle represents area of interest.

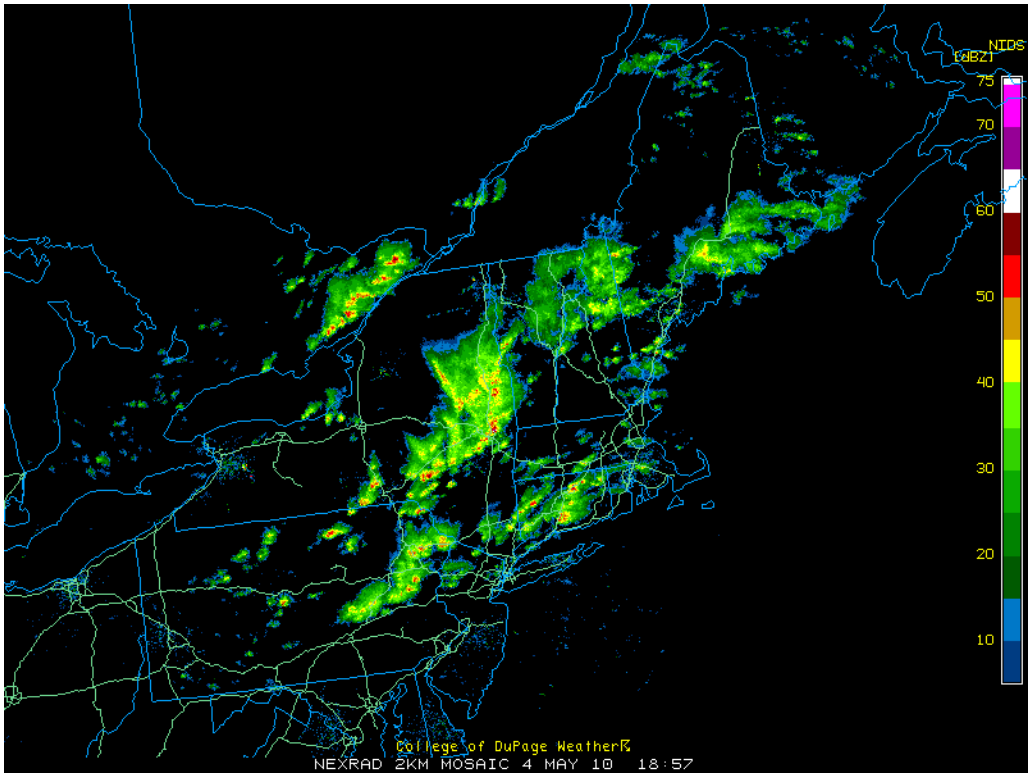

Figure 3.43. Radar reflectivity valid at 1857 UTC 4 May 2010 (source: College of DuPage).

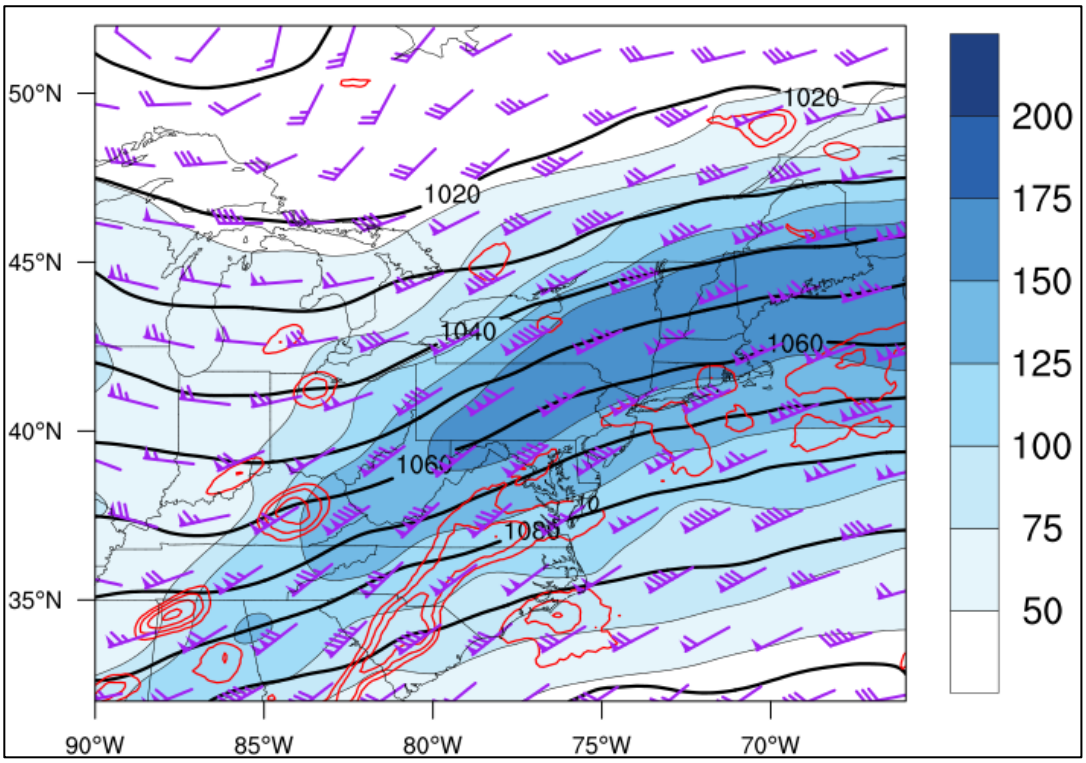

Figure 3.44. As in Fig. 3.34 but for 1400 UTC 4 May 2010.

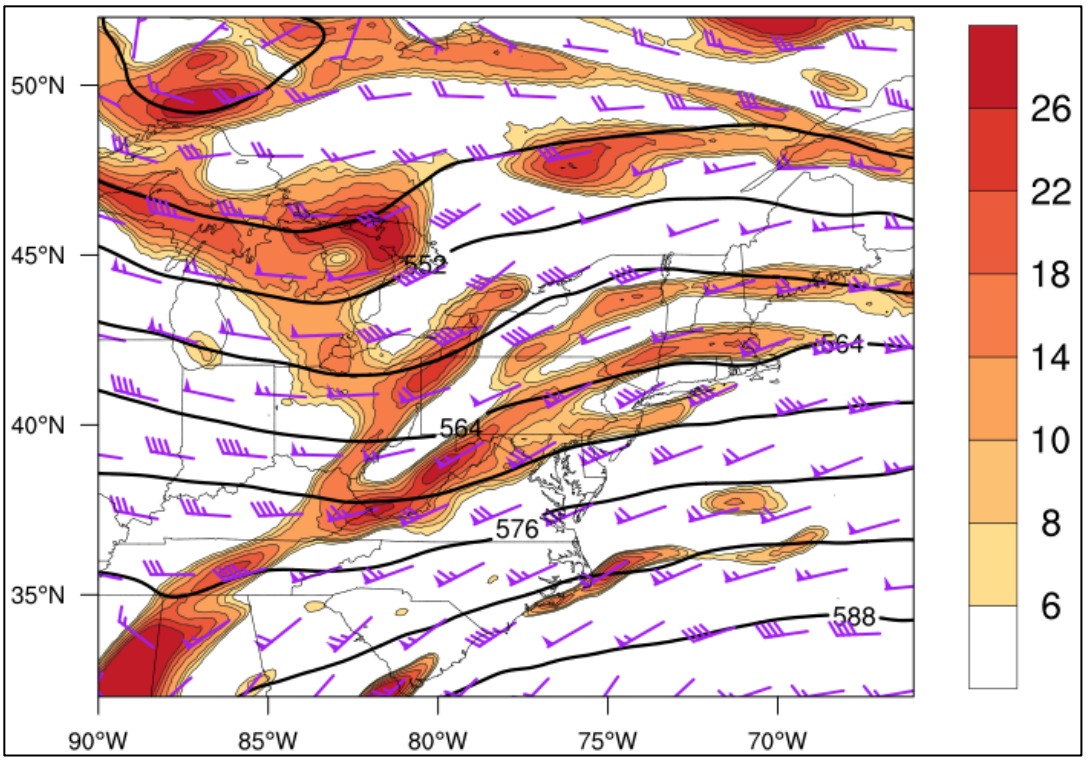

Figure 3.45. As in Fig. 3.35 but for 1400 UTC 4 May 2010.

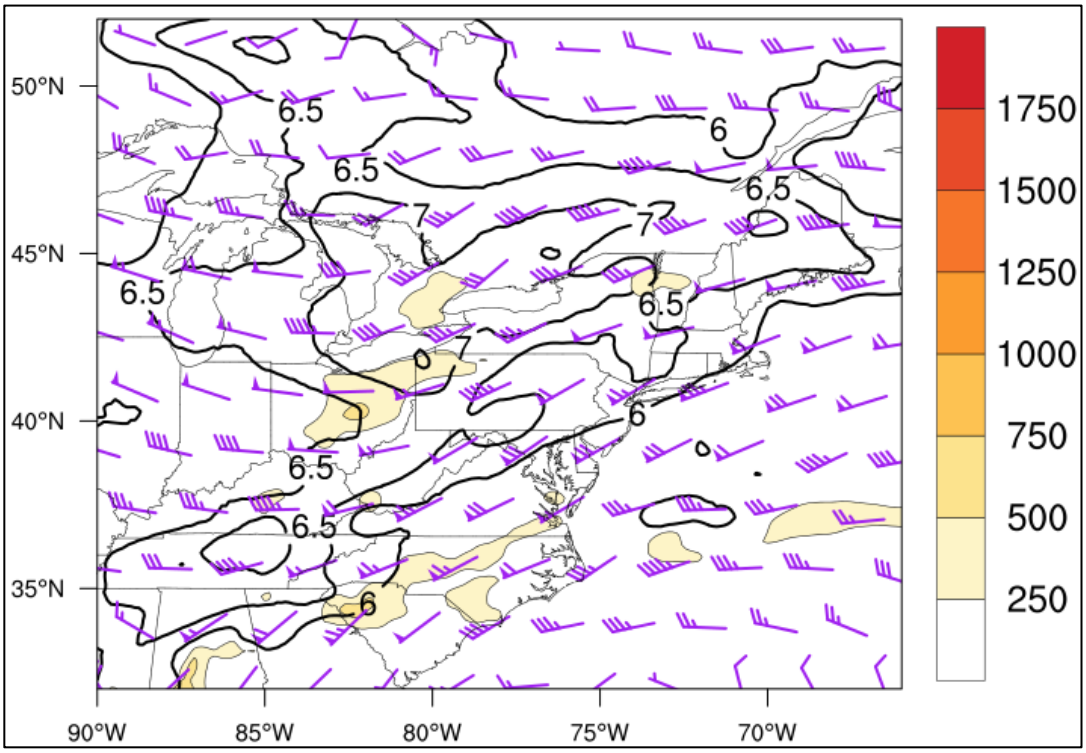

Figure 3.46. As in Fig. 3.36 but for 1400 UTC 4 May 2010.

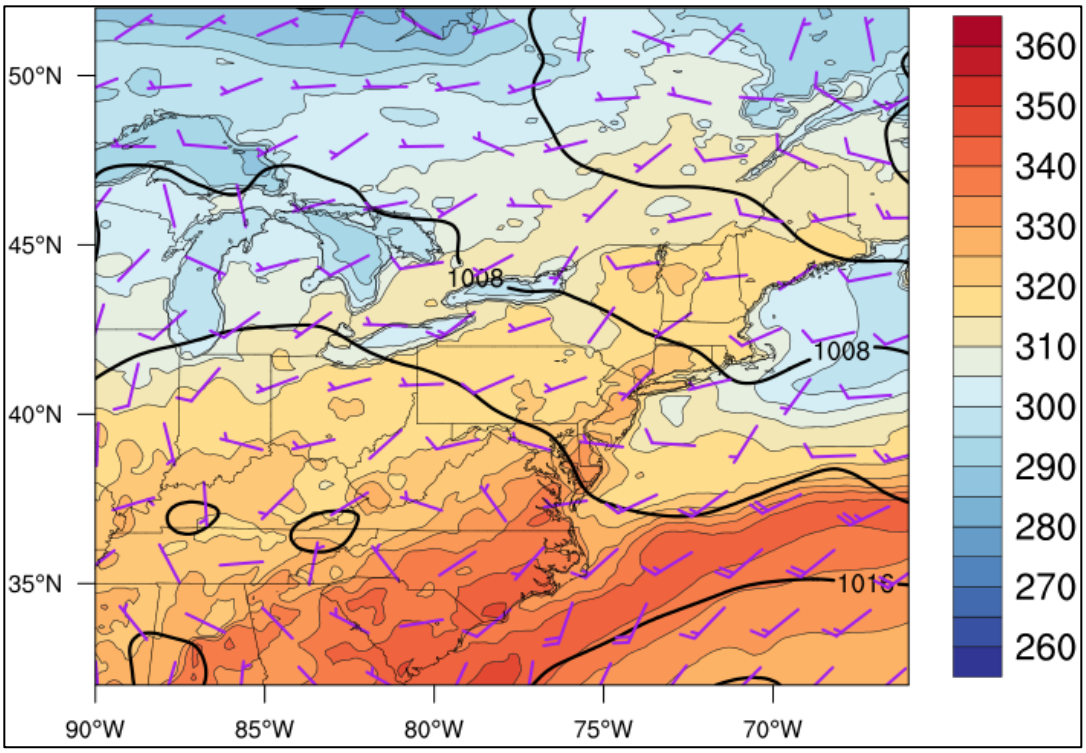

Figure 3.47. Surface equivalent potential temperature (fills, K), MSLP (black contours every 4 hPa), and surface winds (barbed, kt) valid at 1400 UTC 4 May 2010.

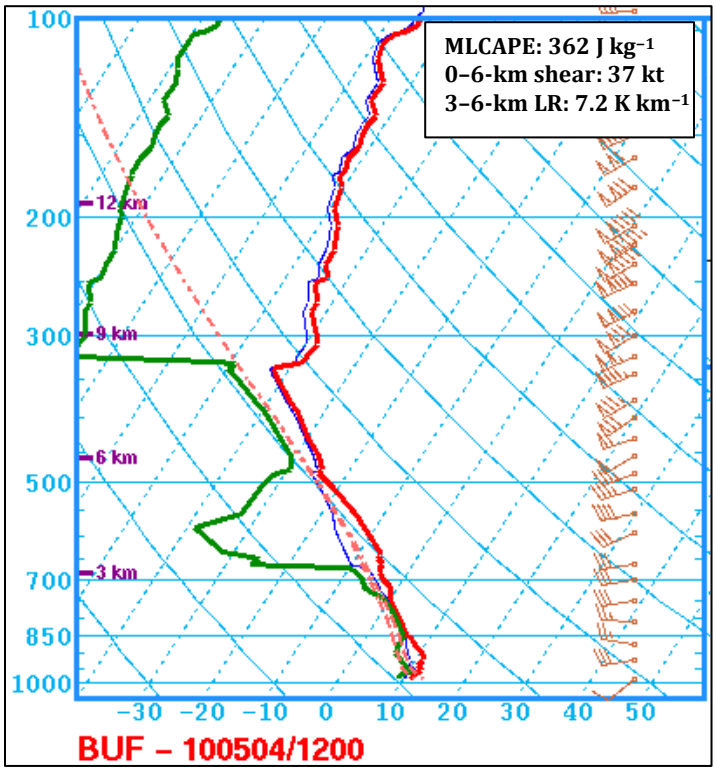

Figure 3.48. Sounding at BUF valid at 1200 UTC 4 May 2010 (source: SPC).

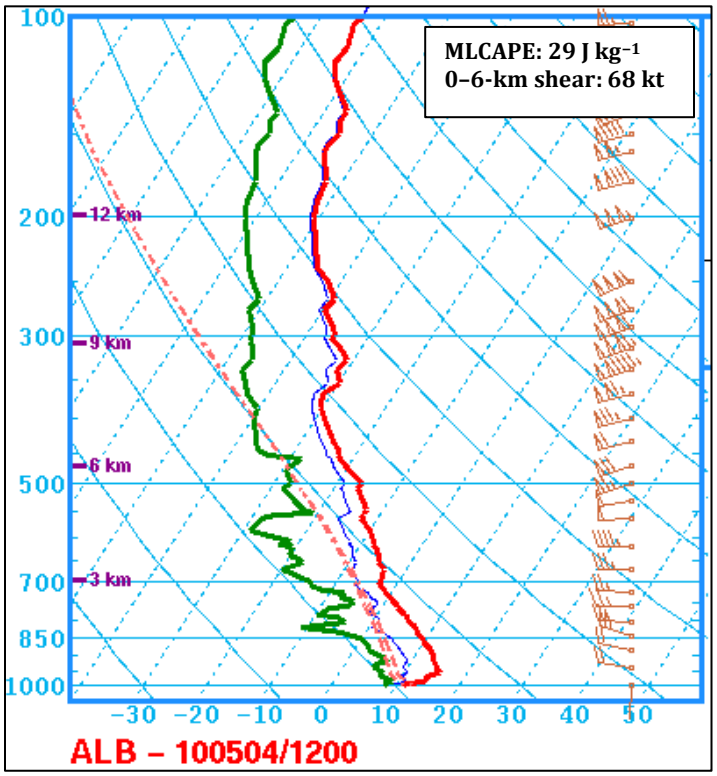

Figure 3.49. Sounding at ALB valid at 1200 UTC 4 May 2010 (source: SPC).

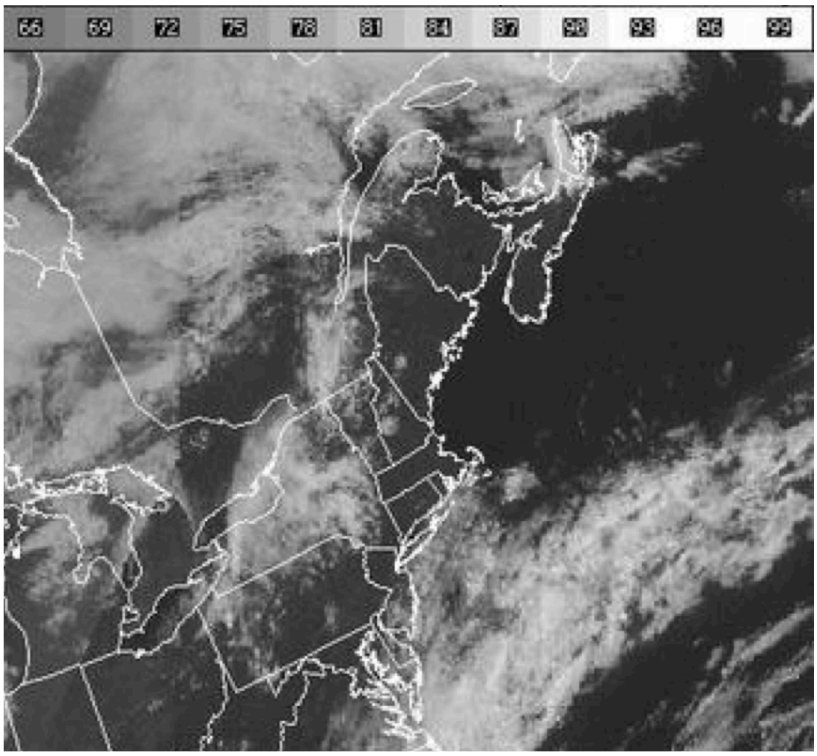

Figure 3.50. Visible satellite imagery valid at 1415 UTC 4 May 2010.

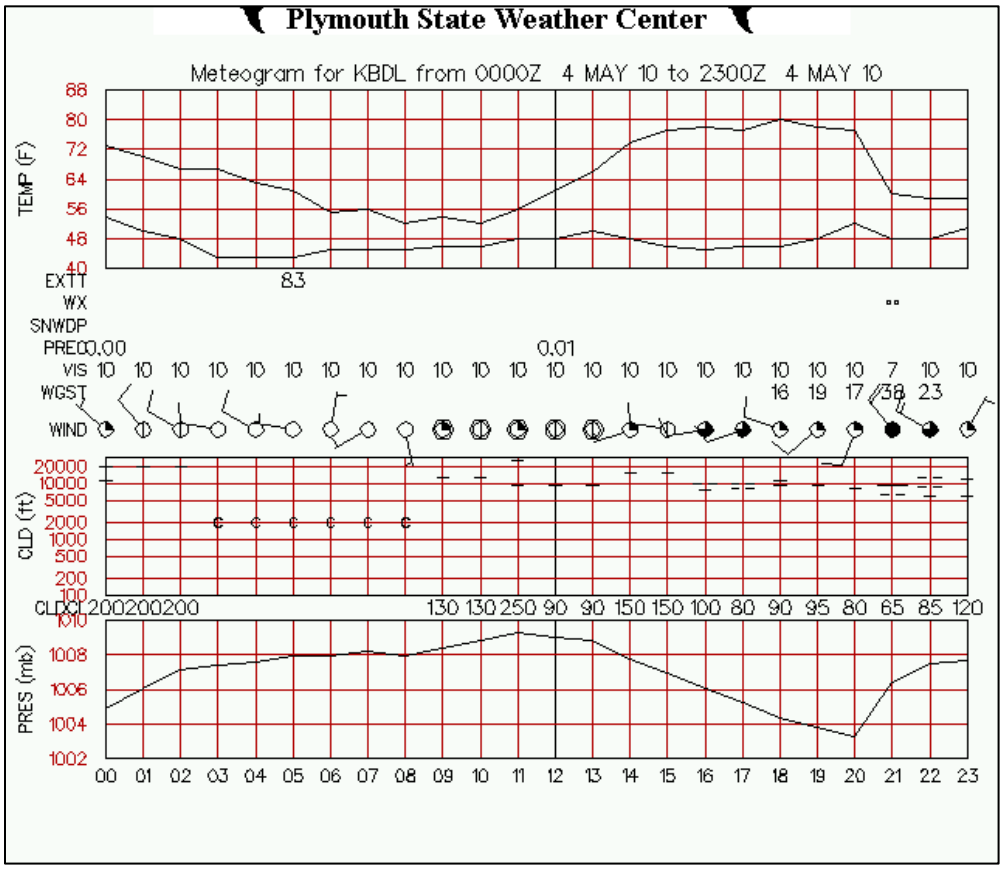

Figure 3.51. Meteogram for BDL valid from 0000 UTC 4 May 2010 to 2300 UTC 4 May 2010. Wind speeds are in knots (source: Plymouth State College).

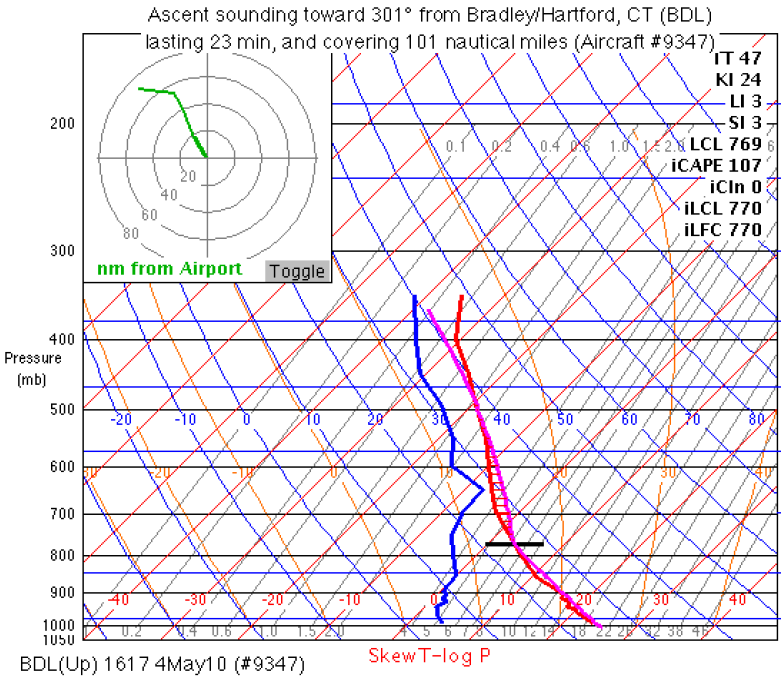

Figure 3.52. Aircraft sounding and computed parcel path using valid METAR data at 1617 UTC 4 May 2010. Sounding is located at BDL.

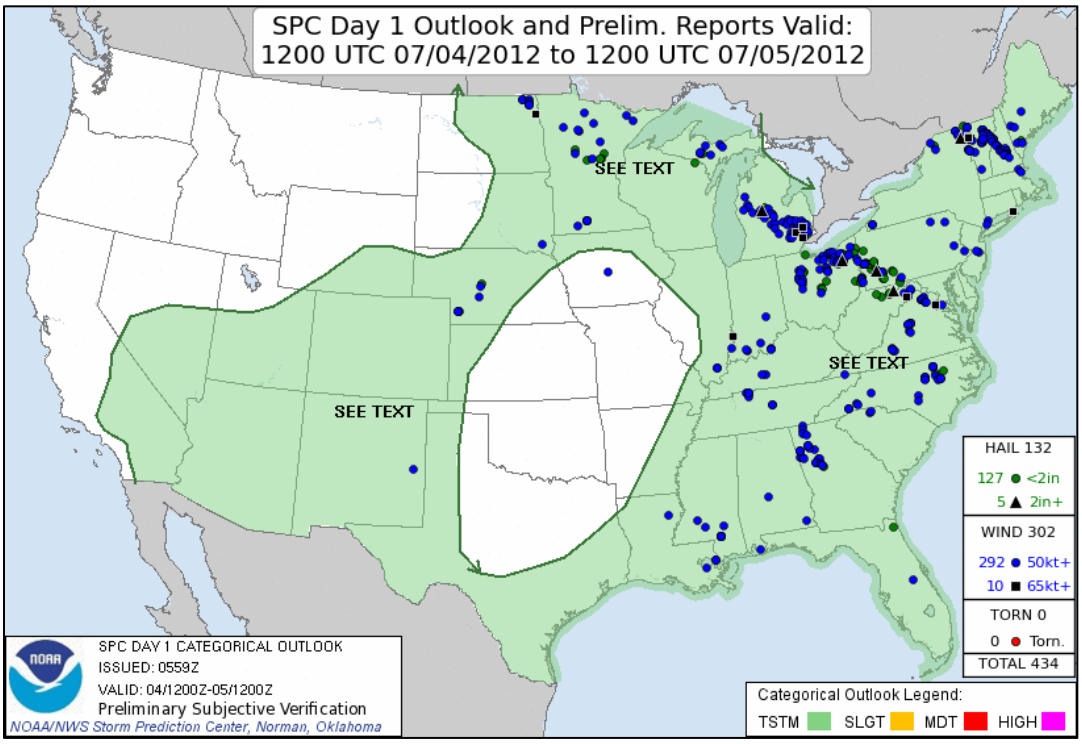

Figure 3.53. SPC 0600 UTC 4 July 2012 severe wind convective outlook valid 1200 UTC 4 July 2012 to 1200 UTC 5 July 2012.

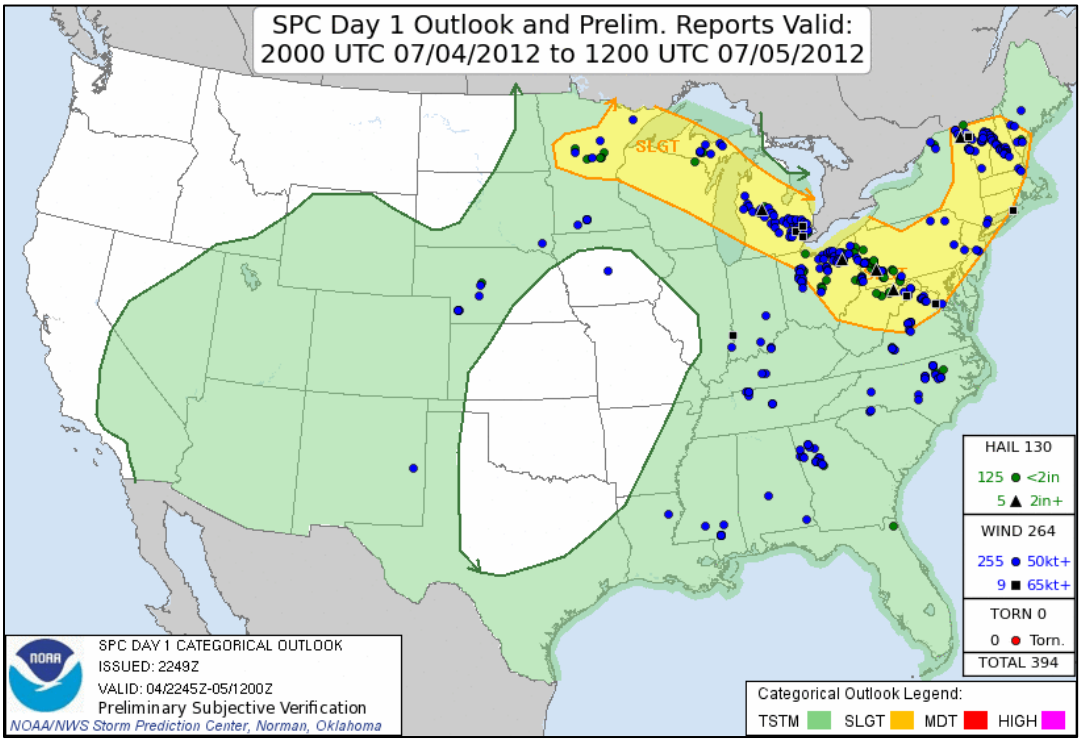

Figure 3.54. SPC 2000 UTC 4 July 2012 severe wind convective outlook valid 2000 UTC 4 July 2012 to 1200 UTC 5 July 2012.

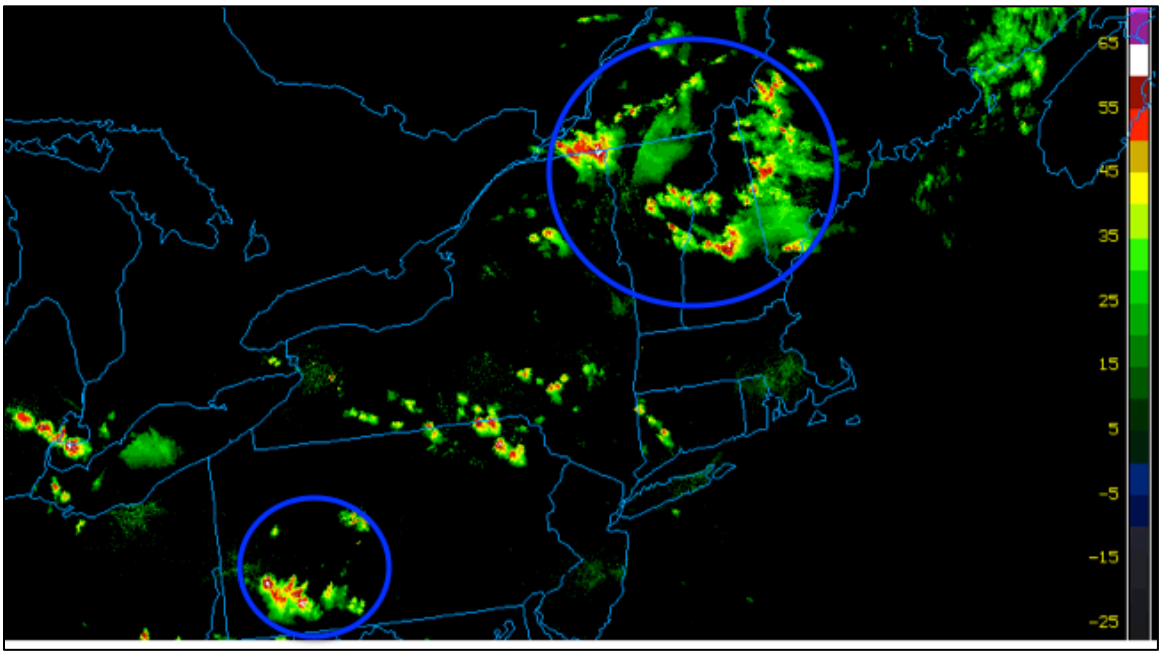

Figure 3.55. Radar reflectivity valid at 2230 UTC 4 July 2012. Blue circles outline the most prolific severe storms (source: College of DuPage).

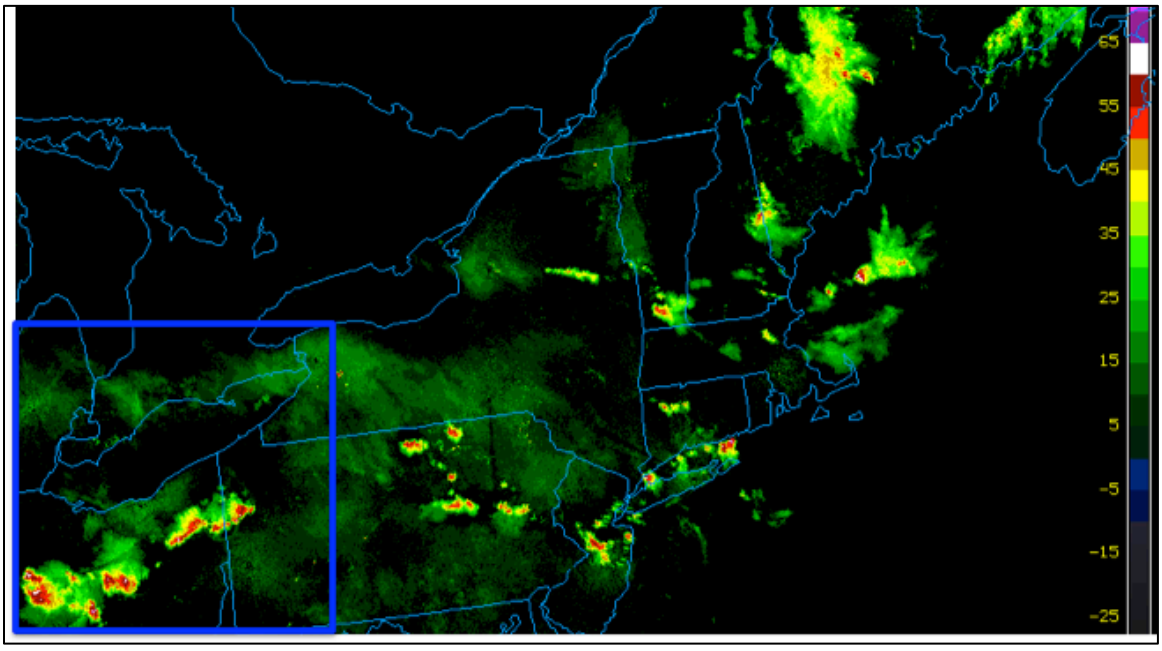

Figure 3.56. Radar reflectivity valid at 0230 UTC 5 July 2012. Blue square outlines the area containing the most prolific severe storms (source: College of DuPage).

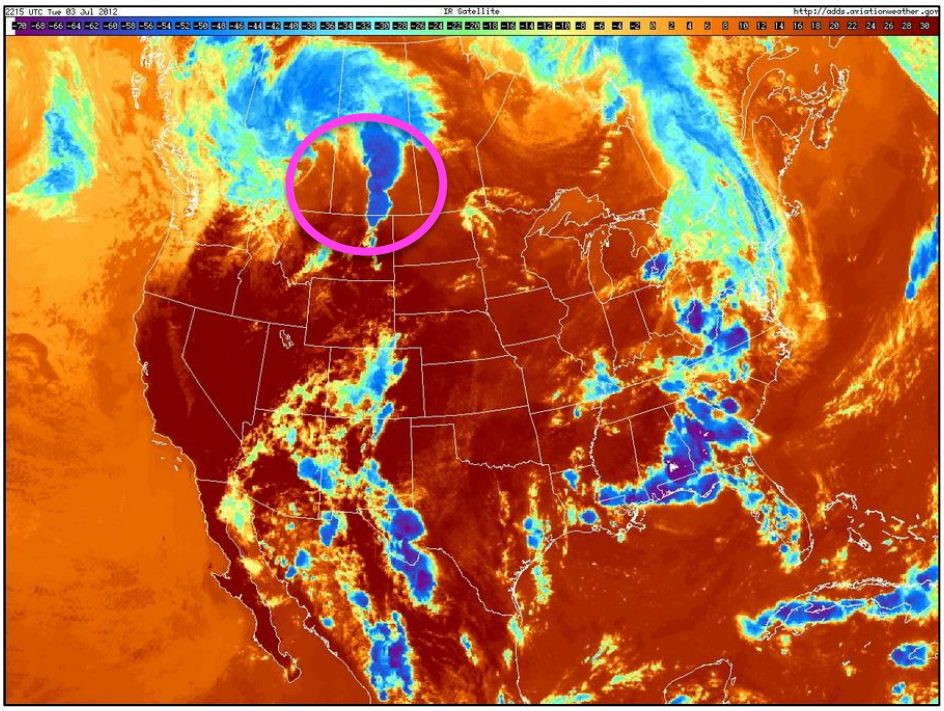

Figure 3.57. Infrared satellite imagery valid at 2215 UTC 3 July 2012. Magenta circle outlines the developing MCS in Saskatchewan.

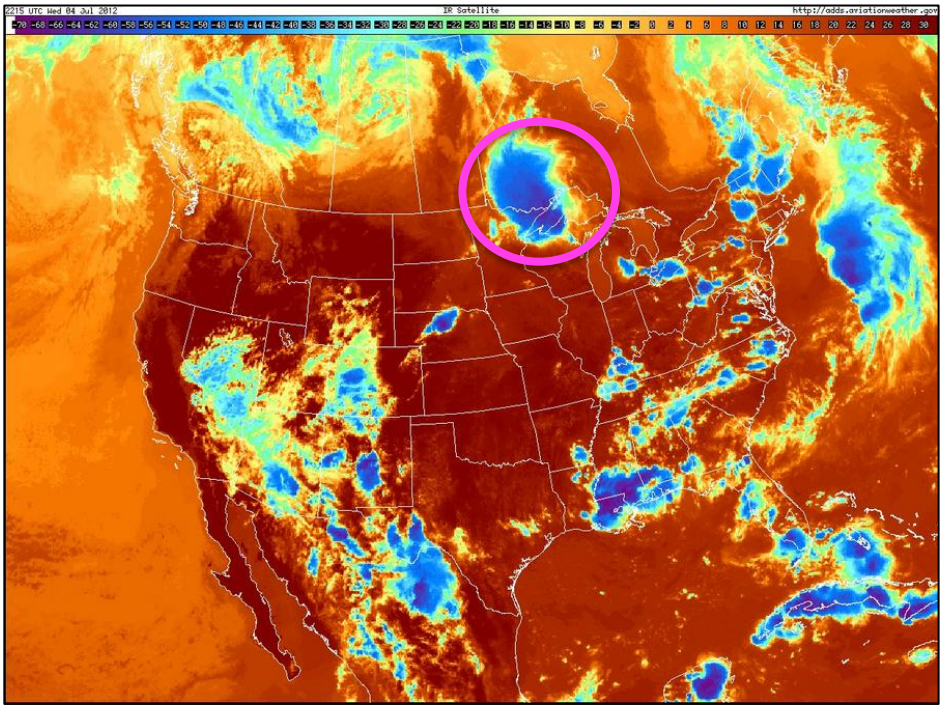

Figure 3.58. Infrared satellite imagery valid at 2215 UTC 4 July 2012. Magenta circle outlines the mature MCS over Ontario and the northern Great Lakes.

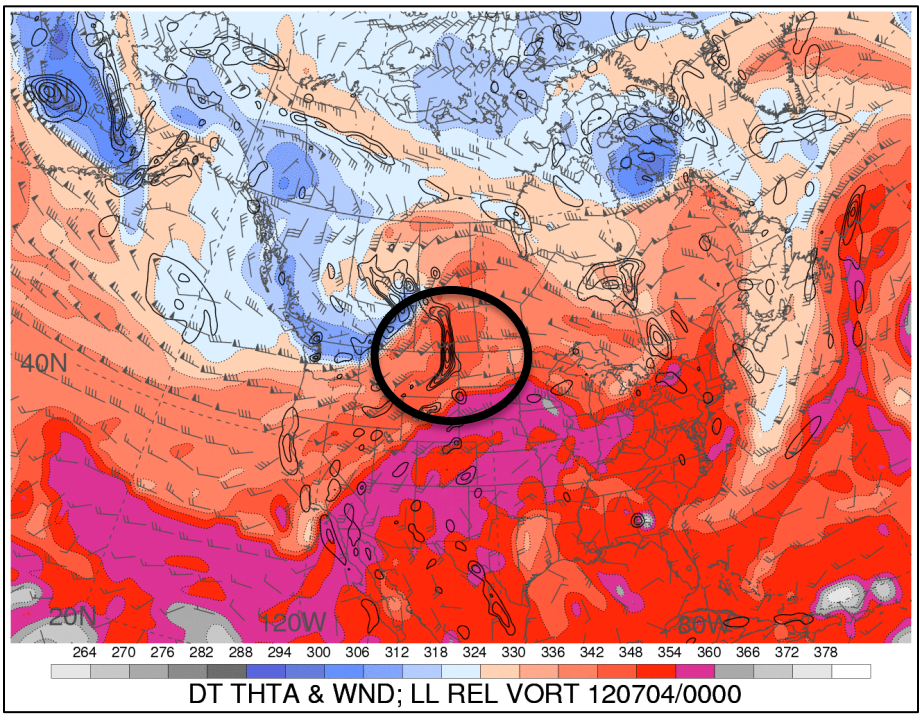

Figure 3.59. Dynamic tropopause (1.5-PVU surface) potential temperature (shaded, K) and wind barbs (kt), 925–850-hPa layer-averaged cyclonic relative vorticity (black contours, every 0.5 x 10^{-4} s^{-1}) at 0000 UTC 4 July 2012. Black circle outlines developing MCS. [Source: Heather Archambault]

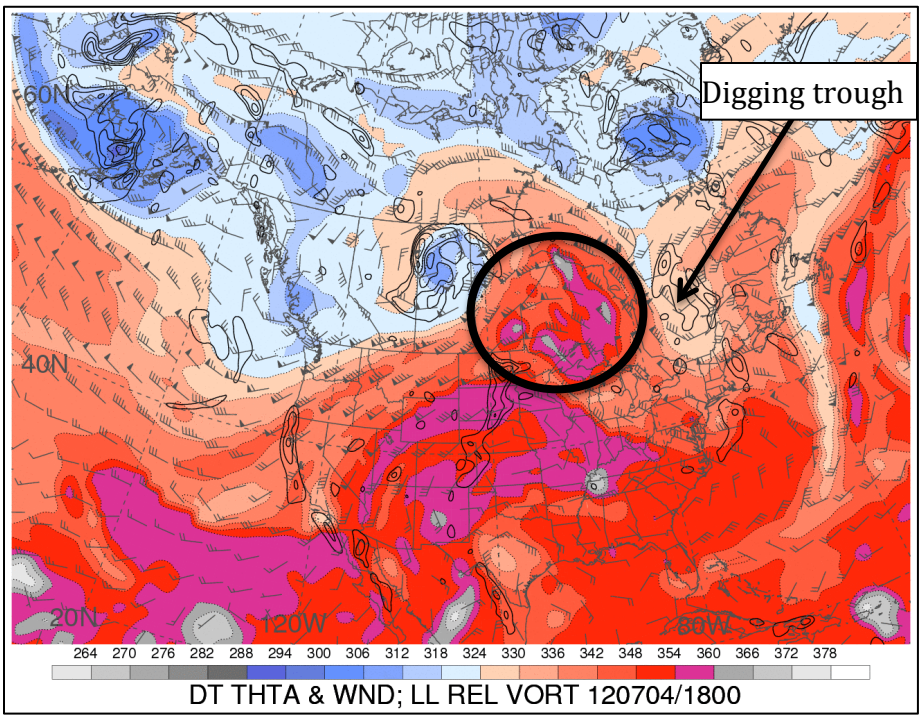

Figure 3.60. As in Fig. 3.58 but at 1800 UTC 4 July 2012. Black circle outlines the ridge strengthened by latent heating associated with convection. [Source: Heather Archambault]

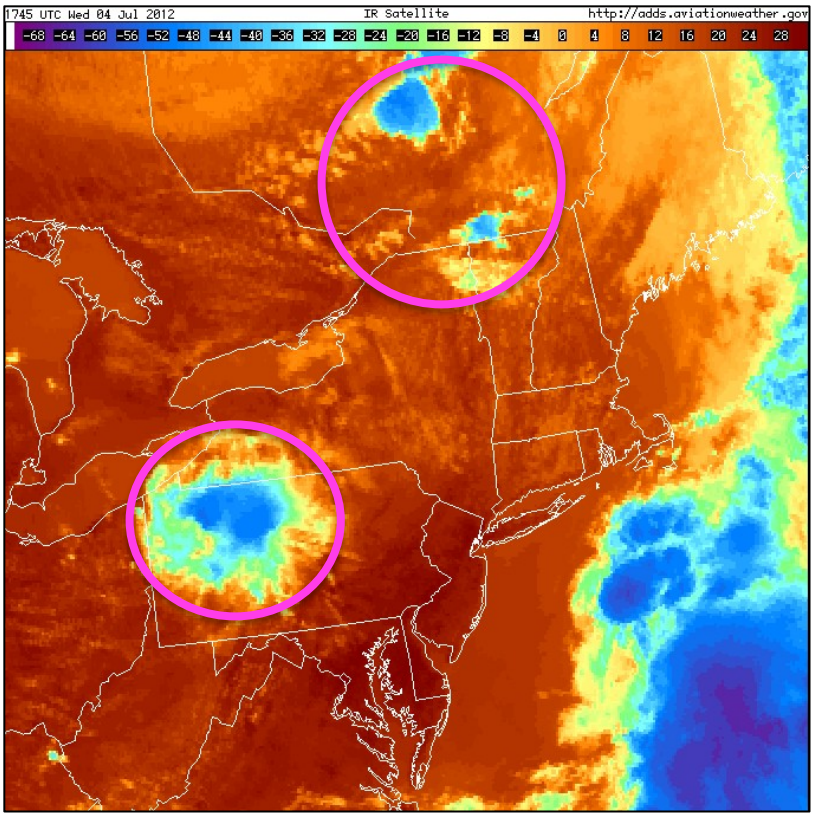

Figure 3.61. Infrared satellite imagery valid at 1745 UTC 4 July 2012. Magenta circles outlines the incipient convection in Quebec (top) and the remnant MCV over PA (bottom).

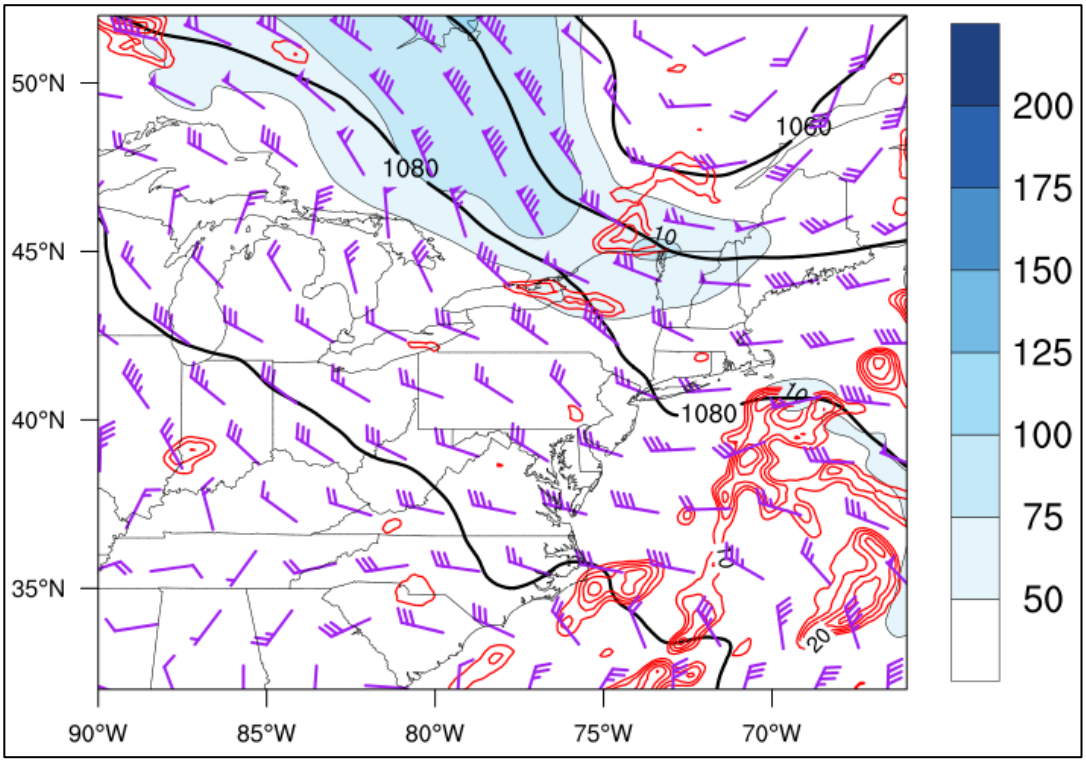

Figure 3.62. As in Fig. 3.34 but at 1800 UTC 4 July 2012 using RAP model analysis data.

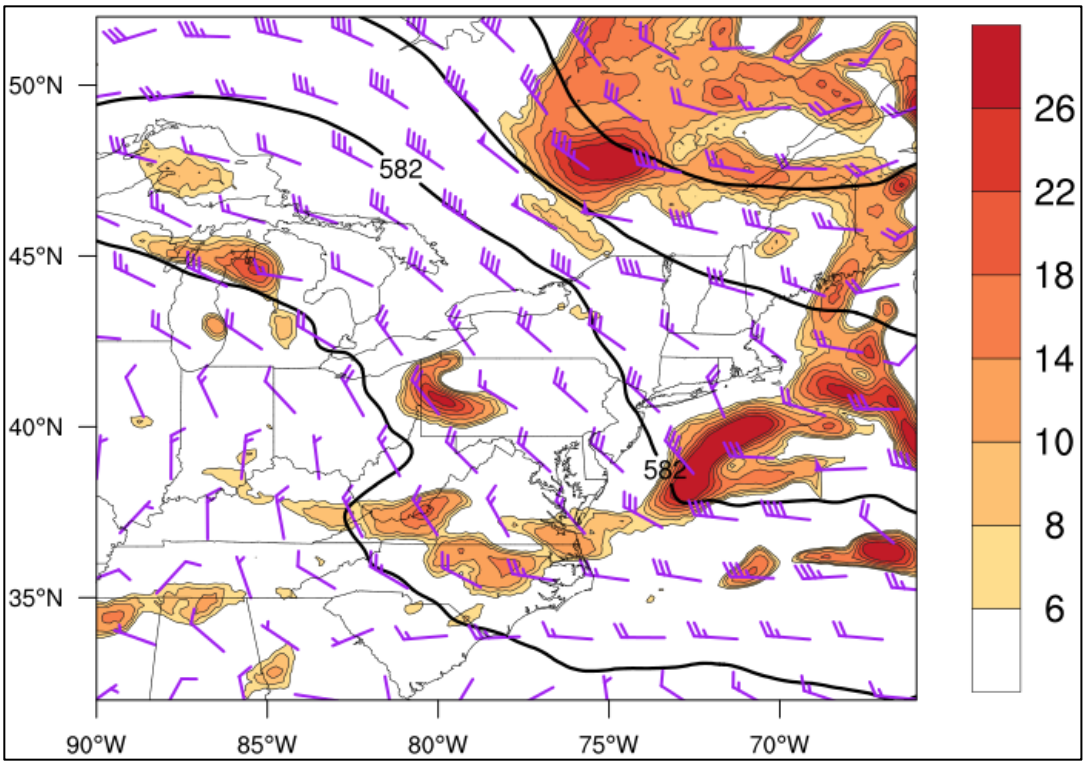

Figure 3.63. As in Fig. 3.35 but at 1800 UTC 4 July 2012.

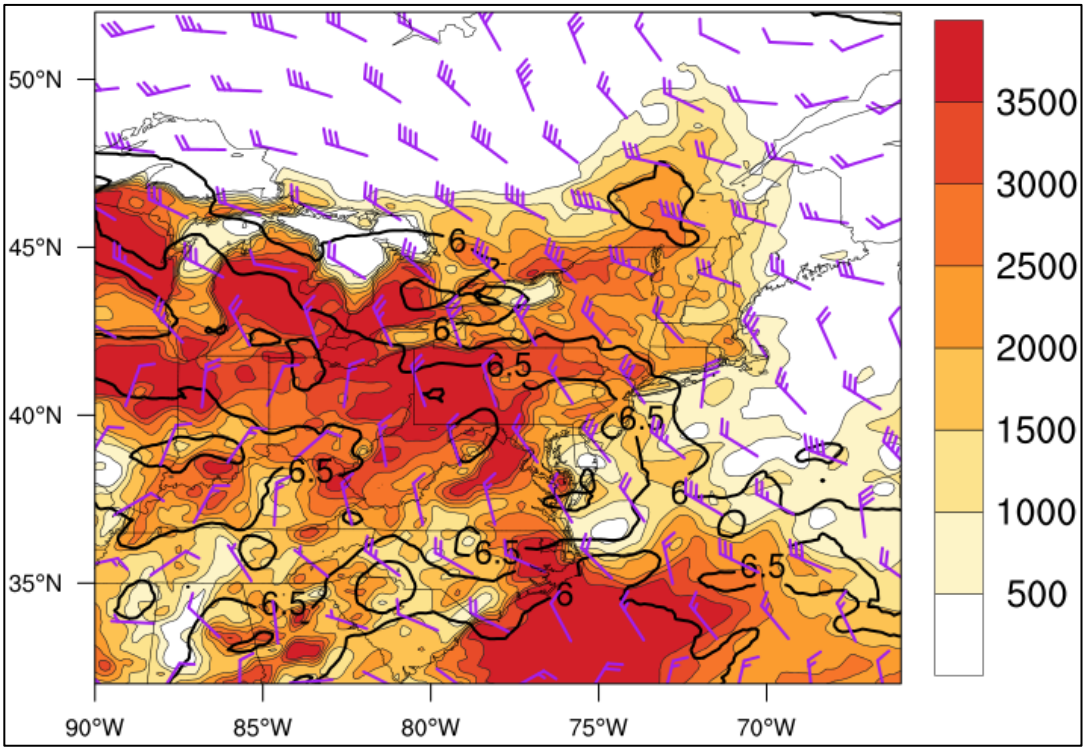

Figure 3.64. As in Fig. 3.36 but at 1800 UTC 4 July 2012 using RAP model analysis data.

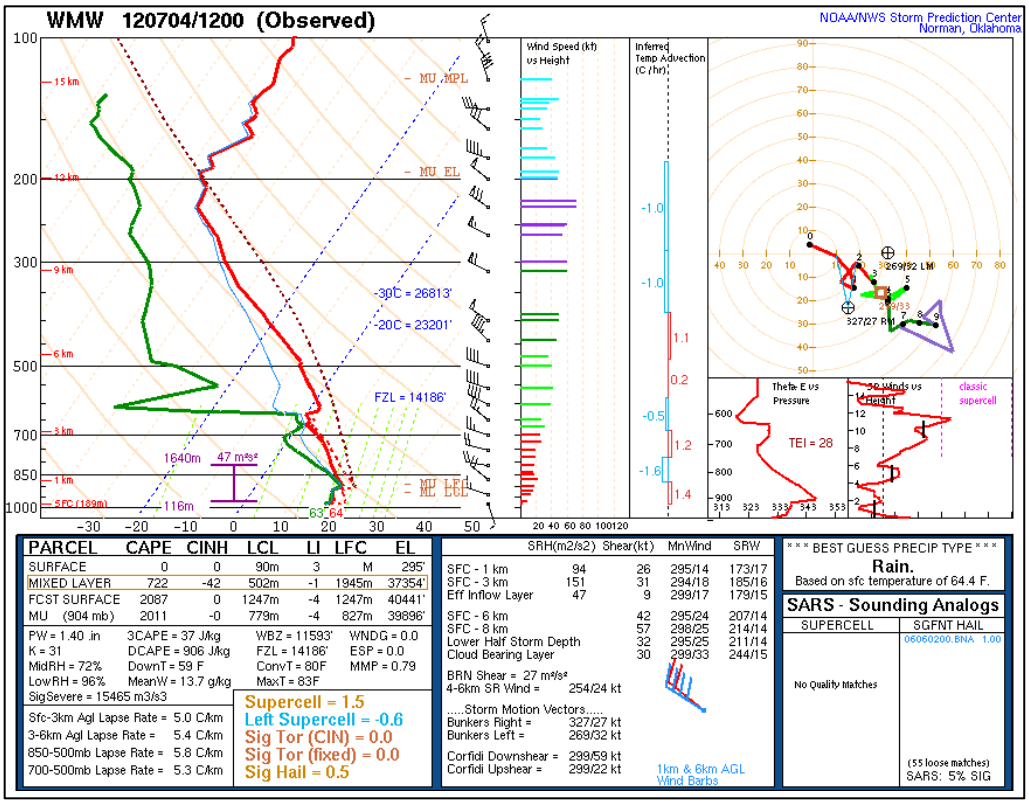

Figure 3.65. Sounding from WMW valid at 1200 UTC 4 July 2012 (source: SPC).

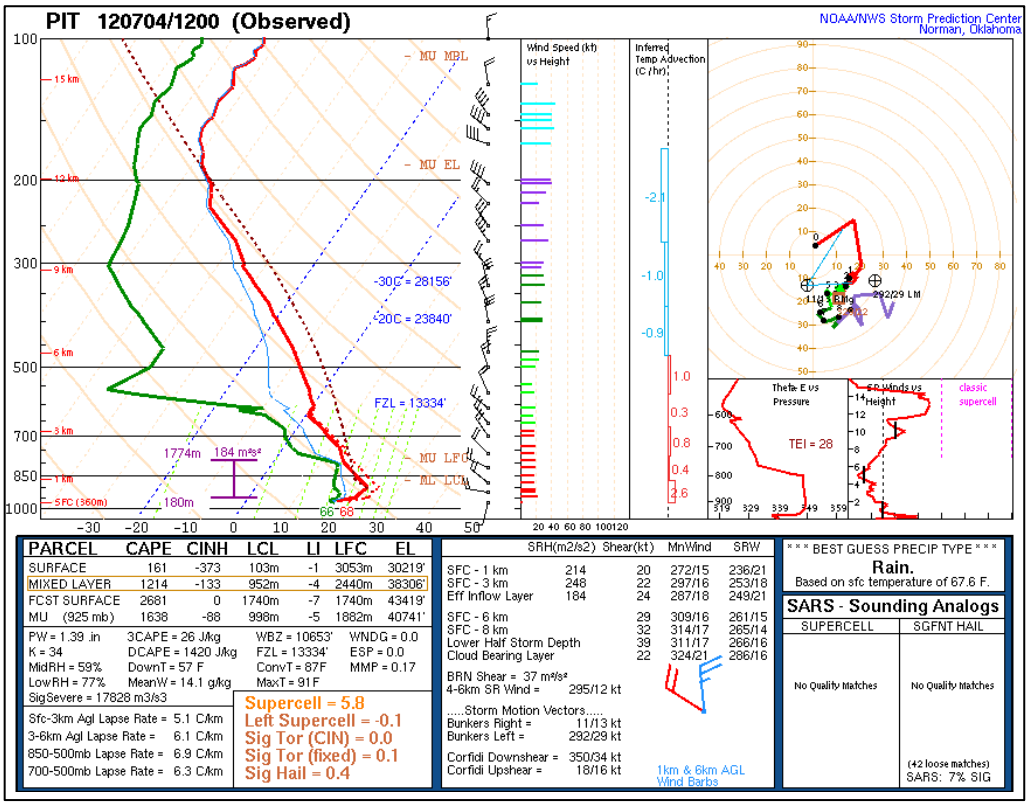

Figure 3.66. Sounding from PIT valid at 1200 UTC 4 July 2012 (source: SPC).

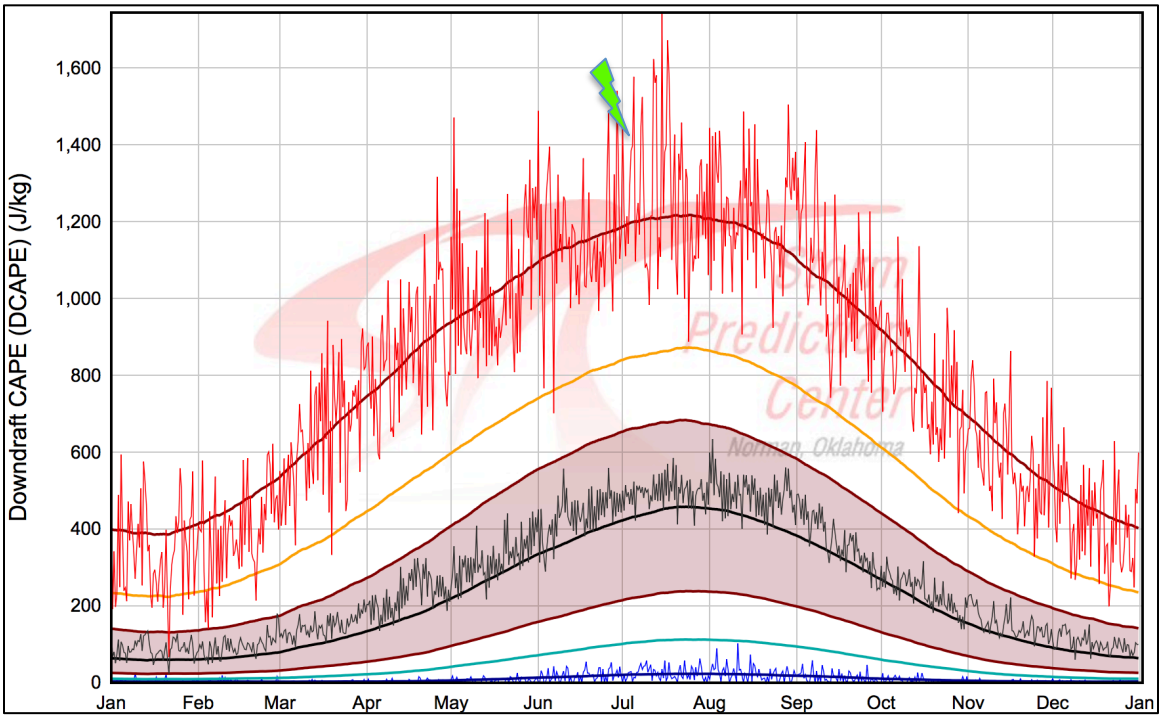

Figure 3.67. As in Fig. 3.39 but for PIT. Green bolt represents observed value at 1200 UTC 4 July 2012 (source: SPC).

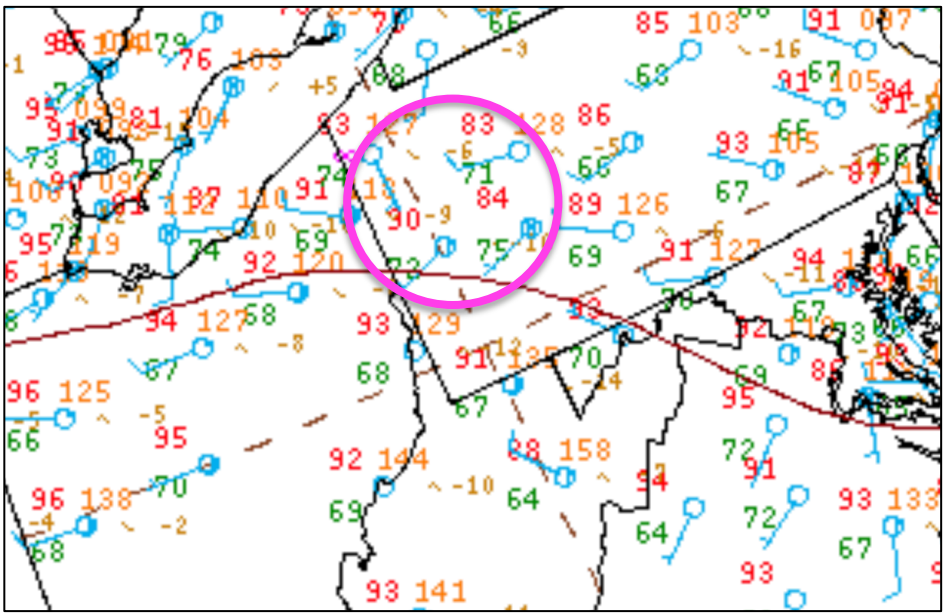

Figure 3.68. Surface observations valid at 1800 UTC 4 July 2012 (source: Weather Prediction Center). Magenta circle denotes area of thermal boundary.

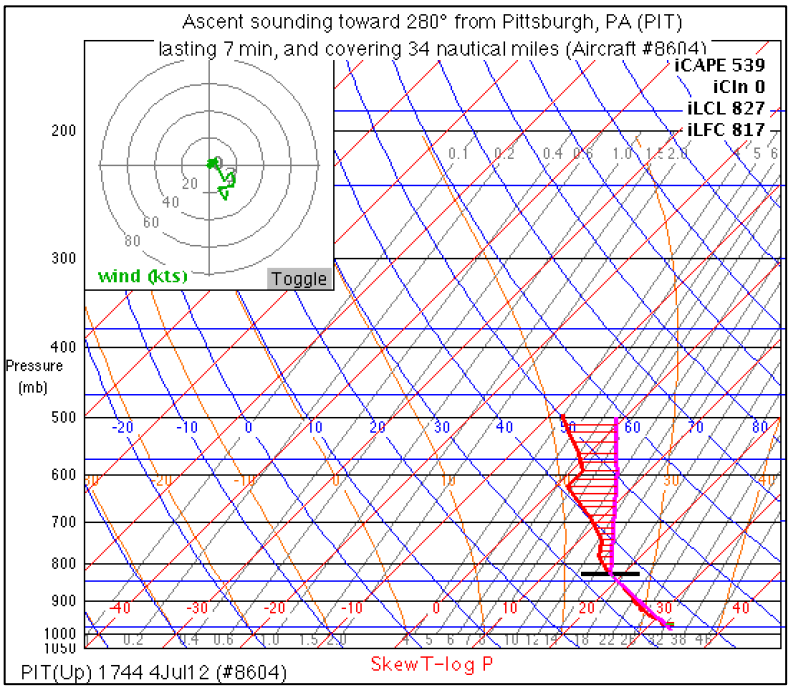

Figure 3.69. Aircraft sounding and computed parcel path using METAR data valid at 1744 UTC 4 July 2012. Sounding is located at PIT.

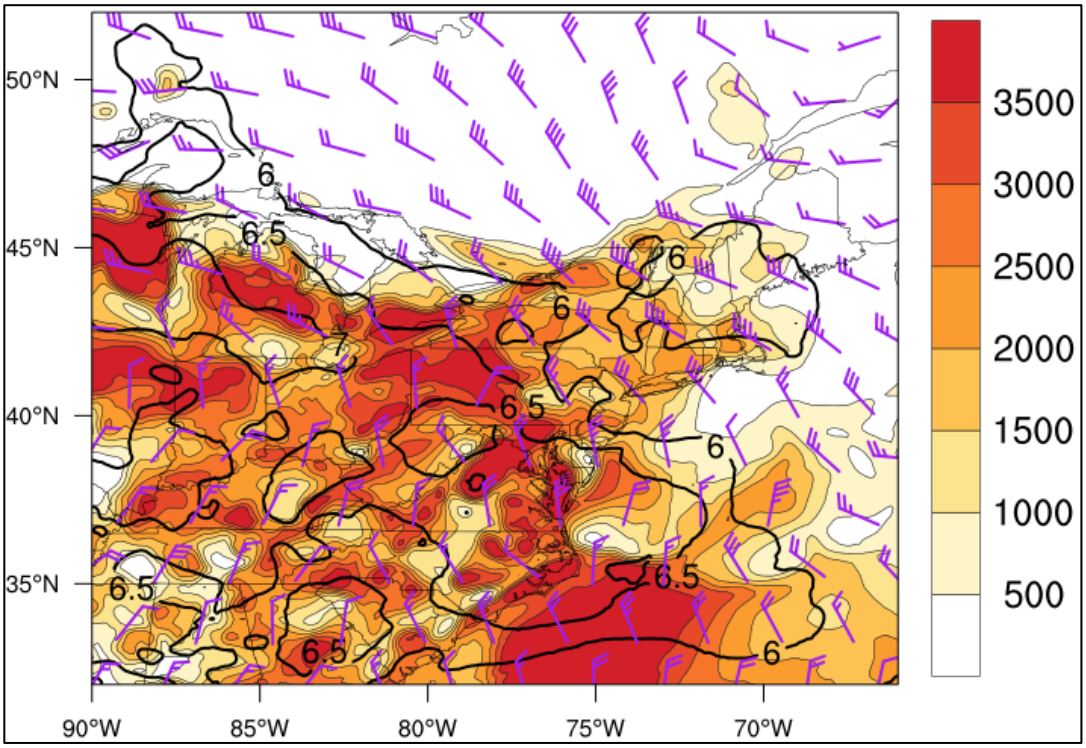

Figure 3.70. As in Fig. 3.36 but for 0000 UTC 5 July 2012 using RAP model analysis data.

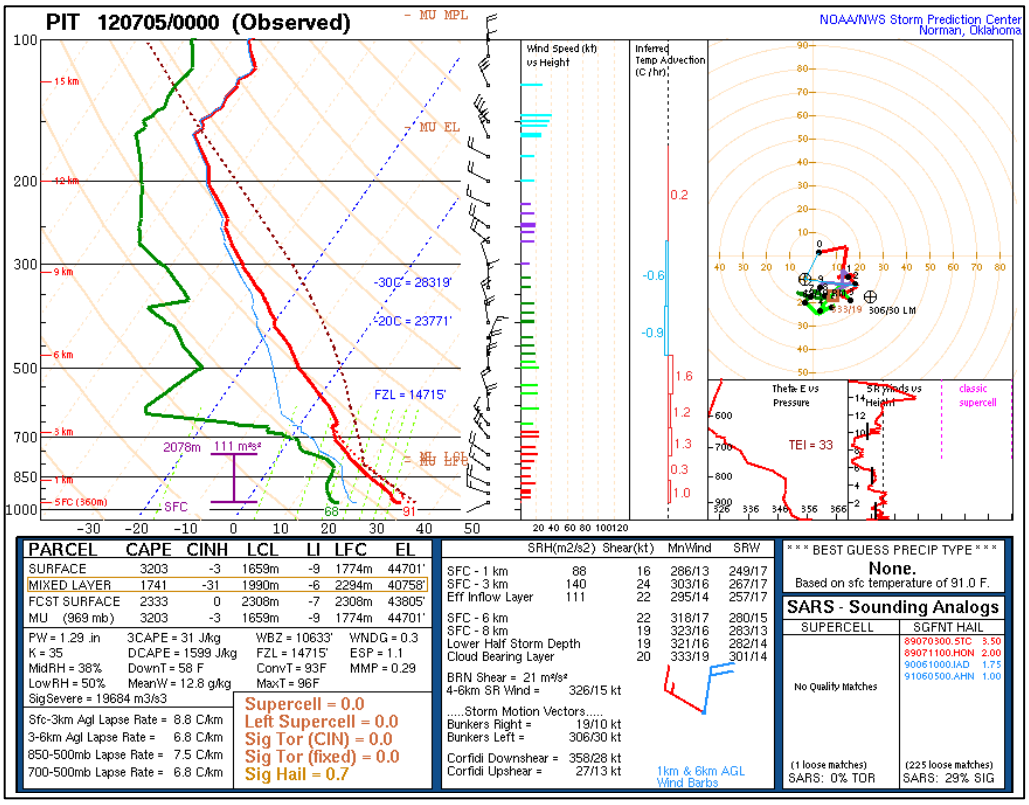

Figure 3.71. Sounding from PIT valid at 0000 UTC 5 July 2012 (source: SPC).

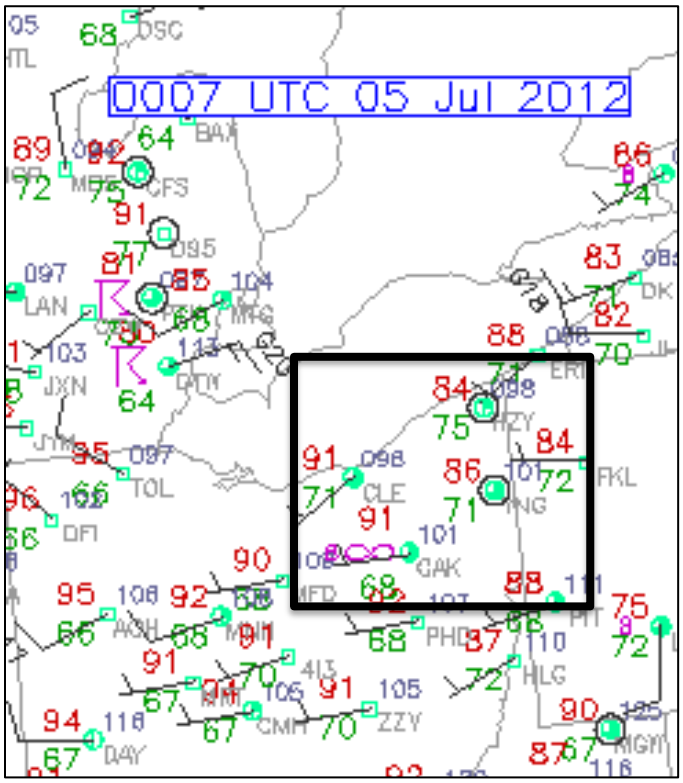

Figure 3.72. Surface observations valid at 0000 UTC 5 July 2012 (source: UCAR). The black box highlights the thermal boundary between CLE, CAK, YNG, and HZY.

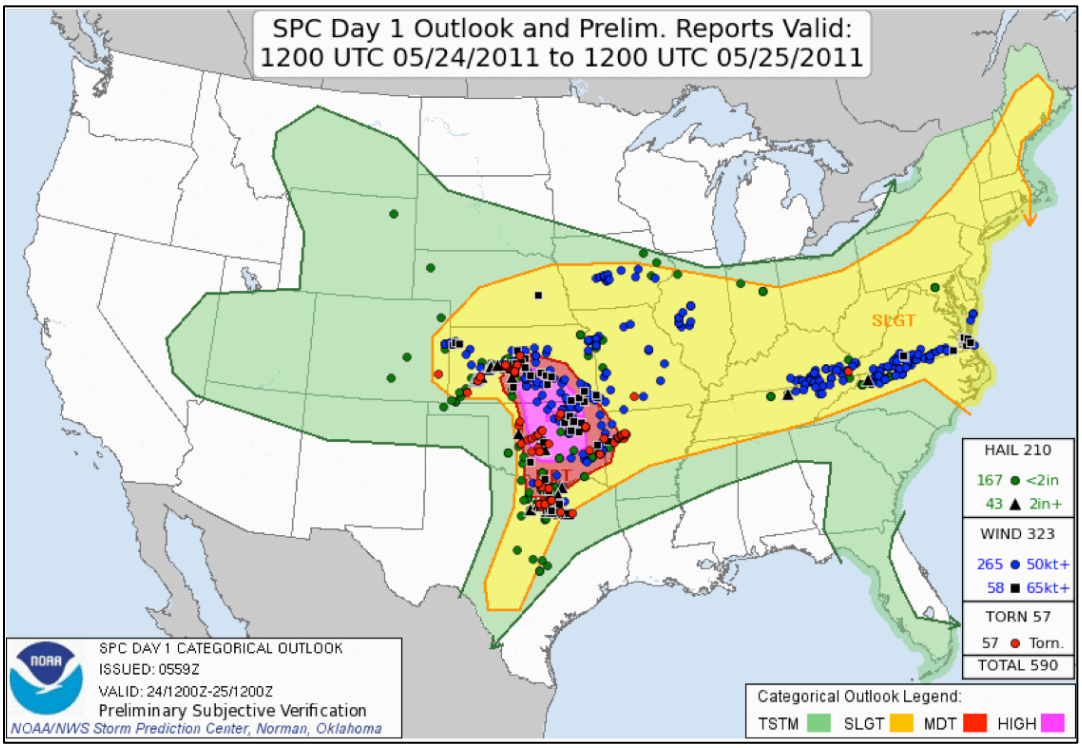

Figure 3.73. SPC 0600 UTC 24 May 2011 severe wind convective outlook valid 1200 UTC 24 May 2011 to 1200 UTC 25 May 2011.

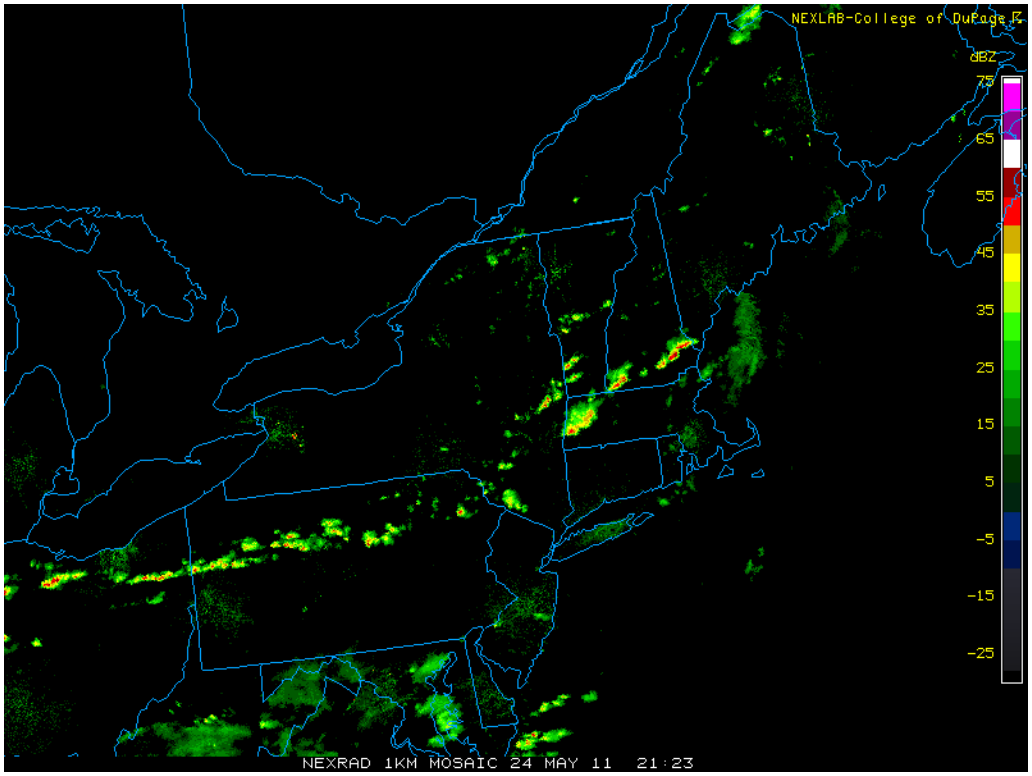

Figure 3.74. Radar reflectivity valid at 2123 UTC 24 May 2011 (source: College of DuPage).

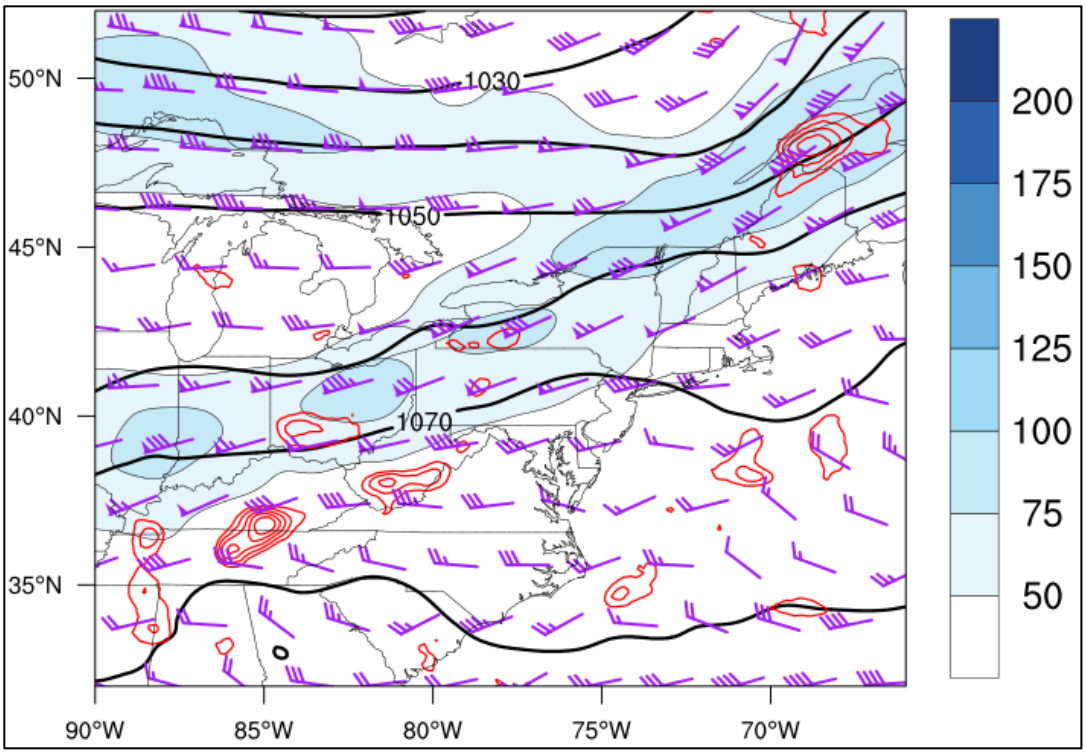

Figure 3.75. As in Fig. 3.34 but at 1200 UTC 24 May 2011.

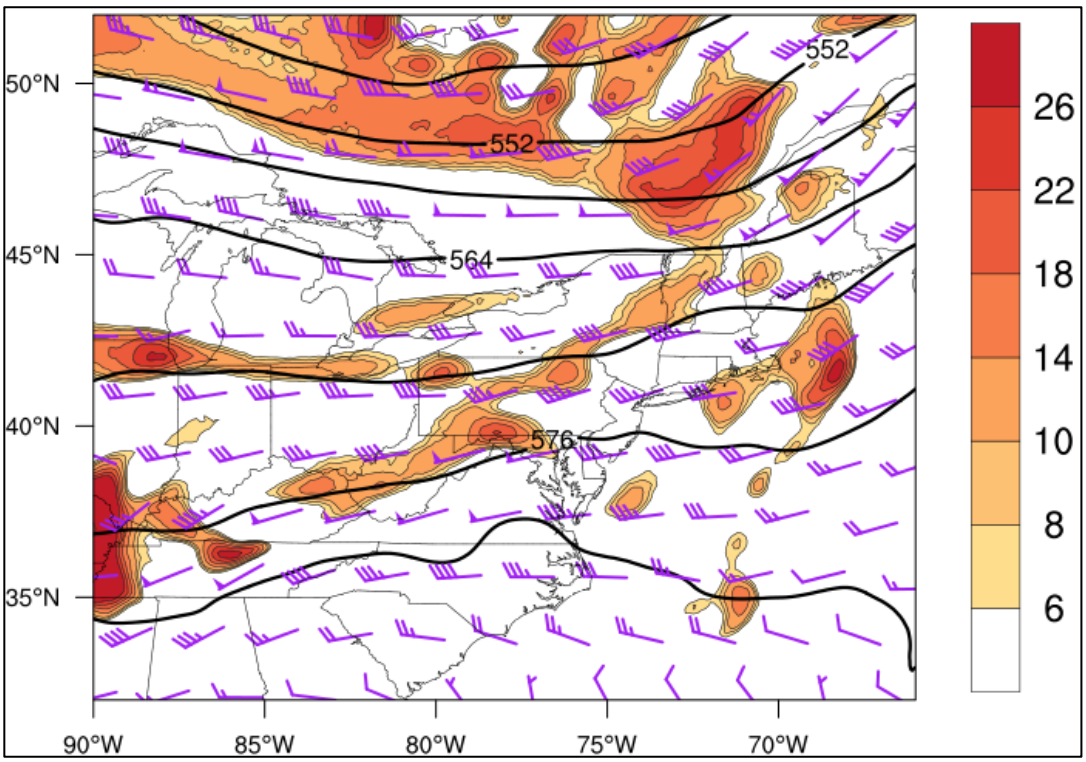

Figure 3.76. As in Fig. 3.35 but at 1200 UTC 24 May 2011.

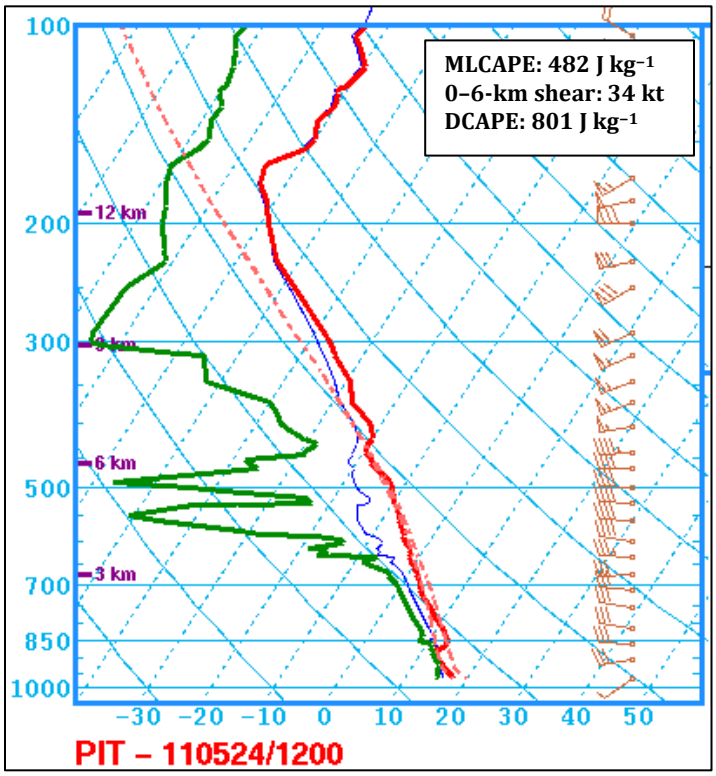

Figure 3.77. Sounding at PIT valid at 1200 UTC 24 May 2011 (source: SPC).

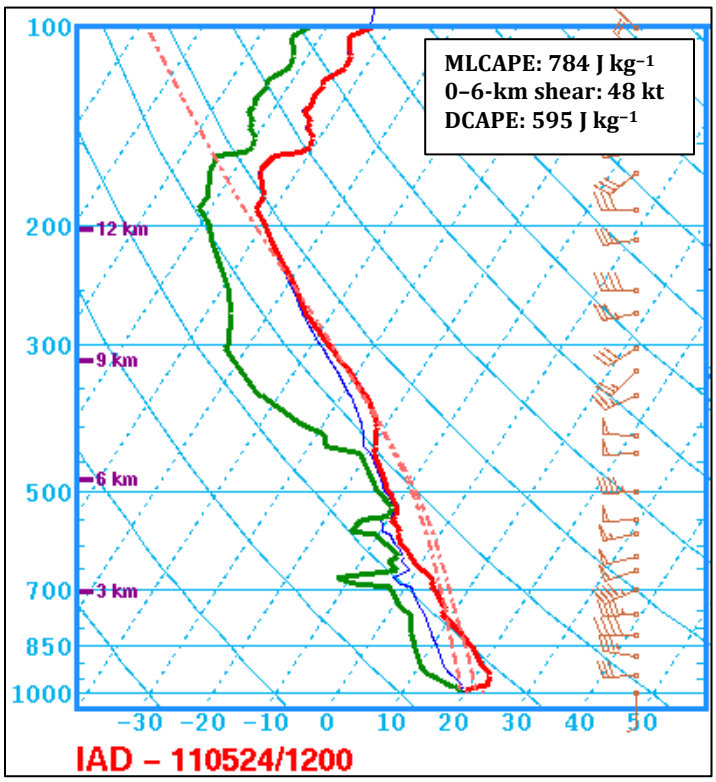

Figure 3.78. Sounding at IAD valid at 1200 UTC 24 May 2011 (source: SPC).

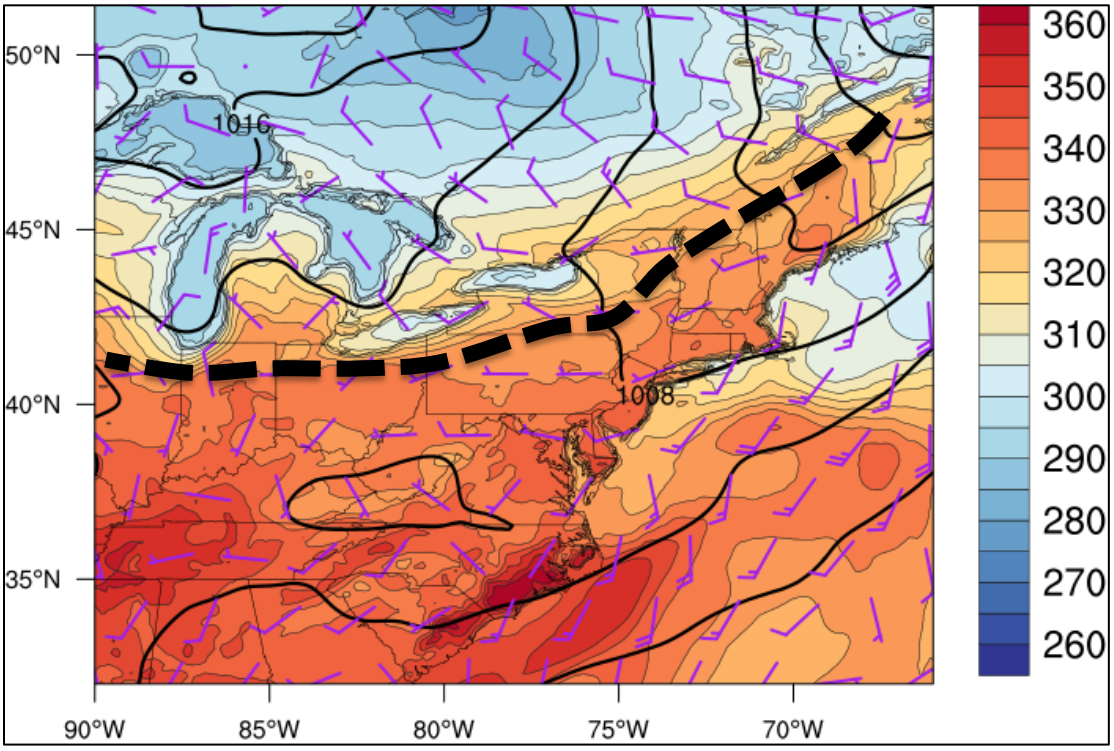

Figure 3.79. As in Fig. 3.47 but at 2200 UTC 24 May 2011. The heavy dashed line indicates the position of the cold front.

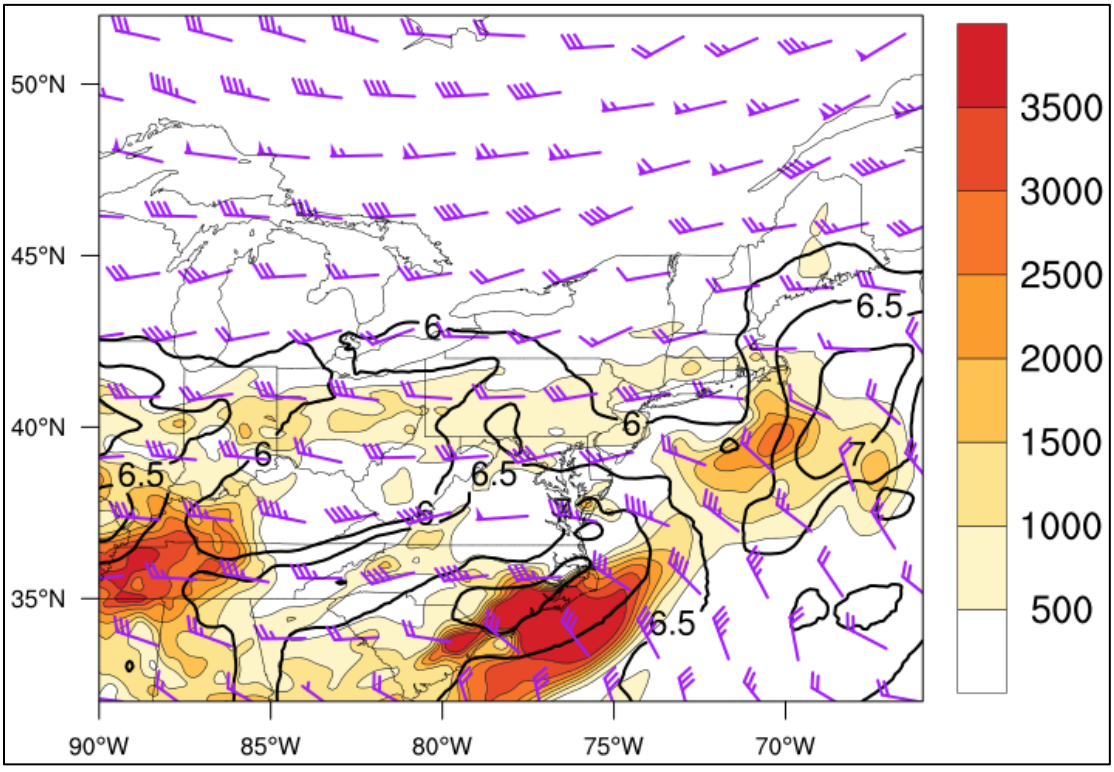

Figure 3.80. As in Fig. 3.36 but at 2200 UTC 24 May 2011.

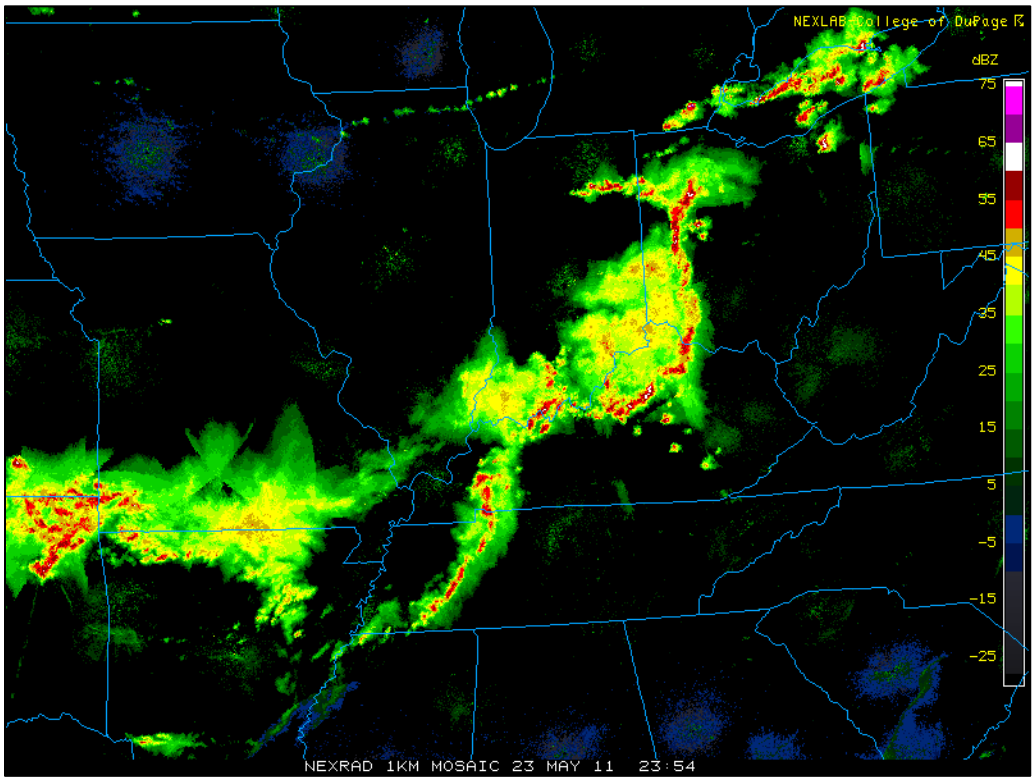

Figure 3.81. Radar reflectivity valid at 2354 UTC 23 May 2011 (source: College of DuPage).

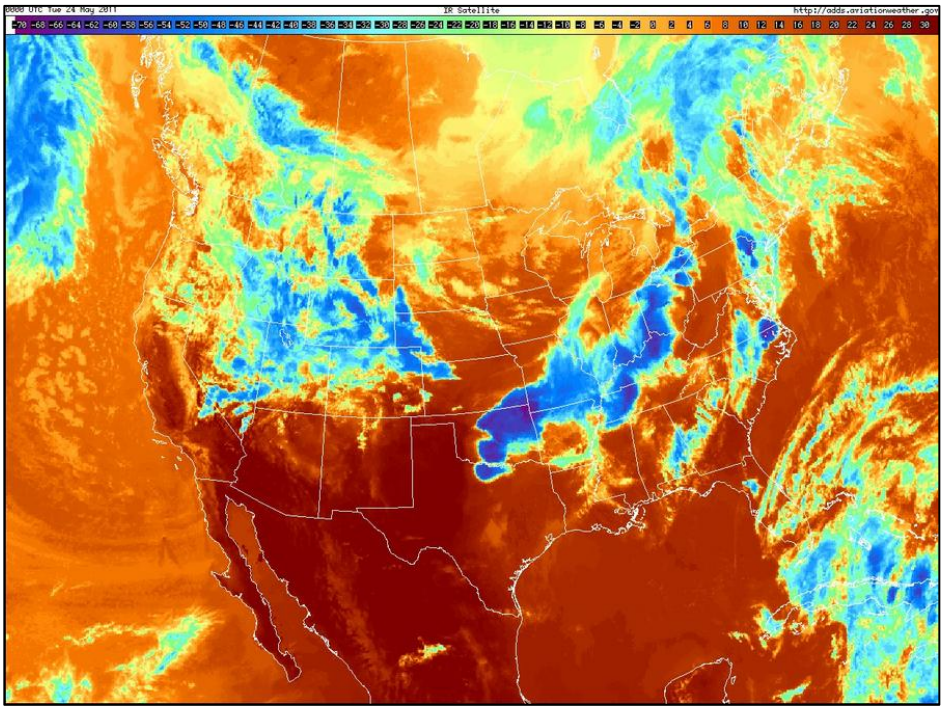
Figure 3.82. Infrared satellite imagery valid at 0000 UTC 24 May 2011.

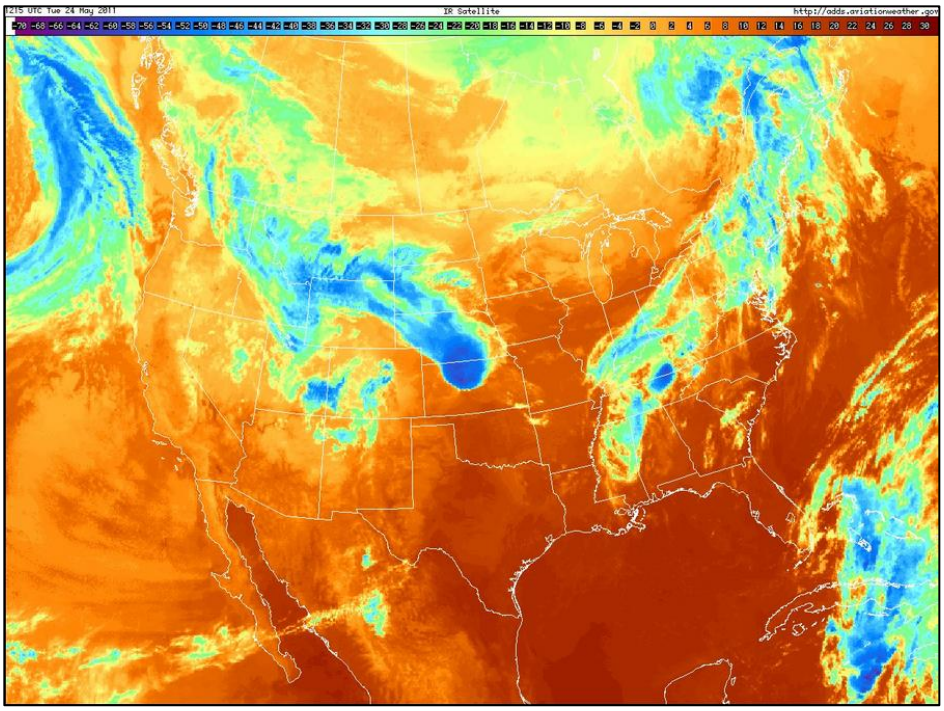

Figure 3.83. Infrared satellite imagery valid at 1215 UTC 24 May 2011.

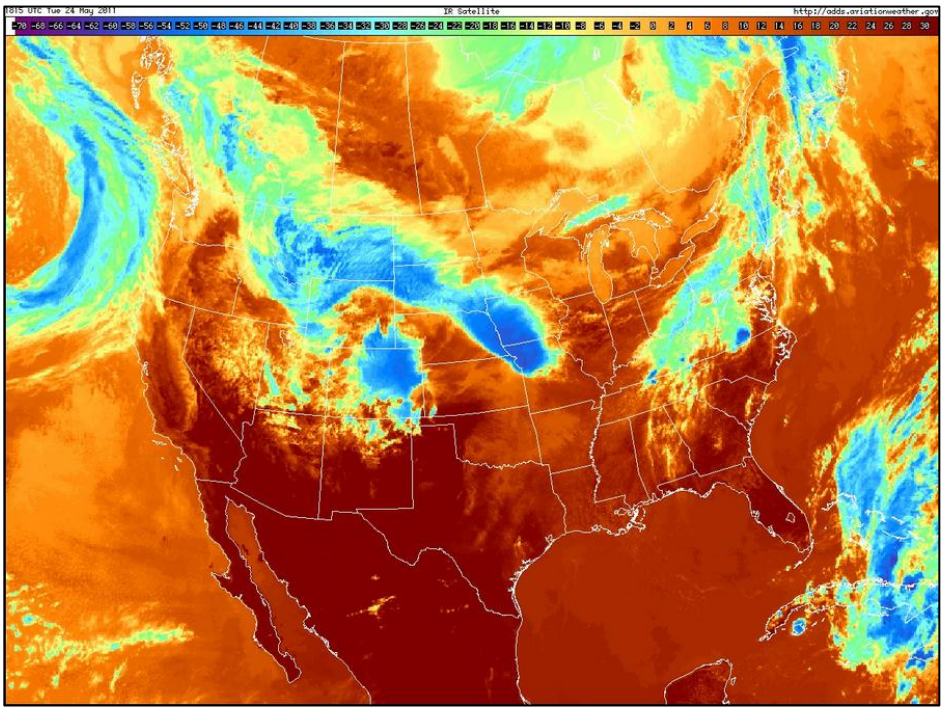

Figure 3.84. Infrared satellite imagery valid at 1815 UTC 24 May 2011.

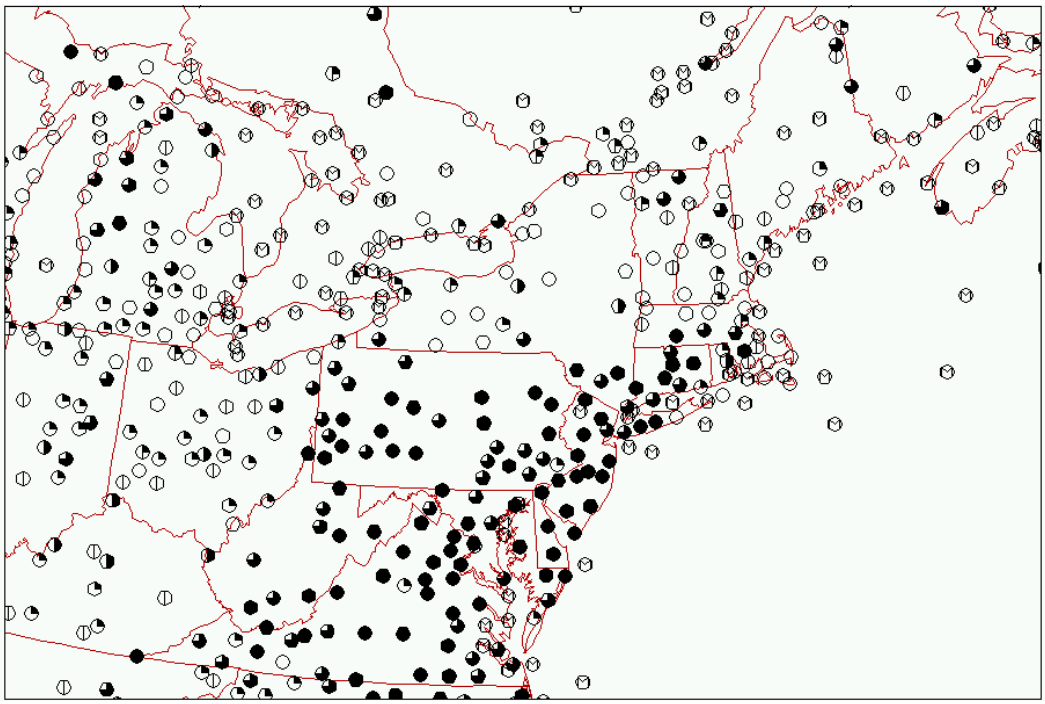

Figure 3.85. Surface observations of sky cover valid at 1800 UTC 24 May 2011 (source: Plymouth State College).

4. Discussion and suggestions for future work

4.1 Discussion

4.1.1 Skill scores

The slight risk skill scores for the CONUS region agree with the results of Hitchens and Brooks (2012), finding little trend in POD, a decreasing trend in FAR, and an increasing trend in TS through the 1980–2013 period. Slight differences arise between the 80 × 80 km verification grid used in Hitchens and Brooks (2012) and the 40 × 40 km grid used in the present study. The increase in annual severe report count shown in Fig. 3.1 coincides with the increase in severe report area illustrated in Fig. 1.14. The increase in severe reports results from both an increase in the number of severe weather days and an increase in the number of severe reports per event (Figs. 3.2 and 3.3). It is hypothesized this increase in severe reports is a result of increasing population and the advent of mass-produced digital communication devices to facilitate expedited reporting of severe weather damage to NWS forecast offices over a larger area.

The Northeast domain shares similar trends with the CONUS but has better overall verification scores. Slight risk outlooks in the Northeast are more likely to contain a higher percentage of severe reports occurring within the domain than the CONUS (Fig. 3.4). The author wishes to emphasize that the skill scores presented herein are using the slight risk category alone. A similar analysis using the see text or the more recent marginal outlook category would likely increase POD scores across both domains. Lower FAR scores in the Northeast indicate less false alarm area within slight risk outlooks than the CONUS. Threat scores in the Northeast are higher during the majority of the study period indicating slight risk outlooks are better indicators of severe weather over the Northeast than the CONUS. Domain and sample size should be

considered when interpreting skill score results. The Northeast domain has larger IQRs through most years in the study period for POD, FAR, and TS. The rarity of slight risk events in the Northeast likely exacerbates the variability of the skill scores due to a lower sample size relative to the CONUS (Fig. 3.5). Additionally, the smaller spatial size of the Northeast likely contributes to slight risk skill score variability. Slight risk outlooks covering a larger portion of the domain are more likely to capture a larger percentage of severe reports within the domain. Alternatively, slight risk outlooks that mainly reside outside the Northeast but have a small portion of outlook area within the Northeast can drastically affect POD and FAR scores. An event may have no reports occurring in the small outlook area within the Northeast and score a high FAR. Similarly, the small outlook area could have a large number of reports clustered within it, leading to a high POD score. Therefore, more variability in skill score should be expected for the Northeast domain.

4.1.2 Climatology

The climatology in this study sought to identify Northeast high-impact severe weather events with high spatial coverage while controlling for the increase in severe weather reporting with time. The technique, described in chapter 2, is applied from 1980–2013 and identifies 825 high-impact events representing the top 32% of severe weather events in the Northeast. A total of 224 events are categorized as type 1 and all type 1 events have a POD score of zero. Out of the 224 type 1 events, 204 events have no 0600 UTC slight risk outlook in the Northeast domain, suggesting type 1 events are characterized by the absence of slight risk outlooks rather than misplaced outlooks. With an average of 7 type 1 events per year and no discernable trend

through the period, low POD events continue to be a forecasting challenge through 2013. Type 2 events are rare with 42 events occurring between 1980–2013 and a heavy bias towards the early half of the period. Considering only 5 events occur between 2003–2013, type 2 events, as they are defined in chapter 2, have become a less significant forecasting challenge through the end of 2013. It is important to note the strict criteria used in this study to identify type 2 events using the highest 25th percentile of false alarm area and the lowest 25th percentile of severe report area. High FAR events with small slight risk outlooks are not well sampled using this approach and the analysis is biased towards events with unusually large false alarm areas. Conversely, good events have increased from 1980–2013, suggesting improved placement of slight risk outlooks in the Northeast through the latter half of the period.

Monthly variability of high-impact events (Fig. 3.10) resembles the climatology of severe reports in the northeast U.S. (Fig. 1.5). Through the summer months of JJA, 70% of high-impact events and 69% of type 1 events occur, suggesting low POD events follow the high-impact climatology during the peak severe weather season in the Northeast (Fig. 3.10). The remainder of the year suggests there is no month where type 1 events occur substantially more often than high-impact and good events with a notable exception in January. Of the 5 high-impact events in January, 4 are classified as type 1, however with a limited number of cases, no conclusions concerning the cause of the poor predictive skill in January are hypothesized. May contains the highest percentage of Type 2 and good events relative to high-impact events while type 1 events occur marginally less frequently than climatology. It is hypothesized that during the springtime when severe weather events are most frequent across the CONUS, and the conditions leading to these events are more synoptically evident (Johns and Doswell 1992), forecasters are more likely to issue slight risk outlooks in the CONUS domain. The Northeast may be influenced by this

increased tendency, especially in the southwest portion of the domain where systems of Midwest origin can propagate into the domain and slight risk outlooks can extend into OH, WV, and PA accordingly.

Low-predictive skill events tend to occur in less common midlevel flow regimes. Northwesterly, northerly, and southerly 500-hPa flow produce type 1 events with higher relative frequency than high-impact or good events (Figs. 3.11 and 3.12) and have lower (though not significantly lower) threat scores than southwesterly and westerly cases (not shown). Considering the smaller sample size of northerly cases, the difference between the number of good events and type 1 events remains drastic. It is hypothesized the rarity of high-impact events under northerly flow—17 events over the 1980–2013 period—inhibits pattern recognition of severe weather precursors, decreasing predictive skill in northerly flow regimes.

Using a MUCAPE and 1000–500-hPa shear phase space bisected by the median MUCAPE and 1000–500-hPa shear of all high-impact events in the Northeast, type 1 events were found to occur under lower shear and comparable MUCAPE conditions relative to good events. This relationship was found to exist across all midlevel flow regimes. Additionally, threat scores for high-impact events are significantly lower under weak shear conditions than strong shear conditions. High deep-layer shear is beneficial to the development of multicellular systems and supercells through the separation of updrafts and downdrafts. Low-shear conditions likely reduce forecaster confidence in upscale growth of convection and mask the potential for widespread severe weather. However, LC11 found large variability in 0–6-km shear magnitudes for northeast severe weather (Fig. 1.9c). Furthermore, Hurlbut and Cohen (2014) note deep-layer shear is not a significant discriminator of severe report magnitude in the northeastern U.S. Therefore, forecasts attempting to use shear as the primary discriminator of the magnitude of the

severe weather threat will not accurately address severe weather occurring in marginal and low-shear environments.

4.1.3 Composites

The event-centered composites for type 1 and good events under northwesterly flow have similar synoptic patterns while type 1 events generally have more subtle features. A weaker jet characterizes type 1 events and more pronounced curvature of the upstream ridge coinciding with weaker midlevel ascent upstream of the event center than the good events. The lack of upper-level forcing for type 1 events likely decreases forecaster confidence in the severe weather threat relative to the good events. Additionally, weaker midlevel lapse rates and winds upstream of the event center reduce advection of steeper lapse rates into the region for type 1 events. Steep lapse rates, particularly elevated mixed layers, are associated with high-impact severe weather over the Northeast (Banacos and Ekster 2010). It is hypothesized stronger lapse rates in the good cases likely increase forecaster confidence in a high-impact severe weather threat and encouraged slight risk issuance for the Northeast. Enhanced baroclinicity northwest of the good event composite center induces higher shear values in the region while a stronger meridional pressure gradient strengthens horizontal momentum over the Northeast. The combination of higher shear and instability upstream of the good event center, relative to the type 1 composite, likely results in improved forecast performance for the northwesterly flow cases amidst generally poor mean forcing for both composite categories. It is hypothesized sub-grid scale forcing mechanisms unresolved and/or misrepresented by the CFSR, such as lake-sea boundaries,

outflow boundaries, and terrain-induced circulations, likely play a role in initiating northwesterly type 1 severe convection.

Southwesterly type 1 events have a less amplified upper-level trough, weaker attendant midlevel ascent, and weaker flow aloft relative to good events, decreasing confidence in large-scale forcing for severe weather. While synoptic forcing for ascent is greater in the southwesterly type 1 events than the northwesterly type 1 events, the weaker upper-level support relative to the good southwesterly events likely discourages issuance of slight risk outlooks for type 1 southwesterly events. The prominent closed surface cyclone in the good composite suggests good agreement with classic conceptual models of severe convection within the warm sector of midlatitude systems whereas the type 1 MSLP field indicates a weaker surface trough and less baroclinicity, reducing shear and forcing for ascent. It is hypothesized the weaker surface trough, along with reduced shear and horizontal momentum aloft relative to the good events decreases forecast confidence in severe weather occurrence during the type 1 events.

Both westerly flow composites suggest a shortwave within the upper-level flow upstream of the event center. The good event composite indicates more midlevel ascent, faster 65-kt 250-hPa winds, and an amplified trough at 500 hPa upstream of the event center relative to the type 1 composite, increasing confidence in forcing for severe convection. Higher PW values upstream of the good event center coincide with enhanced MUCAPE and provide a stronger signal for vigorous convection than the type 1 composite. Additionally, a thickness ridge develops immediately upstream of the good event center and contributes to a stronger warm sector over the event center relative to the type 1 composite. It is hypothesized that higher shear, midlevel ascent, and moisture upstream of the event center contribute to higher confidence in severe weather for the good events. The composites show some signal of an upper-level trough, but the

sheer number of events in the westerly flow composites dampens the trough signal due to variability in space and amplitude. Therefore, while mesoscale forcing mechanisms poorly resolved by the CFSR may play a role in initiating convection, upper-level shortwaves may also contribute to enhancing the severe weather threat in type 1 and good cases.

4.1.4 Case studies

4.1.4.1 18–19 August 2009

The 18 August 2009 event is representative of a westerly LSHC type 1 event in the Northeast. Similar to the westerly flow composite, the jet is displaced to the north and the similarly displaced midlevel trough provides minimal upper-level forcing and deep-layer shear over the area of highest severe report density. Model-derived SBCAPE in excess of 1000 J kg^{-1} across the Northeast, together with MLCAPE ~2000 J kg^{-1} derived from proximity soundings, provides ample potential energy to sustain convection. Given the benign upper-level pattern consisting of a departing shortwave to the east and a trough axis displaced over the northern Great Lakes, deep-layer vertical wind shear is exceedingly weak across the domain. At PIT, the 0–6-km shear is ~12 kt, but with notably higher values ~25 kt between 0 and 3 km. Similarly, WAL has 12 knots of 0–6-km deep-layer shear, but lacks substantial shear in the lower-levels.

Forcing for convection is limited due to homogeneous surface conditions and meager synoptic scale forcing. Therefore, small-scale boundaries serve as a focus for convective initiation. Storms initiate along the southern shore of Lake Erie as well as within the complex terrain of the Appalachian Mountains in PA, NY, MD, and VA. These storms propagate toward the east encountering ~5–10 kt of 0–3-km shear, substantially lower than the area of convective

initiation around PIT. In cases with strong tropospheric flow, vertical advection of horizontal momentum is a large contributor to producing severe winds at the surface. However, on 18 August 2009, weak winds ~10–20 kt at 500 hPa were observed across PA, MD, and VA where severe weather reports were most frequent. The 1200 UTC 18 August WAL sounding depicts a dry layer around 600 hPa that contributes to a DCAPE value of 1294 J kg^{-1} relative to the 510 J kg^{-1} observed at PIT. This anomalously large DCAPE value, above the 91-day maximum average for 18 August, indicates the potential for large negative buoyancy for rain-cooled parcels around 600 hPa. Under these conditions, the severe wind reports across the domain are likely a result of strong downdrafts caused by anomalously large DCAPE within the observed discreet cells and small line segments. Additionally, aircraft data suggests LCL heights around 818 hPa, high enough to allow saturated descending parcels to evaporatively cool through an ~180 hPa thick sub-saturated layer and descend more rapidly.

The lack of strong synoptic forcing for the event, combined with the low vertical wind shear values, likely contributed to poor predictive performance. Storms propagated from a moist 1000–500-hPa environment near PIT toward WAL, which was characterized by similarly large MLCAPE values ~2000 J kg^{-1}, much larger DCAPE values ~1300 K kg^{-1}, and weak shear <12 kt below 6 km. It is hypothesized the evolution of the convection into storms capable of producing numerous severe wind reports at the surface as they crossed into a drier environment, characterized by >1200 J kg^{-1} DCAPE, was unexpected.

4.1.4.2 4–5 May 2010

The case of 4 May 2010 represents a HSLC westerly type 1 event over the Northeast. In contrast to the first case study and the type 1 westerly composite, upper-level flow was substantial across the northeast with both poleward jet entrance region dynamics and an approaching mid-level vorticity maximum influencing the convective initiation location. Model-derived SBCAPE was exceedingly weak, remaining below 500 J kg^{-1} across most of the region, due to low surface dewpoints ranging from 8 to 11 °C, but 850–500-hPa lapse rates in excess of 6.5–7 K km^{-1} were in place over the western Northeast domain. Deep-layer shear between 35–50 kt provided a favorable dynamic environment for upscale growth of convection.

A weak surface trough coinciding with the land-lake boundaries of Lake Erie and Lake Ontario provided a focus for early convection within the moist environment in place near BUF. As convection quickly propagated eastward, the storms encountered drier air in the boundary layer. However, diabatic heating through solar insolation destabilized the boundary layer ahead of the growing MCS and provided a favorable environment for vertical advection of the strong horizontal tropospheric flow over the region. Aircraft and sounding data ahead of the advancing MCS indicate high LCL heights ~770 hPa and a well-mixed boundary layer, supporting vertical advection as well as enhanced evaporative cooling of saturated parcels.

The lack of substantial CAPE, low moisture across the Northeast, and the subtle surface forcing accompanying the MCS likely contributed to the poor forecast performance of this case. The transition between the moist convective initiation environment around BUF to the environment around ALB and BDL characterized by LCL heights ~770 hPa in the late afternoon and evening also presents a forecasting challenge. In this scenario, storms were maintained within the drier environment due to strong midlevel forcing concomitant with a shortwave vorticity maximum and steep mid-and-low level lapse rates. Despite the ≤500 J kg^{-1} SBCAPE

and correspondingly weak upward vertical motions within the convection, strong to severe surface winds were generated through a combination of vertical advection of horizontal momentum along a steep lapse rate and enhanced evaporative cooling of saturated parcels below the cloud base.

4.1.4.3 4–5 July 2012

The case of 4 July 2012 represents a complicated type 1 northwesterly flow event with high CAPE and variable amounts of deep-layer shear. Over the prior 24 hours, a large area of deep convection over the northern Great Plains and southern Saskatchewan created a ridge of high potential temperature on the DT downstream. The enhanced northerly flow on the eastern flank of the convectively enhanced ridge amplified a trough of 324–330 K potential temperature on the DT over southern Hudson Bay, resulting in the southward propagation of the trough towards the northern Northeast states. The associated 500-hPa vorticity maximum provided forcing for ascent and enhanced deep-layer shear to 45 kt in southern Quebec in the presence of >1500 J kg^{-1} SBCAPE around the time of convective initiation at 1800 UTC with higher amounts of SBCAPE across the US–Canadian border. This combination of forcing, ample shear and moderate SBCAPE provided support for multicellular and discreet convection capable of producing severe wind and hail across the northern tier of the Northeast.

Meanwhile, western PA had lower deep-layer shear ~20 kt and little upper-level forcing for ascent in the presence of an upstream ridge at 500-hPa as indicated by the 1800 UTC RAP analysis. Instability was extreme around PIT, exceeding 3500 J kg^{-1} of model-derived SBCAPE.

Similar to the 18 August 2009 case, DCAPE at PIT was anomalously high at 1200 UTC in excess of 1400 J kg^{-1}, eclipsing the climatological maximum average value for the day.

Triggering mechanisms for severe weather in the southern Great Lakes region were subtle around 1800 UTC. Residual cloud cover from early morning convection established an insolation gradient throughout the day, resulting in a thermal boundary in western PA within the complex terrain of the Appalachians. It is hypothesized upslope flow on the western side of the mountains, along with the forcing provided by the aforementioned thermal boundary initiated convection in southwest PA. The nascent storms occur amidst anomalously high DCAPE ~1400 J kg^{-1} and, in the presence of 20 kt of RAP-analyzed 0–6-km vertical wind shear, were able to produce severe wind due to large negative buoyancy of rain-cooled parcels. Additionally, aircraft data indicates LCL heights around 827 hPa and a well-mixed boundary layer, suggesting evaporative cooling of saturated parcels may have enhanced downdraft velocities.

The second round of convection in the southern Great Lakes region, initiating after 0000 UTC, benefits from continued extreme instability across western PA and eastern OH. The PIT sounding at 0000 UTC indicates 3203 J kg^{-1} SBCAPE coincident with an 8.8 K km^{-1} 0–3-km lapse rate. Additionally, DCAPE rose to 1599 J kg^{-1} and persisted in the weakly sheared environment. Similar to the first round of convection at 1800 UTC, a low-level thermal boundary is evident in the surface observations in northeast OH. It is hypothesized this thermal boundary, the land-lake interface along the southern shore of Lake Erie, and the weak low-level warm air advection indicated by the veering wind profile in the 0000 UTC PIT sounding contribute to convective initiation in the absence of strong upper-level and/or frontal forcing. The incipient convection, in the presence of 24 kt 0–3-km shear, >3000 J kg^{-1} SBCAPE, and nearly 1600 J

kg^{-1} DCAPE, grows upscale to a bowing line segment producing a swath of severe wind reports in OH and PA.

The upstream convection and the associated diabatic heating over the northern tier of the central U.S. and south-central Canada likely contributed to the low predictive skill of the event, especially the series of storms in the northern Northeast that benefitted from an amplified Canadian trough. The associated vorticity maximum in southern Quebec provided forcing for ascent, enhanced deep-layer shear, and cooler temperatures aloft over the northern Northeast, providing a favorable dynamic and thermodynamic environment for severe weather. Severe convection at 1800 UTC over western PA occurred in weak deep-layer shear ~20 kt in the absence of significant synoptic forcing for ascent. These factors, along with the early morning convection and the associated solar heating gradient from residual clouds likely prevented adequate anticipation of the severe weather threat. The thermal boundary, a result of the gradient in solar heating, provided additional forcing for ascent and a focus for convective initiation in combination with upslope flow within the Appalachian Mountains in western PA. The longevity of the cloud cover associated with the early morning convection was likely not anticipated. For similar reasons, the severe convection occurring after 0000 UTC presents a forecasting challenge. Forcing and deep-layer shear remain weak and mesoscale boundaries likely play a significant role in convective initiation. However, low-level shear and highly anomalous DCAPE values are indicative of an enhanced severe wind threat for these storms and the updated 2000 UTC 4 July convective outlook correctly captures the severe reports produced by the evening system in the southern Great Lakes.

4.1.4.4 24–25 May 2011

The 24 May 2011 case represents a westerly type 2 event under HSLC conditions. SPC issued a slight risk convective outlook for the majority of the Northeast domain citing a shortwave ejecting eastward into the Ohio valley, a cold front advancing into New England, and diurnal boundary layer destabilization as factors that increased the severe weather threat across the region. Deep-layer shear between 30–40 kt provides a marginally supportive dynamic environment for upscale growth of convection ahead of the encroaching cold front acting as a potential triggering mechanism for convective initiation. Storms initiate along the frontal boundary, but never grow upscale or produce much severe weather aside from 2 hail reports in MD.

Convection in the Missouri and Ohio valleys the day prior produced substantial cloud cover. The high RH air associated with the previous convection was advected by the broad cyclonic upper-level flow towards the Northeast. By 1200 UTC 24 May, clouds overspread a large portion of the Northeast ahead of the advancing cold front. In the presence of broad cyclonic flow, the clouds persisted and remained a significant feature across much of the Northeast at 1800 UTC. It is hypothesized that the clouds inhibited diurnal heating and boundary layer destabilization, preventing the requisite instability to develop and support severe convection.

Similar to the 4 July 2012 case, upstream convection likely played an important role in the evolution and the poor predictive skill of the event. In this case, residual clouds from earlier convection overspread the Northeast and prevented substantial boundary layer destabilization, which SPC cited as a contributing factor to the severe weather threat. It is hypothesized accurate

prediction of the expansive cloud cover over the Northeast and its detrimental effect on CAPE generation would lead to improved forecast performance for this event.

4.1.5 Applications of research to operational forecasting

The composite results presented in section 3.3 provide evidence of when type 1 events are likely to occur. By and large, atmospheric precursors are similar in character but smaller in magnitude for type 1 events relative to events with good predictive skill. This is likely due to the inherent variability of severe convection in the Northeast and the compositing technique used in the present study. Composites presented here for each flow regime are categorized based on the predictive skill rather than the phenomenological nature of the events.

To showcase the synoptic and mesoscale details of environments with low-predictive skill, several case studies were undertaken and 4 are presented in section 3.4. The case studies are representative of several modes of low-predictive skill severe weather in the Northeast. Due to the similarity of type 1 northwesterly low-shear events when conducting the case study analysis, a conceptual model is shown in Fig. 4.1. The model illustrates the lack of strong synoptic triggering mechanisms for this type 1 category with the upper-level jet and surface boundary well removed from the area of convective initiation. Convective initiation occurs along land-lake boundaries or within high terrain and often in an environment with a moist planetary boundary layer (PBL). As convection propagates eastward, storms encounter higher LCL heights and anomalously high DCAPE values generally above the 80th percentile of DCAPE values in the station sounding climatology. This drier environment provides greater negative buoyancy to

rain-cooled parcels and enhanced evaporative cooling of saturated parcels within the boundary layer, increasing the risk for severe wind at the surface despite the reduced environmental shear.

By summarizing the common environmental attributes associated with low-shear type 1 events, the conceptual model provides a basis for "pattern recognition" prior to type 1 event occurrence. However, significant variability exists between type 1 events and the case study and conceptual model results presented herein should be used concurrently with other forecasting techniques when forecasting under marginal conditions.

4.2 Suggestions for future work

This study focuses on atmospheric precursors of severe weather events with low-predictive skill at 1200 UTC and 1800 UTC of the event day. Additional work may control for the time of convective initiation and further categorize events by diurnal cycle. While Hurlbut and Cohen (2014) found the first severe report of severe events typically occurs between 1800 and 2000 UTC, controlling for the diurnal cycle of convection may reduce the variability of the composites. Cluster analysis using empirical orthogonal function techniques performed on CFSR data to group cases by trough location may further reduce variability of the results as shortwave troughs are smoothed substantially within the composites in section 3.3. Considering the environment 24–48 hours prior to convective initiation may expand the applicability of this approach to assess synoptic differences between poorly predicted and well-predicted events in the days leading up to severe weather in the Northeast

Through the course of this study, the author discovered the CFSR has limited capabilities simulating the thermodynamic environment of convectively active days relative to observed

soundings and RUC/RAP model data. This is likely due to assumptions inherent in the boundary layer parameterization within the model as well as coarse model resolution. The 0.5° horizontal resolution struggles to resolve the complex terrain that characterizes the Northeast region. Composite analysis using reanalysis data with higher horizontal resolution may reveal connections to terrain features that the current study can only confirm through case study analysis. Additionally, higher resolution reanalysis data may resolve the mesoscale environment with more fidelity and more accurately simulate boundary layer processes, leading to better correlations between the observed thermodynamic parameters and those in the model analyses.

Lastly, Hurlbut and Cohen (2014) did not find shear to be a significant discriminator of the severity of severe weather events in the Northeast. The findings of this study show high-impact severe weather events occur frequently under low-shear conditions. While DCAPE offers some theoretical understanding for downdraft strength and subsequent wind speeds at the surface, the parameter requires significant violations of parcel theory (i.e. diabatic cooling of the parcel through evaporation of rain falling into it) and does not account for the enhanced evaporational effects of a dry boundary layer below the cloud base. Investigation of the convective mechanisms involved in generating severe winds at the surface in the absence of strong vertical wind shear will contribute to a better understanding of the true severe wind threat within low-shear environments.

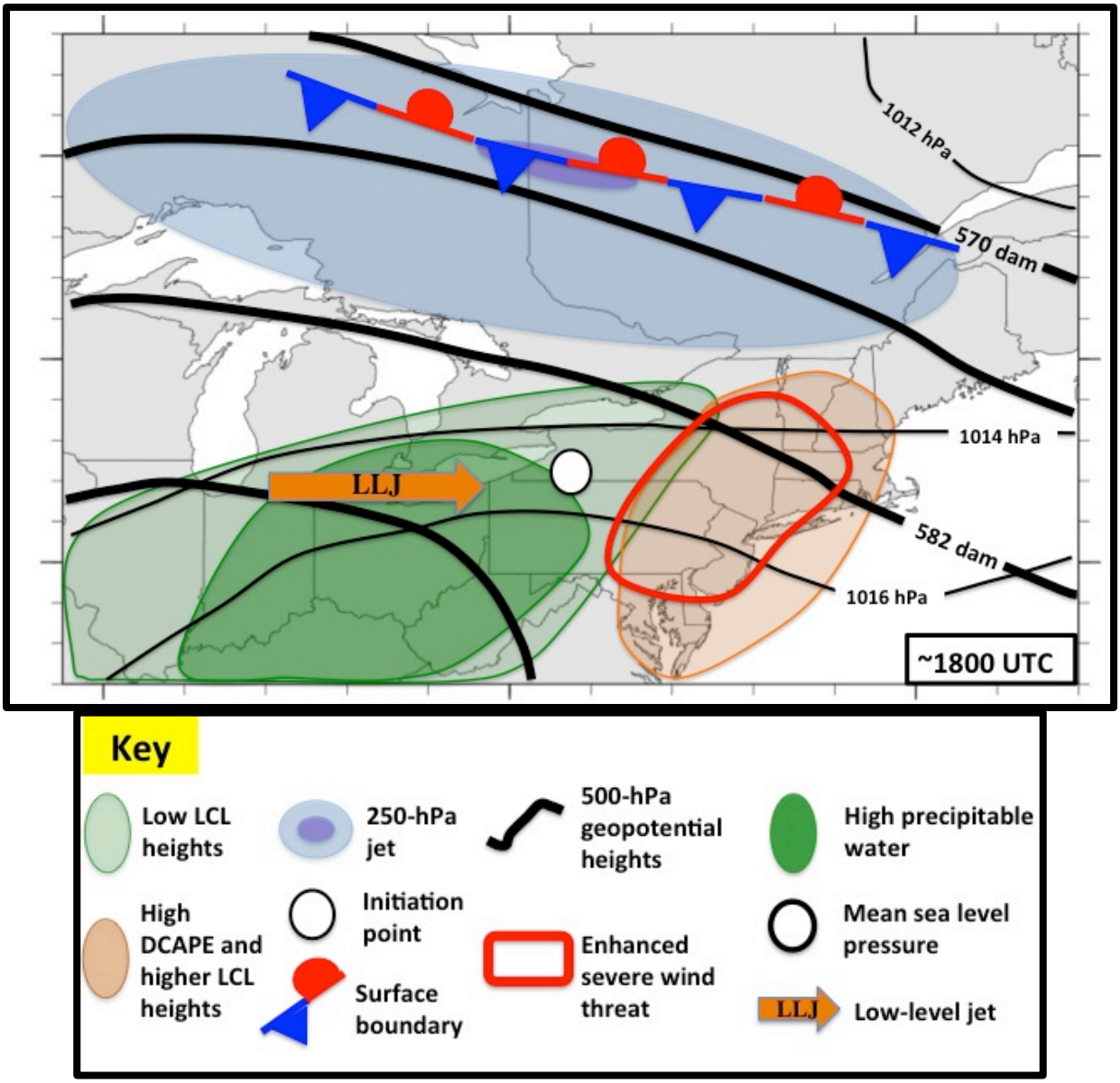

Figure 4.1. Schematic for northwesterly type 1 events under low-shear conditions. Background map is provided solely for scale. Upper-level forcing is weak and well removed from the point of convective initiation. The surface front, displaced to the north, is provided to illustrate the homogeneous surface temperatures and the lack of frontal forcing in the region of interest.

REFERENCES

Bosart, L. F., A. Seimon, K. D. LaPenta, and M. J. Dickinson, 2006: Supercell tornadogenesis over complex terrain: The Great Barrington, Massachusetts, tornado on 29 May 1995. *Wea. Forecasting,* **21,** 897–922

Banacos, P. C., and M. L. Ekster, 2010: The association of the elevated mixed layer with significant severe weather events in the northeastern United States. *Wea. Forecasting*, **25**, 1082–1102

Cohen, A. E., M. C. Coniglio, S. F. Corfidi, and S. J. Corfidi, 2007: Discrimination of Mesoscale Convective System Environments Using Sounding Observations. *Wea. Forecasting*, **22**, 1045–1062.

Coniglio, M. C., D. J. Stensrud, and M. B. Richman, 2004: An observational study of derecho-producing convective systems. *Wea. Forecasting,* **19,** 320–337

Corfidi, S. F., 1999: The birth and early years of the Storm Prediction Center. *Wea. Forecasting,* **14,** 507–525

Doswell C. A., III, S. J. Weiss, and R. H. Johns, 1993: Tornado forecasting: A review. *The Tornado: Its Structure, Dynamics, Prediction, and Hazards, Geophys. Monogr.*, Vol. 79, Amer. Geophys. Union, 557–571

——, H. E. Brooks, and M. P. Kay, 2005: Climatological estimates of daily local nontornadic severe thunderstorm probability for the United States. *Wea. Forecasting,* **20,** 577–595.

——, ——, and N. Dotzek, 2009: On the implementation of the enhanced Fujita scale in the USA. *Atmos. Res.,* **93,** 554–563.

Evans J. E., K. Carusone, M. M. Wolfson, M. Robinson, E. R. Ducot, and B. Crowe, 2004: Improving convective weather operations in highly congested airspace with the Corridor Integrated Weather System (CIWS). Preprints, *11th Conf. on Aviation, Range and Aerospace Meteorology,* Hyannis, MA, Amer. Meteor. Soc., P1.5 [Available online at https://ams.confex.com/ams/pdfpapers/81276.pdf.]

Evans, J. S., and C. A. Doswell III, 2001: Examination of derecho environments using proximity soundings. *Wea. Forecasting,* **16,** 329–342

Gallus, W. A., Jr., N. A. Snook, and E.V. Johnson, 2008: Spring and summer severe weather reports over the Midwest as a function of convective mode: A preliminary study. *Wea. Forecasting,* **23,** 101–113

Gensini, V. A., T. L. Mote, and H. E. Brooks, 2014: Severe-Thunderstorm Reanalysis Environments and Collocated Radiosonde Observations. *J. Appl. Meteor. Climatol.*, **53**, 742–751.

Hitchens, N. M. and H. E. Brooks, 2012: Evaluation of the Storm Prediction Center's Day 1 Convective Outlooks. *Wea. Forecasting*, **27**, 1580–1585.

—, and —, 2014: Evaluation of the Storm Prediction Center's Convective Outlooks from Day 3 through Day 1. *Wea. Forecasting*, **29**, 1134–1142.

Hurlbut, M. M. and A. E. Cohen, 2014: Environments of Northeast U.S. Severe Thunderstorm Events from 1999 to 2009. *Wea. Forecasting*, **29**, 3–22.

Johns, R. H., and C. A. Doswell III, 1992: Severe local storms forecasting. *Wea. Forecasting*, **7**, 588–612

LaPenta, K. D., L. F. Bosart, T. J. Galarneau Jr., and M. J. Dickinson, 2005: A multiscale examination of the 31 May 1998 Mechanicville, New York, tornado. *Wea. Forecasting,* **20,** 494–516

Lericos, T. P., H. E. Fuelberg, M. L. Weisman, and A. I. Watson, 2007: Numerical simulations of the effects of the coastlines on the evolution of string, long-lived squall lines. *Mon. Wea. Rev.,* **135,** 1710–1731

Lombardo, K. A., and B. A. Colle, 2010: The spatial and temporal distribution of organized convective structures over the Northeast and their ambient conditions. *Mon. Wea. Rev.,* **138,** 4456–4474

—, and —, 2011: Convective storm structures and ambient conditions associated with severe weather over the northeast United States. *Wea. Forecasting,* **26,** 940–956

Mesinger, F., and Coauthors 2006: North American Regional Reanalysis. *Bull. Amer. Meteor. Soc.,* **87,** 343–360

Riley, G. T., and L. F. Bosart 1987: The Windsor Locks, Connecticut tornado of 3 October 1979: An analysis of an intermittent severe weather event. *Mon. Wea. Rev.,* **115,** 1655–1677

Roebber, P. J., 2009: Visualizing multiple measure of forecast quality. *Wea. Forecasting,* **24,** 601–608

Saha, S., and Coauthors, 2010: The NCEP Climate Forecast System Reanalysis. *Bull. Amer. Meteor. Soc.,* 91, 1015–1057

Thompson, R. L., R. Edwards, J. A. Hart, K. L. Elmore, and P. Markowski, 2003: Close proximity soundings within supercell environments obtained from the Rapid Update Cycle. *Wea. Forecasting,* **18,** 1243–1261

Vescio, M. D., and R. L. Thompson, 2001: Subjective tornado probability forecasts in severe weather watches. *Wea. Forecasting,* **16,** 192–195

Wasula, A. C., L. F. Bosart, and K. D. LaPenta, 2002: The influence of terrain on the severe weather distribution across interior eastern New York and western New England. *Wea. Forecasting*, **17,** 1227–1289